ISSN 1028-8546

Azərbaycan Milli Elmlər Akademiyası
Fizika-Riyaziyyat və Texnika Elmləri Bölməsi
Fizika İnstitutu

3

Fizika

Cild

X

2004

Bakı ✵ Elm

QUASI-ELASTIC SCATTERING OF PROTONS INTERMEDIATE ENERGIES ON NUCLEUS

M.M. MIRABUTALIBOV
The Azerbaijan State Oil Academy,
AZ-1007, Baku, Azadlig ave., 20

The expression for the amplitude of quasi-elastic knockout of nucleus from the nuclei by protons of intermediate-energies with the activation of final nucleus has been obtained on the base of quasi-classic theory. The differential cross-section for the quasi-elastic scattering of protons of 1GeV has been determined for approach protons knockout from $1P_{3/2}$,$1P_{1/2}$,$1S_{1/2}$ levels in ^{16}O nucleus . The energies of protons knockout from these levels and the energy of excited hole states have been determined.

In activity on the basis of the quasi-classical approach, developed in [1] is put by the purpose to receive compact expression for amplitude of quasi-elastic knockout of nucleons from nucleus by protons of intermediate energies with excitation of a nucleus residual.

Differential cross-section of reaction *A(p, Np)B* proceeds as follows [2]:

$$d\sigma = (2\pi)^4 \frac{m}{k} dP_1 dP_2 \delta(E_P - E_1 - E_2 - E_N - E_R) \frac{1}{2(2j_i + 1)} \sum_{m\mu_f} |T_{if}|^2 . \quad (1)$$

Here E_P, E_1, E_2 – kinetic energies of dropping, scattering and knockout nucleons, E_N – energy of striping of nucleons accordingly

$$E_R = \frac{P_R^2}{2M_{A-1}}. \quad (2)$$

- recoil energy of a residual nucleus.

The matrix element of transition of a nucleus is represented by the way

$$T_{if} = < f \left| \int dr dx \psi_f^{(-)*}(r) \psi_{\kappa_0}^{*}(x) \vartheta(|r - x|) \rho(x) \psi_i^{(t)}(r) \psi_{nejm}(x) \right| i > \quad (3)$$

Wave functions of the relative movement scattered proton and a knocked out nucleon is received from the solution of Schrödinger equations:

$$\psi^{\pm}(r, k) = exp\left\{ i\left[kr \mp \Phi^{(\pm)}(r, k) \right] \right\} \quad (4)$$

Allowing taking (4) into account (3), after a change of variables $u = r - x$ and using thus series expansion for the distorting member $\Phi(\mathbf{r})$, we have:

$$T_{if} = -\frac{\hbar^2}{(2\pi)^2 \mu_0} < f \left| \int e^{i[q_{эф} - q']u} \rho(x) \psi_{\kappa_{00}}^{*}(x) f_{NN}(q') \psi_{nejm}(x) du dx d\vec{q} \right| i > , \quad (5)$$

where

$$q_{эф} = q + \nabla\Phi(u + x)\big|_{n=0} \quad (6)$$

Two partial potential was replaced by his Fourier-mode of amplitude of nucleon - nucleon interaction, which one has parameterized form [10]:

$$f_{NN}(q') = \frac{ik\sigma}{4\pi}(1 - i\varepsilon_0) e^{-\beta^2 q'^2} \quad (7)$$

Integrating expression (5) on *du* and then *dq'*, we'll receive simple expression for the differential cross-section:

$$d\sigma = \hbar^4 \frac{(2\pi)^6}{k} dP_1 dP_2 \delta(E_P - E_1 - E_2 - E_N - E_R) |f_{NN}(q)|^2 B(q_0) \quad (8)$$

where

$$q_0 = k_i - k_f - k_0 = q - k_0 \quad (9)$$

is equal to the momentum of nuclear nucleon before the act of interaction, $q=k_i-k_f$ - momentum of transfer of a scattering nucleon, k_0 - is a momentum of the knocked out nucleon.

The correlation function $B(q_0)$ is the distorted impulse distribution of nuclear protons in one of a particle condition, and is determined by an overlapping integral of wave

functions of a proton $\psi_t^{(+)}(x)$ in an initial state and two nucleons in an final state $\psi_f^{(-)}(x)$, $\psi_{\mathbf{k}_0}(x)$ by a particle function with a particle function $\psi_{nejm}(x)$ of a nucleus of the target:

$$B(q_0)=\sum_{m,\mu_f}\left|<f|\int dx\psi\, d(x)\rho(x)\psi_{nejm}(x)|i>\right|^2 \quad (10)$$

where

$$\psi(x)=exp\left[iq_0x+i\gamma\chi_1(x)+i\gamma^2\chi_2(x)\right] \quad (11)$$

is accepted , for simplification of expression (11), the mathematical method advanced in is received [1], after which we get:

$$\psi(x) = \Re(x)e^{iq\mathbf{0}x} \quad (12)$$

$$\Re(x) = 1 + i\Phi(x) - 2\beta^2 q_{\mathbf{0}}\nabla\Phi(u+x)\big|_{u=0} - \Phi^2(x)/2 - 2i\beta^2 q_{\mathbf{0}}\Phi(x)\nabla\Phi(u+x)\big|_{u=0} + (2\beta^4 q_{\mathbf{0}}^2 - \beta^2)(\nabla\Phi(u+x)\big|_{u=0})^2 \quad (13)$$

For determination (10) the functions $\rho(x)$ - nucleons density, which depends on features of adopted model of a nucleus, we proceed from the assumption , that each nucleon is estimated as a dot particle and introduces the independent contribution this operator of density:

$$\rho(x) = \rho_0\sum_{\alpha=1}^{A-1}\delta(x - x_\alpha) \quad , \quad (14)$$

where the summation α is conducted on all nucleons of a nucleus – core , x_α- coordinate of a nucleons which is read out from center of gravity of a nucleus.

After quasi-elastic knockout of a nucleon from a nucleus of the target, we'll esteem a nucleus- core as one nucleon outside of filled nuclear envelopes. Further if , that during the process the state of nucleons generated filled shells don't change ,the core - rest can be esteemed as a system consisting of an external nucleon and a frame of a core. Agrees (10), (12) and (14), the template member of transition of a core is determined by value of value,

$$B(q_0) = \rho_0^2\sum_{m,\mu_f}\left|< f\left|\sum_{\alpha=1}^{A-1}\Re(x_\alpha)\psi_{nejm}(x_\alpha)e^{iq_0x_\alpha}\right|i >\right|^2 \quad (15)$$

In a system consisting of a frame of a core and a nucleon, it is possible to enter effective mass which is taking into account their relative movement with the help of following reasoning [3]. Let situation of a nucleons having mass *m*, is described in some coordinate system by a radius-vector $\mathbf{r}_1$, and situation of a remaining part of a core - rest of mass *m(A-2)* by a radius-vector to k_2. Then

$$\sum_{\alpha=1}^{A-1}\Re(x_\alpha)\psi_{nejm}(x_\alpha)e^{iq_{\mathbf{0}}x\alpha} = \Re(r_1 - R_0)\psi_{nejm}(r_1 - R_0)e^{iq_{\mathbf{0}}(r_{\mathbf{1}}-R_{\mathbf{0}})} + (A-2)\Re(r_2 - R_0)\psi_{nejm}(r_2 - R_0)e^{iq_0(r_{\mathbf{2}}-R_0)} \quad (16)$$

Substituting in a right member of this equaling manifestative expression of a radius-vector of center of gravity, all core - rest $R_0 = \frac{r_1 + r_2(A-2)}{A-1}$ and allowing a result in (15), we have

$$B(q_0) = \rho_0^2\sum_{m,\mu_f}(< f\left|\left[\psi_{nejm}(rm_e)e^{iq_0\mathbf{r}m_e} + (A-2)\psi_{nejm}\left(\frac{r}{(A-1)}\right)e^{-\frac{iq_0r}{(A-1)}}\right]\Re(rm_e)|i >\right)^2 \quad , \quad (17)$$

where $r=r_1-r_2$ determines relative position of a nucleon and frame of a nucleus-core , and effective mass $m_e = \frac{A-2}{A-1}$, which is taking into account relative movement of a nucleon and a core.

$\psi_{nejm}(r,\theta,\varphi)$ is determined from the solution of a no relativistic Schrödinger equations for spherically - symmetrical potential with allowance for the spin - orbital interplay. Thus the wave function is represented as:

$$\psi_{nejm}(r,\theta,\varphi) = \frac{u_{nej}(r)}{r}\Phi_{ejm}(\theta,\varphi) \quad (18)$$

Schrödinger equations then we shall record so

$$\left\{\frac{d^2}{dr^2}-\frac{\ell(\ell+1)}{r^2}+\frac{2m}{\hbar^2}[E-U(r)]\right\}u_{nej}=0 \qquad (19)$$

Numerous experiments on scattering of nucleons on nucleus indicate that the potential of a harmonic oscillator more approaches for description of light nucleus, therefore nuclear potential is chosen by this way

$$U(r)=\frac{m\omega^2}{2}r^2+V_{\ell s}(r)\ell s, \qquad (20)$$

Where m – mass of a nucleon, ω - oscillation frequency of a classic oscillator, $ls=\frac{\{j(j+1)-l(l+1)-s(s+1)\}}{2}$ - - receives values $\frac{l}{2}$ for $j=l+\frac{1}{2}$ and $\frac{l(l+1)}{2}$, for . The intrinsic values of an equation (19) look like:

$$E_{nej}=E_{ne}+\Delta_{(n)e} \qquad (21)$$

Here $\Delta_{(n)e}=\frac{|V_{es}|(2l+1)}{2}$ - spacing interval between formicate levels, which one is determined from following known expression:

$$\Delta_{(n)\ell}=-20\ell sA^{-\frac{2}{3}}M\text{эВ} \qquad (22)$$

thus

$$E_{n\ell}=\hbar\omega\left(2n+l+\frac{3}{2}\right), \qquad (23)$$

where

$$\hbar\omega=\frac{\hbar^2}{ma^2} \qquad (24)$$

As the A (p, Np)B are investigated in reacting in light nucleus, it is necessary to result expressions of radial wave functions for 1C and $1P$ - state:

$$u_{1s}(r)=\pi^{-\frac{3}{4}}a^{-\frac{3}{2}}\exp\left(-\frac{r^2}{2a^2}\right) \qquad (25)$$

$$u_{1p}(r)=\left(\frac{8}{3}\right)^{\frac{1}{2}}\pi^{-\frac{1}{4}}\left(\frac{r}{a}\right)\exp\left(-\frac{r^2}{2a^2}\right) \qquad (26)$$

Parameter a in these wave functions expresses with the help (23) and (21) through energy of nucleons separation E_{nej};

$$a^2=\frac{\hbar^2(2n+\ell+3/2)}{m(E_{n\ell j}-\Delta_{(n)\ell})} \qquad (27)$$

Now we shall consider expression (17), being a correlation function of an exited nucleon and frame of a core. At its calculations it is necessary to select a coordinate system, let's select $0_z \uparrow\uparrow r$. It means that the exited nucleon is displaced in a direction inverse to a momentum of a nucleus of recoil.

After the count (18) in (17) we have.

$$B(\text{ъ}_{\text{и}} \rightarrow \text{ъ}_{\phi})=\frac{\rho_0^2}{4\pi}\left|\int r^2 и_f(r)и_i(r)\wp(r)dr\right|^2 S(j_i, j, j_f) \qquad (28)$$

where

$$S(j_i, j, j_f)=4\pi\sum_{m,\mu_f}\left|\left(\Phi_{j_f\mu_f}, Y_{jm}, \Phi_{j_i\mu_i}\right)\right|^2 , \qquad (29)$$

the so-called statistical factor, which one expresses through factors of vectorial addition. The exact form (29) is given in [3], and $\wp(r)$ receives following form

$$\wp(r)=\left\{и_{jm}(rm_e)e^{iq_0rm_e}+(A-2)и_{jm}\left(\frac{r}{(A-1)}\right)e^{-\frac{iq_0r}{(A-1)}}\right\}\Re(rm_e) \qquad (30)$$

Using the formulas of vectorial addition [4], we receive

$$B(j_i\rightarrow j_f)=\rho_0^2\frac{(2l+1)}{4\pi}<j_i1/2l0|j_f1/2>^2\left|\int u_f(r)u_i(r)\wp(r)r^2dr\right|^2 \qquad (31)$$

Thus, for differential cross-section of quasi-elastic knockout of nucleons one particle excitation of a residual nucleus

$$\frac{d^3\sigma}{d\Omega_2 d\Omega_1 dE_1} = (2\pi)^6 \frac{\hbar^4 m}{k} E_1^{1/2} \cdot E_2^{1/2} \left| f_{NN}(q) \right|^2 B(j_i \rightarrow j_f) , \qquad (32)$$

Where the energy knockout of a nucleon possess the value

$$E_2 = E_p - E_1 - E_N - E_R \qquad (33)$$

also is determined with the help (2) and law of conservation of momentum

$$P_R = \hbar k_i - \hbar k_1 - \hbar k_0 \qquad (34)$$

At quasi-elastic knockout of nucleons nucleus of recoil gain a vacant hole site in a shell, from which one the proton is released, and the energy of separation is equal to energy of one of a particle state. As in the beginning the nucleus A reposed, the momentum of a nuclear nucleon (q_0) up to the act of interaction was considered equal on value, but opposite in direction to the momentum of a nucleus of recoil in a final state. Therefore its value can be found from a law of conservation of momentum (34), $q_0 = -P_R = -\hbar k_{A-1}$ .Thus, knowing energy of taking off nucleon's and angles of their departure, it is possible directly to determine of energy and momentum distributions of one of particle state in concrete shells. Differential cross-section of quasi-elastic scattering of protons with energy 1 GeV is computed for a ^{16}0 nucleus. The analysis, basically, was shown to analysis of the form of correlation distributions and relative outputs of protons from different nuclear shells. The nucleus ^{16}0 can release protons from levels $1P_{3/2}, 1P_{1/2}, 1S_{1/2}$, therefore differential cross-section is counted for each of these cases and the outcomes are adduced in a fig. 1.

Besides in this figure for comparison, the theoretical curves counted in [5] with Hartri - Fok by wave functions are adduced. The calculations, basically, are made for an angle $\theta_2 = 61^0$ of departure of sluggish protons at a fixed scattering angle $\theta_1 = 13.4^0$ of a fast proton. Thus oscillator parameter a was "free", with the help which one the noticeable resemblance of theoretical differential cross-section with experimental is obtained.

In the table the counted energy of one of particle levels in nucleus ^{16}0 at the conforming values of oscillator parameter are adduced. Besides for comparison, the experimental values of energies of one of particle levels are adduced [5].

As it is shown at a fig. 1, power distribution of protons, corresponds two maximal in the range of energies 860 MeV and 930 MeV, for levels $P_{1/2}$ и $P_{3/2}$ and it is possible to explain these distributions from distributions on momentums of protons located at the conforming one particle level. The maiden maximum corresponds to invading of a ground state ($1/2-$)) and ($3/2-$). The second maximum corresponds to an exited state in a nucleus of the rest ^{15}N. In this figure a curve depicting knockout of protons from $S_{1/2}$ state with a maximum in the range of energies 870 MeV also is adduced.

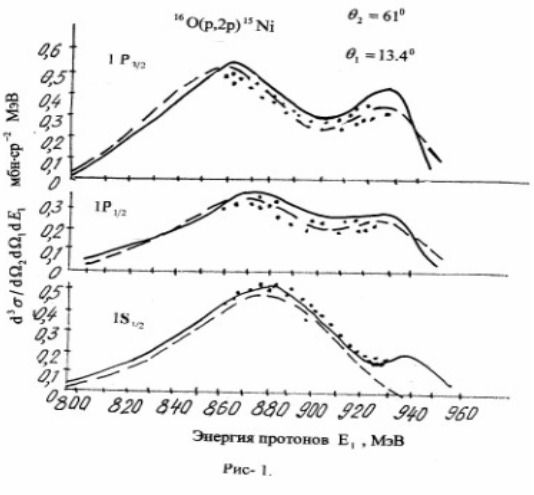

Fig. 1. Differential cross-sections of reaction of quasi-elastic knockout of protons from different shells of a nucleus ^{16}0. Continuous lines - outcome of the present activity, the shaped lines - are counted with Hartri-Fok by wave functions [5], point - experimental data.

Table 1

Theoretical and experimental values of energies one of particle state in a nucleus

nucleus	levels	a Fm	E_{lj} (MeV)	$E^{\bullet}_{lj}$ (MeV)	E_{lj} (Eкs) (MeV)
^{16} O	$1P_{3/2}$	2.27	18.6	15.98	19.6
	$1P_{1/2}$	2.55	12.8	10.74	13.0
	$1S_{1/2}$	1.28	38.1	33.19	39.2

The satisfactory description of the of correlation distributions' form and relative outputs of protons on the one hand, testifies that the count of distorting of surges and mathematical methods, used in calculations the amplitudes, of process are precise enough. On the other hand, consent of one-particle power spectrums both with experimental data,

and with curves of cross-sections counted with Hartri-Fok by wave functions, allow to make a conclusion, that this theoretical gear well describes A(p, Np) B - reaction, and nucleus structure. Therefore it can be applied for a quantification of differential cross-sections of quasi-elastic interaction of nucleons in a series of nucleus.

[1] *M.M. Mirabutalibov*.ANSA PHYSICS, 7.60.2001.

[2] *M. Goldberger, T. Watson.* T. The theory interactions. M. "Mir", 1967.

[3] *A.S. Davidov.* The theory of an atomic nucleus ."Fiz-mat izd" M. 1958.

[4] *V.G. Solovuyev.* The theory of an atomic nucleus. . M." Energoizd" 1981.

[5] *A.A. Vorobyev, O.B. Dotsenko etc.* SA USSR LINF pr.-1076,38,1985.

M.M. Mirabutalıbov

ORTA ENERJİLİ PROTONLARIN NÜVƏDƏN KVAZİELASTİKİ SƏPİLMƏSİ

Kvaziklassik nəzəriyyəyə əsasən, protonların nüvədən kvazielastiki səpilməsi prosesində nüvədən nuklon qoparılarkən qalıq nüvəsinin həyəcanlaşması zamanı, səpilmə amplitudasının ifadəsi analitik şəkildə tapılmışdır. ^{16}O nüvəsinin $1P_{3/2}$,$1P_{1/2}$,$1S_{1/2}$ enerji səviyyələrindən protonların qoparılması prosesi üçün differensial effektiv kəsik hesablanmış, həmin səviyyələrdən protonun qoparılma enerjisi və nüvənin bir zərrəcikli həyəcanlaşma enerjisi tapılmışdır.

М.М.Мирабуталыбов

КВАЗИУПРУГОЕ РАССЕЯНИЕ ПРОТОНОВ ПРОМЕЖУТОЧНЫХ ЭНЕРГИЙ НА ЯДРАХ

На основе квазиклассического подхода, развитого автором, получено компактное выражение для амплитуды квазиупругого выбивания нуклонов из ядер протонами промежуточных энергий с возбуждением ядра остатка.

Дифференциальное сечение квазиупругого рассеяния протонов с энергией 1 ГэВ, вычислено при выбивании протонов из уровней $1P_{3/2}$,$1P_{1/2}$,$1S_{1/2}$ в ядре ^{16}O. Определены энергия выбивания протонов из этих одночастичных уровней и энергия возбуждения дырочных состояний.

Received: 03.06.04

STM SURFACE TOPOGRAPHY AND UV PHOTOCONDUCTIVITY OF InSe, GaSe LAYER SEMICONDUCTORS

ZARBALIYEV MAHARRAM ZARBALI OGLU
Institute of Physics National Academy Science of Azerbaijan Republic
Az-1143, Baku, H. Javid ave., 33

Photoconductivity spectra of InSe, GaSe layer semiconductor samples in the region of high energy ($hv>>E_g$) and surface topography receiving by Scanning Tunneling Microscope (STM) method of these samples have been investigated. The results both photoconductivity and STM investigation showed that surface and bulk electron behaviors not so different. These allow investigate electron transitions in depth of adsorption edge by simple photoconductivity method. STM surfaces topography unfolds new usage perspectives for layered crystals InSe, GaSe.

Layer semiconductors InSe, GaSe due to peculiarity of their crystalline structure are characterized by practical absence ragged chemical bounds on a surface. Due to this property their surface distinguishes weak adsorption ability. As consequence of before stated conditions the lower density of surface states allows to register high photosensitivity in a wide spectral range including ultraviolet (UV) area of spectra [1].

It is known that electronic properties of these crystals are not so anisotropy as their mechanical properties. These crystals are easily cleaved and almost without special technological processing it is possible to receive samples rather the big area surfaces with monolayer.

Researches of Auger spectra investigation have showed are that surface concentration of adsorbents on InSe and GaSe surfaces two or three order is lower than surfaces of "usual" semiconductors [2].

On the one hand the above-stated properties of crystals InSe and GaSe allow to create on their basis photosensitive devices in a wide spectral range, especially in short-wave area of a spectrum, and on the other hand to study of behaviors optical transitions in depth of absorption edge by means of a photoconductivity method, where $hv>>E_g$. Characteristic spectral dependences photoconductivity of layered semiconductors InSe and GaSe on fig.1 are resulted at the room temperature.

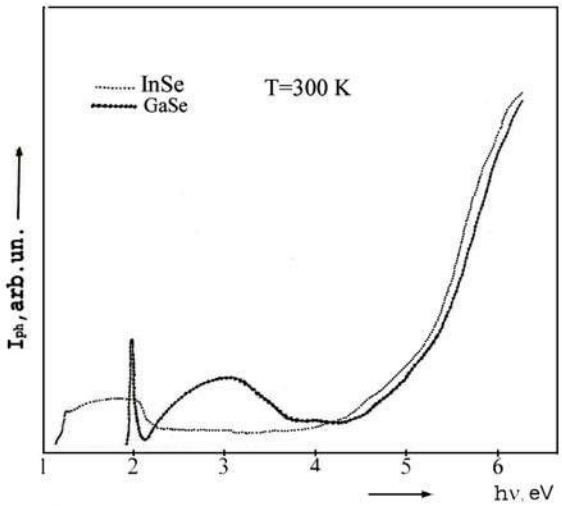

Fig.1. Photoconductivity spectra of InSe and GaSe layer semiconductors in the usual geometry (light being incident normally to the layer surface and contacts being installed upon the illuminated surfaces) of measurement in 1 – 6 eV region.

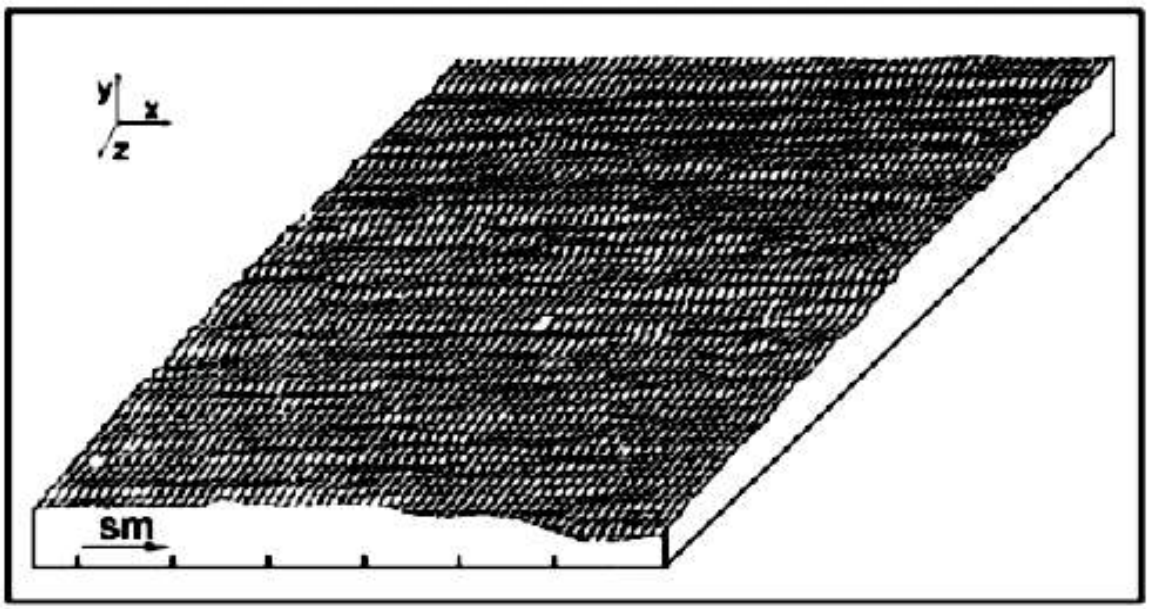

Fig.2. Scanning Tunneling Microscope method surface topography of InSe layer semiconductor samples in air. Size of image is correspondent to 280x280 A^o /cm on **x** and **y** direction, 60 A^o /cm on z direction.

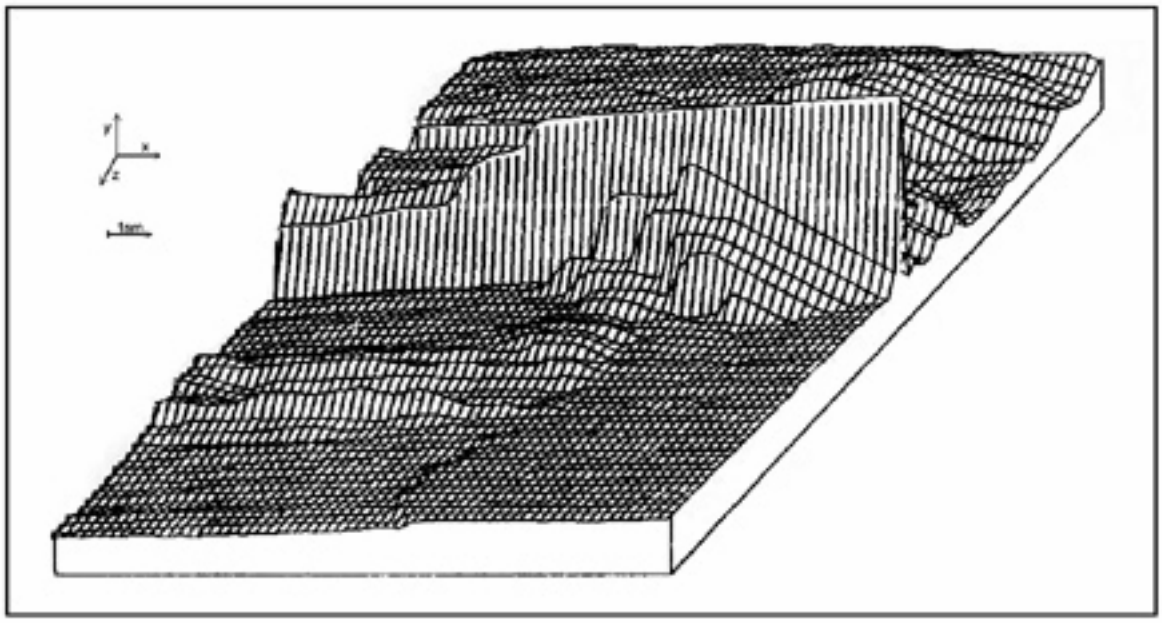

Fig.3. Scanning Tunneling Microscope method surface topography of InSe layer semiconductor samples in air where mechanical cleaving occurred in different layers far one from another. Size of image is correspondent to sizes on fig.2.

For present purposes the surface topography of samples InSe have been studied by the STM method in air. Before receiving topography images of given samples have been investigated of photoconductivity spectrums and were observed high photosensitivity, particularly in UV areas of a spectrum. On fig.2 the characteristic topography image of InSe samples surface is shown by STM method. These pictures distinctly show on reception favorable circumstance rather big areas of monolayer surfaces by the mechanical cleaved. On alongside with the assertion on surface of samples InSe crystal is absent significant inclusions, nevertheless in some places of topography images differences for scans are clearly visible. The height of these differences corresponds approximately to ~12–15 A^{o}. It can be concluded that on a surface can be have a place that defects of layers as a transition crystal lattice translation from one layer to another. Another event shown in Fig.3 where mechanical cleaving occurred in different layers far one from another and differences between scans much more than depth one or two layers.

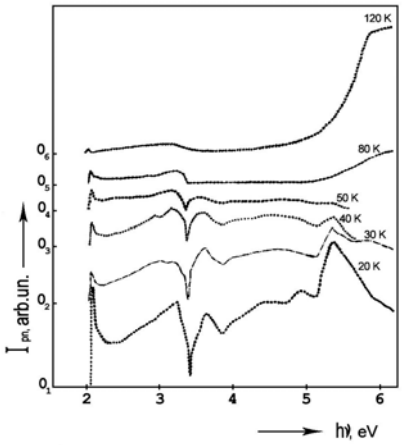

Fig.4. Photoconductivity spectra of GaSe layer semiconductors at different temperature.

Despite of the specified defects it is possible to observe separate sites of a surface with practical consisting of one monolayer. Due to opportunity STM it is easily possible to define on surface areas of layered semiconductors InSe and GaSe suitable for creation UV sensitive detectors and with manipulation simple technology it is possible to fabricate cheep UV devices.

The received results for samples from InSe layer crystals one can say with confidence can be attributed to samples of GaSe layer crystals.

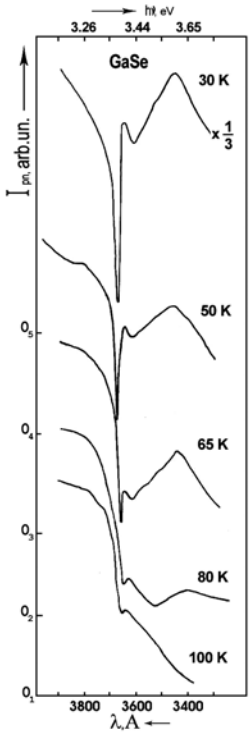

Fig.5. Photoconductivity spectra of GaSe layer semiconductors near deep exciton state.

It has been marked, that high photosensitivity in depth of absorption edge allows to studies the nature of optical transitions in this spectrum region. The spectrum of photoconductivity registered on sample GaSe are shown on fig.4 at various temperatures. Apparently from fig.1 and fig.4 photoconductivity spectrums of samples InSe and GaSe despite of increase adsorption coefficient factor photoconductivity signal decrease (~2-3 eV in InSe, ~3-4 eV in GaSe) is observed. Energy interval of this spectrum area coincides with spectrum area which optical transitions have excitons nature. Temperature influences research on photoconductivity spectra of InSe and GaSe layer semiconductors samples show an opportunity rather precise registration deep excitons transitions in these crystals for estimate their binding energy and Bohr radii. Temperature dependence photoconductivity spectra of these GaSe samples are shown on fig.4.

Thus in InSe and GaSe layered semiconductors were observed two types exciton states. One are formed between absolute extremes of a conductivity and a valet zone and it is typical Wannier-Mott type excitons, others correspond to excitations localized near the atomic site, possess the great binding energy (~90-100 meV), in small Bohr radii (~8 A^o), poorly participate in photoconductivity, and can be attributed to intermediate type excitons. Photoconductivity spectra of GaSe near deep exciton state at the different temperatures are resulted on fig.5. Deep exciton states originate from direct transitions between states which have atomic-like wave functions. It is easy to annihilate these excitons mainly at the low temperature than rather dissociate and consequently their contribution on photoconductivity registered as deep minima.

The photoconductivity and STM investigation of layer semiconductors InSe, GaSe are show that bulk and surface electron behavior of given crystals is approximately identically, more conclusions for bulk behaviors almost can be attributed to surface. At least monolayer surface of InSe, GaSe layer crystal can be utilized as easy prepare natural semiconductor plane surface for building on this a new nanometer devises and these blocks.

[1] *O.Z. Alekperov, M.O. Godjaev, M.Z. Zarbaliev and R.A. Suleymanov*. Solid State Commun. 1991, vol. 77, pp. 65-67.

[2] *E.Y. Salaev, M.O. Godjaev, G.L. Belenkii and L.N. Alieva.* Doklady Academii Nauk Azerb. SSR. 1986, 42, 15.

Məhərrəm Zərbəli oğlu Zərbəliyev

InSe, GaSe LAYLI YARIMKEÇİRİCİLƏRİNİN STM SƏTH TOPOQRAFİYASI VƏ SPECTRİN ULTRABƏNÖVŞƏYİ OBLASTINDA FOTOKEÇİRİCİLİYİ

InSe, GaSe laylı yarımkeçirici nümunələrin yüksək enerji oblastında ($hv>>E_g$) fotokeçiriciliyi və həmin nümunələrin Skanirəedən Tunel Mikroskopu (STM) metodu ilə səth topoqrafiyası tədqiq edilmişdir. STM və fotokeçiricilik metodlarının hər ikisindən alınan nəticələr göstərir ki, səthi və həcmi elektron xassələri bir-birindən çox fərqlənmir. Bu da udulma kənarından dərin oblastda elektron keçidlərinin təbiətini sadə fotokeçiricilik metodu ilə öyrənməyə imkan verir. STM səth topoqrafiyası InSe, GaSe laylı kristallarının yeni məqsədlər üçün istifadəsinə yollar açır.

Зарбалиев Магеррам Зарбали оглы

ПОВЕРХНОСТНАЯ ТОПОГРАФИЯ ПО МЕТОДУ СТМ И УФ ФОТОПРОВОДИМОСТЬ СЛОИСТЫХ ПОЛУПРОВОДНИКОВ InSe, GaSe

Исследованы спектры фотопроводимости образцов слоистых полупроводников InSe, GaSe и поверхностная топография этих же образцов методом Сканирующей Туннельной Микроскопии (СТМ). Результаты, полученные обоими методами показывают, что электронные свойства поверхности и объема не сильно отличаются. Это позволяет изучать электронные переходы в глубине края поглощения простым методом фотопроводимости. Поверхностная топография по методу СТМ открывает возможности использования этих кристаллов в новых других целях.

Received: 26.05.04

THE FEATURES OF THE SCATTERING OF ELECTROMAGNETIC AND ACOUSTIC WAVES IN THE WATER BOUNDARY LAYER OF THE ATMOSPHERE

A.SH. MEKHTIYEV, T.M. TATARAYEV, L.N. FARADGEVA
The Azerbaijan National Space Agency of National Academy of Sciences

On the basis of exploration of the processes of small-scale dependence of the sea and atmosphere conducted in the Caspian Sea [6-9] were examined some features of the scattering of electromagnetic and acoustic waves in the water boundary layer of the atmosphere.

INTRODUCTION

The solution of the problems of radiophysics and hydrophysics demands to study the influence of the turbulent structure of the atmospheres water boundary layer on the scattering of electromagnetic and acoustic waves in it. The regime of the turbulence in the atmosphere's water boundary layer practically depends on the extent of the windy waves development defining by the attitude c/u_*, where c-phase velocity of the main energycarrying surface wave, u_*-dynamic velocity of wind. The vast scientific literature [1-3] is dedicated to the methods of theoretical calculation of the fluctuation phenomena's in the water boundary layer and their experimental research. A few of works are dedicated to the research of features of the scattering of electromagnetic and acoustic waves although the remote probe of the ocean and the sea has a big meaning. So our work is dedicated to the revealing of the influence of the turbulence's regime in the water boundary layer of the atmosphere on the scattering electromagnetic and acoustic waves in it.

TEORETICAL FOUNDATIONS

Some features of the scattering of electromagnetic and acoustic waves in the water boundary layer of the atmosphere are examined in the dependence on the phase of development of the windy waves on the basis of the exploration conducted in the Caspian Sea [7; 8] with following suppositions:

a) The thermal stratification in the water layer of the atmosphere is close to neutral that is the Richardson number reaches to zero (Ri→0).

b) Electromagnetic and acoustic waves are spread at the altitude $Z>Z^o$, where Z^o-height; vertical profiles of meteorological parameters are declined from the logarithmic law higher than the height.

The scattering of the electromagneting and acoustic waves passing through the turbulent medium (it is an atmosphere and sea) is a main cause of fluctuations of the refractive coefficient. The refractive coefficient of the atmosphere [1; 3; 4] is a function of the temperature, wind velocity and humidity.

For the description of the scattering of electromagnetic and acoustic waves flows in the volume V containing the turbulence we must determine the average value $\overline{d\sigma}$ - effective section of the dispersion in this volume in any directions $\vec{q}$.

This value is determined by the following formulas mentioned in [3,4].

In the case with electromagnetic waves:

$$\frac{\overline{d\sigma}}{V \cdot d\Omega_e} = 2^{-\frac{14}{3}} \cdot K^{\frac{1}{3}} \cdot \sin^2\alpha \cdot \left[A^2 \cdot \left(B^{(T)} \cdot \overline{N_T} + B^{(e)} \cdot \overline{N}_E \cdot B^2\right) \cdot \overline{\varepsilon}^{-\frac{1}{3}}\right] \cdot \left|\sin\frac{V}{2}\right|^{-\frac{14}{3}} \quad (1)$$

and in the case with acoustic waves:

$$\frac{\overline{d\sigma}}{V \cdot d\Omega_a} = 2^{-\frac{14}{3}} \cdot K^{\frac{1}{3}} \cdot \cos^2 v \left[\frac{c_1 \cdot \cos^2\frac{v}{2} \cdot \overline{\varepsilon}^{-\frac{2}{3}}}{c^2_0} + \frac{B^{(T)} \cdot \overline{N}_T \cdot \overline{\varepsilon}^{-\frac{1}{3}}}{4 \cdot \overline{T}^2}\right] \cdot \left|\sin\frac{v}{2}\right|^{-\frac{11}{3}} \quad (2)$$

Here $K=\frac{2\pi}{\lambda}$ - wave number, α - angle between vectors $\vec{p}$ (whose the unit vector is perpendicular to the direction of the spreading of waves and describes its polarization) and $\vec{q}$; c_1- constant , equal 1,5 ; c_0- average speed of the spreading of acoustic waves in the air ; $\overline{N}_T$ and $\overline{N}_E$ -parameters characterizing the velocities of inhomogeneties alignment of temperature and specific density at the expense of the molecular effects , v - angle of waves' scattering , $\overline{T}$ - absolute average temperature , $\overline{E}$ - average specific humidity , Ω - spatial angle , $\overline{\varepsilon}$ - average velocity of dissipation of the turbulent energy , $B^{(T)}$ and $B^{(E)}$- constant values about unity ;

$$A=10^{-6} \cdot \left(79\frac{\overline{P}}{\overline{T}^2}\right) \cdot \left(1+\frac{15600}{\overline{T}} \cdot \overline{E}\right);$$

$$B=7800 \Big/ \left(1 + \frac{15600}{\overline{T}} \cdot \overline{E}\right) \quad (3)$$

where $\overline{P}$ - average atmosphere's pressure.

According to the theory by Monin - Obukhov [2] in the case of thermal stratification, close to neutral, is used the following formulas:

$$\overline{\varepsilon} \approx \frac{u_*^3}{k \cdot z},$$

$$\overline{N}_T \approx \frac{k \cdot u_* \cdot T_*^2}{z}, \qquad (4)$$

$$\overline{N}_E \approx \frac{k \cdot u_* \cdot E_*^2}{z},$$

where u_* , T_* , E_* - accordingly gauges of the velocity of wind, temperature and humidity.

These values we can determine through flows of quantity of the momentum τ, the heat q_T and the humidity W_E in the following way:

$$u_* = \sqrt{\frac{\tau}{\rho}},$$

$$T_* = -\frac{q_T}{k \cdot u_* \cdot c_p \cdot \rho_a}, \qquad (5)$$

$$E_* = -\frac{W_E}{k \cdot \rho_a \cdot u_*},$$

where c_p and ρ_a - specific heat capacity and density of the air, k - constant of Carmana.

The direct natural measuring of the vertical flows of quantity of τ , q_T and W_E demand to use high-sensitive and expensive devices. So by solution of the problem of small-scale interaction of the atmosphere and the sea we must pay attention to the definition of the mentioned flows through easy-measurable exterior parameters [2]

:

$$\delta u = \overline{u}_a - \overline{u}_w \cong u_a;$$

$$\delta\overline{T} = \overline{T}_w - \overline{T}_a \qquad (6)$$

$$\delta\overline{E} = \overline{E}_w - \overline{E}_a$$

where $\overline{u}$; $\overline{T}$; $\overline{E}$ -average velocity of wind , temperature , density of air and indices "a" and "w" refer to the standard height their measuring and marine surface .

So vertical flows we can express in the following way:

$$\tau = \rho_a \cdot c_a \cdot \overline{u}_a^{\,2},$$

$$q_T = \rho_a \cdot c_T \cdot \overline{u}_a \cdot \delta\overline{T}, \qquad (7)$$

$$W_E = \rho_a \cdot \overline{u}_a \cdot \delta\overline{E},$$

where c_a ; c_T ; c_e - coefficients of the marine surface resistance, the transfer of heat and evaporation.

Then with help of the equations (5) we can receive:

$$T_* = \left(\frac{c_T}{\sqrt{c_a}}\right) \cdot \left(\overline{T}_a - \overline{T}_w\right),$$

$$E_* = \left(\frac{c_E}{\sqrt{c_a} \cdot k}\right) \cdot \left(\overline{E}_a - \overline{E}_w\right) \qquad (8)$$

If to use the received scales the formulas (4) will have a following form:

$$\varepsilon = \frac{u_*^{\,3}}{k \cdot z},$$

$$\overline{N}_T = \left(\frac{u_*}{k \cdot z}\right) \cdot S_1 \cdot \left(\overline{T}_a - \overline{T}_w\right), \qquad (9)$$

$$\overline{N}_E = \left(\frac{u_*}{k \cdot z}\right) \cdot S_2 \cdot \left(\overline{E}_a - \overline{E}_w\right)$$

where $S_1 = \frac{c_T^{\,2}}{c_a}$; $S_2 = \frac{c_E^{\,2}}{c_a}$ (10)

.

Having defined a wave number as $2\pi/\lambda$ and having inserted the formulas (9) in (1) and (2) we can receive the following formulas:

$$\frac{\overline{d\sigma}}{V \cdot d\Omega_e} = \frac{2^{-\frac{14}{3}} (2\pi)^{1/3} \cdot \lambda^{-\frac{1}{3}}}{(k \cdot z)^{2/3}} \cdot \sin^2\alpha \left[A \cdot \left(B^{(T)}\right) \cdot S_1 \cdot \left(\overline{T}_a - \overline{T}_w\right) + B^{(E)} \cdot S_2 \cdot \left(\overline{E}_a - \overline{E}_w\right)^2 \cdot B^2\right] \cdot \left|\sin\frac{\nu}{2}\right|^{-\frac{11}{3}} \qquad (11)$$

$$\frac{\overline{d\sigma}}{V \cdot d\Omega_w} = \frac{2^{-\frac{14}{3}} (2\pi)^{\frac{1}{3}} \cdot \lambda^{-\frac{1}{3}}}{(k \cdot z)^{2/3}} \cdot \cos^2\nu \cdot \left[\frac{c_1 \cdot \cos^2\frac{\nu}{2} \cdot \varepsilon^{-\frac{2}{3}}}{c_o^{\,2}} + \frac{B^{(T)} \cdot \overline{N}_T \cdot \varepsilon^{-\frac{1}{3}}}{4\overline{T}^2}\right] \cdot \left|\sin\frac{\nu}{2}\right|^{-\frac{11}{3}} \qquad (12)$$

As it is seen from the formulas (11) and (12) parameters S_1 and S_2 enter the number of parameters determining the diffusion of waves. The last are determined with help of the coefficients c_a , c_T and c_e . As it is shown in the articles [5,7] one of the main parameters determining the dynamic processes in the water boundary layer is "waves' age "(which characterize the extent of the development of windy waves) expressed c/u_* . According to [5] the values $c/u_* \le 25-30$ correspond to the regime of the developing waving, $c/u_* \approx 30-40$ - the developed waving and $c/u_* \ge 40$ - the decadent waving.

RESULTS

For the definition of the dependence of the scattering of electromagnetic and sound waves on the extent of development of windy waves as it seen from (11) and (12) we must explore the variability of parameters S_1 and S_2 defined by the coefficients c_a , c_T and c_E . However up to now we have not a lot of experimental works which are dedicated to the study of the connections these coefficients with characteristics of the interaction wind are fields and surface waves. But we have a lot of experimental data which allow defining the variability of the parameter of roughness z_0 or c_a in a dependence on the characteristics of interaction of the sea and atmosphere.

So the task of the definition of the vertical flows of heat and moisture is tried to solve with help of the calculation of unit parameter z_0 .

In the article [5] on the basis of the natural measuring of characteristics of the interaction of the sea and atmosphere in the wide range of the variability of exterior hydrometeorological conditions of the coefficients c_a , c_T and c_E were approximated by the following formulas :

$$c_a \approx 1{,}2\cdot 10^{-3}\cdot\left(\frac{z^0\cdot u_*}{V}\right) \qquad (13)$$

$$c_T \approx c_E \approx 10^{-3}\cdot\left(\frac{z^0\cdot u_*}{v}\right) \qquad (14)$$

where $v \approx 0{,}15\ cm^2/sec$ is a coefficient of the kinematic viscosity of the air.

These formulas were received by the data of the direct measurement of τ , q_T and w_E . The conducting of the measuring in the different hydrometeorological conditions permitted authors to define the dependence z_0 and u_* on the parameter c/u_* , so far as u_* is stimulatingly determined by direct and indirect methods.

It is known that the development of the surface waves is escorted by the formation of the unstationary boundary layer of atmosphere. The connection between characteristics of the water boundary layer of atmosphere and the surface waves according to the data of the natural measuring is detail described in the work [6]. On the basis of the mathematical models of the atmosphere's boundary layer [7,8] we can receive the following formulas for its characteristics:

$$z^0 = \frac{u_\infty{}^2\cdot\rho_w\cdot\beta}{\rho_a\cdot g^3}\cdot\left[\frac{4}{3}\cdot\left(\frac{c}{u_\infty}-\gamma\right)\right]^3\cdot\frac{\xi\cdot e^{-\xi}}{1-e^{-\xi}} \qquad (15)$$

$$\frac{c}{u_\infty} = \left(1-e^{-\xi}\right)^{-1} - \frac{1}{\xi}\quad ;\ \frac{c}{u_*} = \frac{10}{3}\cdot\left(\frac{c}{u_\infty}-\gamma\right) \qquad (16)$$

where u_∞ - wind velocity on an upper bound of the wave's boundary layer, g - speeding up of free fall (acceleration due to gravity); β -constant, equal 10^{-2} ; γ -constant coefficient; $\xi = \frac{u_\infty\cdot k}{u_*}$.

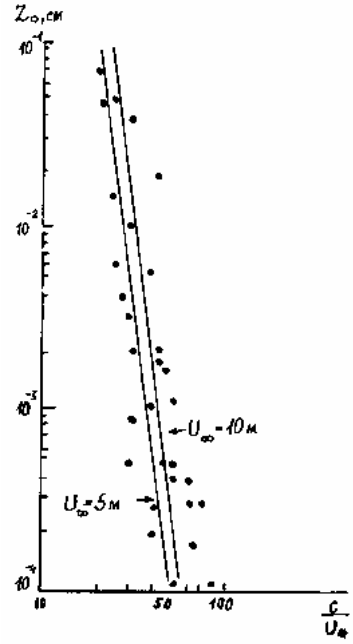

Fig.1. The dependence of the parameter of roughness on c/u_* .

The comparisons (15) and (16) with the experimental data has shown that its better conformity is achieved by γ =0,25.

The dependence of the parameter of roughness z_0 on the stage of the development of windy waves c/u_* according to the data of natural measuring in the Caspian Sea [7, 9] is shown on the fig.1. As it seen from the figure 1 the calculating and experimental points are coordinated quite satisfactorily.

Inserting the formula (15) in (13) and (14) and using (10) we can receive:

$$S = S_1 \approx S_2 = 8{,}4 \cdot 10^{-4} \left\{ \frac{{u_\infty}^3 \cdot k \cdot \rho_w \cdot \beta}{g \cdot \gamma \cdot \rho_a} \cdot \left[\left(\frac{c}{u_\infty} - \gamma \right) \cdot \frac{u}{3} \right]^3 \right\} \cdot \frac{e^{-\xi}}{1 - e^{-\xi}} \qquad (17)$$

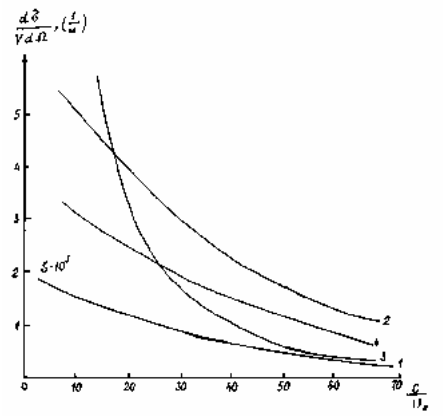

Fig.2. The dependence of characteristics of the scattering of electromagnetic and acoustic waves on c/u_*.

Such method simplifies to make calculation of the scattering according to the formulas (11) and (12), in which S enters.

The dependence of the parameter S on the stage of the development of windy waving (curve 1) is shown on the fig.2.

By constructing the figure $u_{10} = 10\, m/s$.

As it is seen from the figure when the parameter c/u_* increases from 10 to 70 the value S decreased up to1,5 times.

If to use $S = S_1 = S_2$ in the formulas of calculation of the scattering of electromagnetic and acoustic waves in the water layer of the atmosphere (11) and (12) after the foolproof transformations we are receiving:

$$\frac{\overline{d\sigma}}{V \cdot d\Omega_e} = \frac{2^{-\frac{14}{3}} \cdot (2\pi)^{1/3} \cdot \lambda^{-\frac{1}{3}} \cdot S}{(k \cdot z)^{2/3}} \cdot \sin^2 \alpha \left[B^{(T)} \left(\overline{T}_a - \overline{T}_w \right)^2 + B^{(E)} \cdot \left(\overline{E}_a - \overline{E}_w \right)^2 \cdot B^2 \cdot A^2 \right] \cdot \left| \sin \frac{v}{2} \right|^{-\frac{11}{3}} \qquad (18)$$

$$\frac{\overline{d\sigma}}{V \cdot d\Omega_a} = \frac{2^{-\frac{14}{3}} \cdot (2\pi)^{1/3} \cdot \lambda^{-1/3}}{(k \cdot z)^{2/3}} \cdot \cos^2 \cdot v \cdot \left[\frac{c_1 \cdot k^2 \cdot {\overline{u}_\infty}^2}{\xi^2 \cdot c_0} + \frac{B^{(T)}}{4} \cdot S \cdot \left(1 - \frac{\overline{T}_w}{\overline{T}_a} \right)^2 \right] \cdot \left| \sin \frac{v}{2} \right|^{-\frac{11}{3}} \qquad (19)$$

Then inserting the formula (17) in (18) and (19) and taking into consideration (15) and (16) we can construct graphs of the dependence of characteristics of the scattering on the extent of development of windy waving. We have constructed the dependences of the scattering on parameter c/u_* for several cases.

The curve 2 (fig. 2) shows the dependence of the parameter $\overline{d\sigma}/(V \cdot d\Omega_e)$ on c/u_* by $\lambda = 0{,}081$;

$|\delta E| = 0{,}001^{2/2}$; $\gamma = 0{,}25$; $\overline{P} = 1000 mb$;

$u_\infty = 10\, m/s$; $v = 48^0$ and $z = z_a = 10_m$.

But a reverse scattering by such methods is shown on the curve 4. Analogous dependence corresponds to the curve 3.

CONCLUSION

On the basis of analysis of the results of theoretical and experimental explorations of the turbulent water layer of the atmosphere and its interaction with windy waves is shown that the characteristics of the mentioned interaction have an influence on the scattering of electromagnetic and acoustic waves in it.

So the scattering of the waves rather quickly decreases by the increasing of the parameter c/u_*, characterizing the extent of the development of windy waves.

[1] *A.S. Monin.* Some characteristics of the acoustics' scattering in the turbulent atmosphere. Acoustic Journal, 1967, vol. 7, №.4, pp.457-461.

[2] *A.S. Monin, A.M. Yaglom*. Statistical hydromechanics, part 1 ("Nauka", Moscow. 1965, 639

[3] *A.S. Monin, A.M.Yaglom*. Statistical hydromechanics, part 2, "Nauka", Moscow. 1967, 720.

[4] *V.I. Tatarsky.* The propagation of the waves in the turbulent atmosphere. "Nauka", Moscow. 1967, 548.

[5] *S.A. Kitaygorodskiy, Yu.A. Volkov*. About the roughness parameter of the sea surface and the calculation of the turbulent flows of the momentum of water boundary layer of the atmosphere. Proceeding of the Academy of Sciences of USSR, Series Physics, Atmosphere and Optics, vol.1. №.9, 1965, pp. 873-988.

[6] *O.A. Kuznetsov, G.N. Panin*. The roughness of the sea surface and some characteristics of the atmosphere turbulence. The first meeting of the oceanology, Moscow, Issue 1. 1977, p.96.

[7] *A.Yu. Benilov, A.I. Gumbatov, M.M. Zaslavskiy, C.A. Kitaygorodskiy*. About the evolution of water boundary layer of the atmosphere by generation of windy waves. The first meeting of the oceanology. Moscow, Issue 1, 1977, p.89.

[8] *N.I. Achmedov, Ya.Z. Gadshie, A.I. Gumbatov, T.M. Tatarayev*. Non-stationary models of the development of the turbulent boundary layer over sea of the finite depth by generation of the surface wind wave. Oceanology, vol.31, Issue 1 1987, pp.52-56.

[9] *G.B. Valter, S.P. Zubkovskiy, T.M. Tatarayev, M.Z. Kholmenskiy, I.R.Tsvang*. The exploration of the spectrums of the atmospheric turbulence above the sea at the Caspian water station. (Academy of Science of the USSR; series of physics of the atmosphere and the ocean; 1976, vol. 12; No3; pp.244-254.

A.Ş. Mehdiyev, T.M. Tatarayev, L.N. Fərəcova

ATMOSFERİN SUYANI QATINDA ELEKTROMAQNİT VƏ SƏS DALĞALARININ SƏPİLMƏSİNİN XÜSUSİYYƏTLƏRİ

Xəzərdə kiçik miqyaslı «dəniz-atmosfer» qarşılıqlı təsirinin eksperimental tədqiqatları nəticələri əsasında suyanı atmosfer qatında elektromaqnit və akustik dalğaların səpilməsi qanuna uyğunluqları araşdırılmışdır. Müəyyən edilmişdir ki, göstərilən atmosfer qatında elektromaqnit və akustik dalğaların səpilmə xarakteristikaları dalğa rejiminin inkişaf mərhələsini xarakterizə edən c/u_* parametrindən ciddi asılıdır.

А.Ш. Мехтиев, Т.М. Татараев, Л.Н. Фараджева

ОСОБЕННОСТИ РАССЕЯНИЯ ЭЛЕКТРОМАГНИТНЫХ И ЗВУКОВЫХ ВОЛН В ПРИВОДНОМ СЛОЕ АТМОСФЕРЫ

На основе результатов экспериментальных исследований мелкомасштабного взаимодействия «море-атмосфера» на Каспии проанализированы закономерности рассеяния электромагнитных и акустических волн в приводном слое атмосферы. Установлено, что характеристики рассеяния электромагнитных и акустических волн в указанном слое атмосферы существенно зависят от параметра c/u_* ,характеризующего стадию развития ветровых волн.

Received:24.06.04

THE ENERGY SPECTRUM OF CARRIERS IN KANE TYPE SEMICONDUCTOR MICROCRYSTALS WITH SINQULAR OSCILLATOR POTENTIAL

A.M. BABAYEV
Institute of Physics, Azerbaijan Academy of Sciences,
Baku, Az-1143, H. Javid av. 33

The energy spectrum of light carriers in narrow band gap semiconductor microcrystal are studied theoretically taking into account the nonparabolicity of the electrons, light holes and spin-orbit splitting holes dispersion laws. The confinement potential of microcrystal is approximated as $\lambda r^2+\lambda_1 r^{-2}$, and the dispersion laws are considered within the framework of three-band Kane model. Confinement potential introduced in the Kane equations by non-minimal substation.

In recent years there has been a great interest to the nanostructures, which was developed from narrow-gap semiconductors. In these nanostructures much smaller effective mass of electrons resulting has higher size quantization energy. In order to investigate the optical and kinetic properties of nanostructures it will be possible to observe size quantization energy states. On the other hand in narrow-gap semiconductors the spin-orbit interaction and the non-parabolicity energy spectrum of carriers must be taken into account. It is impossible solve the equation analytically when the confinement potential is added to the Kane equations as scalar potential. Because of this in this study we have added the potential to the Kane equations by non-minimal interaction applied in the works of [1,2]. We refereed to the obtained equation as the singular Kane oscillator by analogy with the Dirac oscillator [2].

Confinement potentials are of the form $V(r)=\lambda\cdot r^2+\lambda_1 r^{-2}$ describe a quantum dot, an antidot, or a quantum ring, depending on the values of λ and λ_1 [3].

In the three-band Kane's Hamiltonian the valence and conduction bands interaction is taken into account via the only matrix element P (so called Kane's parameter). The system of Kane equations including the nondispersional heavy hole bands as in the case of Dirac equation can be written in the following matrix form:

$$(\vec{\sigma}\cdot\vec{k}\cdot P+\text{в}\cdot G-E)Ш=0 \tag{1}$$

In equation (1) 8x8 matrix α,β and G have the following nonzero elements:

$$\alpha_{1,3}{}^{x}=\alpha_{3,1}{}^{x}=-\alpha_{2,6}{}^{x}=-\alpha_{6,2}{}^{x}=-\frac{1}{\sqrt{2}} \tag{2}$$

$$\alpha_{1,5}{}^{x}=\alpha_{5,1}{}^{x}=-\alpha_{2,4}{}^{x}=-\alpha_{4,2}{}^{x}=\frac{1}{\sqrt{6}} \tag{3}$$

$$\alpha_{1,8}{}^{x}=\alpha_{8,1}{}^{x}=\alpha_{2,7}{}^{x}=\alpha_{7,2}{}^{x}=\frac{1}{\sqrt{3}} \tag{4}$$

$$\alpha_{1,3}{}^{y}=-\alpha_{3,1}{}^{y}=\alpha_{2,6}{}^{y}=-\alpha_{6,2}{}^{y}=\frac{i}{\sqrt{2}} \tag{5}$$

$$\alpha_{1,5}{}^{y}=-\alpha_{5,1}{}^{y}=\alpha_{2,4}{}^{y}=-\alpha_{4,2}{}^{y}=\frac{i}{\sqrt{6}} \tag{6}$$

$$\alpha_{1,8}{}^{y}=-\alpha_{8,1}{}^{y}=-\alpha_{2,7}{}^{y}=\alpha_{7,2}{}^{y}=\frac{i}{\sqrt{3}} \tag{7}$$

$$\alpha_{1,4}{}^{z}=\alpha_{4,1}{}^{z}=\alpha_{2,5}{}^{z}=\alpha_{5,2}{}^{z}=\sqrt{\frac{2}{3}} \tag{8}$$

$$\alpha_{1,7}{}^{z}=\alpha_{7,1}{}^{z}=-\alpha_{2,8}{}^{z}=-\alpha_{8,2}{}^{z}=\frac{1}{\sqrt{3}} \tag{9}$$

$$G_{11}=G_{11}=E_g, G_{11}=G_{22}=Д \tag{10}$$

$$Ш=\left(Ш_1,Ш_2,Ш_3,Ш_4,Ш_5,Ш_6,Ш_7,Ш_8\right)^T \tag{11}$$

Here P is the Kane parameter, $E_{.g.}$ - the band gap energy, Δ - the value of spin-orbital splitting and $k_{\pm}=k_x\pm ik_y, \vec{k}=-i\vec{\nabla}$. The zero of energy is chosen at bottom of the conduction band.

Let us carry out the non-minimal substitution

$$\vec{k}\to\vec{k}-i\beta\left(\lambda\vec{r}-i\lambda_1\frac{\vec{r}}{r^2}\right) \tag{12}$$

in Kane system of equations. Expressing all components of the wave function by the first two we obtain two coupled equations for the spin-up and the spin-down conduction band

$$\left(A+BL_z\right)Ш_1+BL_+Ш_2=0 \tag{13}$$

$$\left(A-BL_z\right)\Psi_2+BL_-\Psi_1=0 \tag{14}$$

where

$$A=E_g-E+\frac{P^2(3E+2ДД}{3(Д+E)E}\left(-\nabla^2+л^2r^2+3л+2лл_1+\frac{л_1\left(л_1+1\right)}{r^2}\right) \tag{15}$$

$$B=\frac{2}{3}\frac{P^2\Delta}{E(\Delta+E)}\left(\lambda+\frac{\lambda_1}{r^2}\right) \qquad (16)$$

where L_x, L_y, L_z are angular momentum operator compenents. Sense the problem has a spherical symmetry, we seek a solution to the differential equation in the form $F(r)Ylm(\theta\varphi)$..

By acting upon the equation (11) through the operator L_+ and using commutation relationships for the operators, we obtain $L_+\psi_2$. After substituting this quantity into expression (10), we derive two equations for $F(r)$.

$$\left(A+\frac{B}{2}\mp B(l+\frac{1}{2})\right)F(r)=0 \qquad (17)$$

After substitution of the values of A and B from (15), (16) the equation (17) can be rewritten in the form:

$$\left(\frac{d^2}{dr^2}+\frac{2}{r}\frac{d}{dr}+\frac{2m_n}{\hbar^2}(E'-\frac{l(l+1)}{r^2}\cdot\frac{\hbar^2}{2m_n}-\frac{a}{r^2}-br^2)\right)F(r)=0 \qquad (18)$$

where

$$E'=\frac{E(E-E_g)(E+\Delta)}{3E+2\Delta}\cdot\frac{3}{P^2}\frac{\hbar^2}{2m_n}-\frac{\hbar^2}{2m_n}\left(2\lambda\lambda_1+3\lambda+\frac{2\Delta\lambda}{3E+2\Delta}\left(\frac{1}{2}\mp(l+\frac{1}{2})\right)\right) \qquad (19)$$

$$a=\frac{\hbar^2}{2m_n}\left(\lambda_1(\lambda_1+1)+\frac{2\Delta\lambda_1}{3E+2\Delta}\left(\frac{1}{2}\mp(l+\frac{1}{2})\right)\right) \qquad (20)$$

$$b=\frac{\hbar^2\lambda^2}{2m_n} \qquad (21)$$

The eigenvalues of equations (18) take the following form [5]

$$E^{'}=\frac{\hbar^2\lambda}{2m_n}\left(4n+2+\sqrt{(2l+1)^2+\frac{8m_n}{\hbar^2}a}\right) \qquad (22)$$

The eigenfunctions corresponding to the eigenvalues of equation (18) are

$$F(\xi)=\exp\left(-\frac{\xi}{2}\right)\cdot\xi^2\cdot\Phi\left(-n,2s+\frac{3}{2},\xi\right) \qquad (23)$$

where is the confluent hypergeometric function, n must be non-negative integer, $\lambda=\frac{m_n\omega}{\hbar},\xi=\sqrt{2m_nb}\cdot\frac{r^2}{\hbar}$.

Equation (18) determines the energies of electrons, light holes, and the spin-orbit split-of band of holes. Equation (18) can be useful for analyzing the influence of nonparabolicity on the energy spectrum of electrons in a quantum dot.The singular oscillator equation is obtained from a system of the equations for multiband Hamiltonian describing spectrum of electrons, light and heavy holes in Kane's semiconductors by the method of a non-minimal interaction.

[1] *J. Benitez, R.P. Martinez y Romero* Phys. Rev Lett. 1990, V. 64, 14.

[2] *M. Moshinsky and A .Szezepanik.* J. Phys. A 22, L817 1989.

[3] *Namee Kim, S.J. Lee et all.* Journal of the Korean Physical Society 39, No3, pp.501-505.

[4] *B.M. Askerov.* inetic Effects in Semiconductors (Nauka, Leningrad, 1970.

[5] *L.D.Landau and E.M.Lifshitz*.Quantum Mechanics, 1977, Pergamon press.

A.M. Babayev

SİNGULYAR OSSİLYATOR POTENSİALİNA MALİK KEYN TİPLİ MİKROKRİSTALLARDA YÜKDAŞIYICILARIN ENERJİ SPEKTRLƏRİ

Qadağan olunmuş zonası dar olan yarımkeçirici microkristallarda yüngül yükdaşıyıcıların enerjı spektrləri nəzəri olaraq öyrənilmişdir. Mikrokristallarda saxlayıcı potensial olaraq $\lambda r^2+\lambda_1 r^{-2}$ şəklində götürülmüşdür. Potensial Keyn tənliklərinə qeyri-minimal qarşılıqlı təsir yolu ilə daxil edilmişdir. Yüngül yükdaşıyıcıların enerji spektrlərinin qeyri parabolikliyi nəzərə alınmışdır.

А.М. Бабаев

ЭНЕРГЕТИЧЕСКИЙ СПЕКТР НОСИТЕЛЕЙ ЗАРЯДА В КЕЙНОВСКИХ МИКРОКРИСТАЛЛАХ С ПОТЕНЦИАЛОМ СИНГУЛЯРНОГО ОСЦИЛЛЯТОРА

Найден энергетический спектр и волновые функции кейновского сингулярного осциллятора, описывающего спектр энергии электронов, легких дырок и спин-орбитально отщепленной зоны дырок в квантовой точке с удерживающим потенциалом типа $\lambda r^2+\lambda_1 r^{-2}$.

Received: 14.05.04

KANE TYPE QUANTUM DISK WITH WEAK RASHBA SPIN-ORBIT COUPLING

F.M, HASHIMZADE, A.M. BABAYEV
Institute of Physics of Azerbaijan National Academy of Sciences
Baku, Az-1143, H. Javid ave. 33

S. ÇAKMAK, Ş. ÇAKMAKTEPE
Department of Physics, University of Suleyman Demirel,
Isparta 32260, Turkey

Electrons in Kane type semiconductors quantum disk in presence of Rashba spin-orbital interaction of quantum disk are considered theoretically. A three-level model of the kp theory is used to describe electrons in weak Rashba spin-orbit coupling regimes, taking into account the main features of the band structure in InSb-type semiconductors: a small energy gap, a strong spin-orbit interaction. We calculated the radii, thickness, and coupling strength dependence of Rashba splitting for electrons. It has been seen that the Rashba splitting of the electrons are decreased with the increasing of radius.

Keywords: Spintronics; Rashba spin-splitting; quantum wire

Introduction

The study of semiconductor quantum dots and nanocrystals in recent years has been of great interest from experimental and theoretical points [1]. The interest originates from an ultimate limit of size quantization in solids in those objects. For an ideal quantum dot the electron spectrum consists of a set of discrete levels. This makes the semiconductor quantum dots very attractive for possible applications in micro and nano-opto-electronics [2].

The electron spin plays an important role in the quantum dot design. Spin-dependent effects that are naturally present in quantum dots are of great importance for the emerging field of spintronics. Spintronics is a new branch of electronics where electron spin is the active element for information storage and transport [3]. An example is Rashba spin-orbit coupling [4], which has recently attracted much attention as it is the basis of a spin-controlled field-effect transistor [5]. In [6,7] found analytic solution to the problem of the Rashba spin-orbit coupling in semiconductor quantum dots and calculated the energy spectrum, wave functions, and spin-flip relaxation times using perturbation theory. The above descriptions treat the case of a simple parabolic energy band .

However, the experimental advantages of using narrow-gap semiconductors for the reduced dimensionality systems make it necessary to account for the real band structure of these materials. To consider the nonparabolicity of the electron dispersion in narrow-and medium gap semiconductors take into account the coupling of the conduction and valence bands. This is purpose of our work. We now calculate the total spin-splitting energy in Kane type quantum disk with hard walls both without and with an applied constant axial magnetic field. It has a contribution due the Zeeman effect and another to the Rashba effect. We consider a three-level model-Kane model of the band structure at $k=0$ (the Γpoint).The Γ_6 level (s type symmetry) is separated by the energy gap E_g from the Γ_8 level (p type), which is in turn split off by the spin-orbit interaction Δ from the Γ_7 level (p type). We also omit the free-electron term in the diagonal part and the Paul spin erm, as they give only small contributions to the effective mass and the spin g value of electrons in InSb. The Rashba spin-orbit interaction for conduction band and valence and given by respectively:

$$H_R = R_c(\vec{n}[\vec{k}\vec{J}]) \quad H_v = R_v(\vec{n}[\vec{k}\cdot\vec{J}]) \quad H = R_\Delta(\vec{n}[\vec{k}\vec{J}]) \tag{1}$$

where k is the momentum operator, R_c, R_v, R_Δ is the coupling strength for conduction band, valence band, spin-orbit-splitting band respectively, $J=\{J_x, J_y, J_z\}$ are the angular momentum matrices for $j=1/2$ and $j=3/2$ [8], n is the unit vector in the growth direction. The Kane Hamiltonian is represented in the Bloch basis [9]-

$$1.iSv_1\ 2.iSv_2\ 3.-\frac{1}{\sqrt{2}}(x+iy)v_1\ 4.-\frac{1}{\sqrt{6}}((x+iy)v_2-2zv_1) \tag{2}$$

$$5.\frac{1}{\sqrt{6}}((x-iy)v_1+2zv_2)\ 6.\frac{1}{\sqrt{2}}(x-iy)v_2\ 7.-\frac{1}{\sqrt{3}}((x+iy)\cdot v_2+zv_1) \tag{3}$$

$$8.\frac{1}{\sqrt{3}}((x-iy)\cdot v_1-zv_2) \tag{4}$$

where $v_1 = \begin{pmatrix} 1 \\ 0 \end{pmatrix}$, $v_2 = \begin{pmatrix} 0 \\ 1 \end{pmatrix}$ spin-up and spin-down functions, respectively

- as: $H_K =$

$$\begin{bmatrix} -E & & -\frac{Pk_-}{\sqrt{2}} & \sqrt{\frac{2}{3}}Pk_z & \frac{Pk_+}{\sqrt{6}} & 0 & \frac{Pk_z}{\sqrt{3}} & \frac{Pk_+}{\sqrt{3}} \\ & -E & 0 & -\frac{Pk_-}{\sqrt{6}} & \sqrt{\frac{2}{3}}Pk_z & \frac{Pk_+}{\sqrt{2}} & \frac{Pk_-}{\sqrt{3}} & \frac{Pk_z}{\sqrt{3}} \\ \frac{Pk_-}{\sqrt{3}} & & -E_g - E & 0 & 0 & 0 & 0 & 0 \\ \sqrt{\frac{2}{3}}Pk_z & -\frac{Pk_+}{\sqrt{6}} & 0 & -E_g - E & 0 & 0 & 0 & 0 \\ \frac{Pk_-}{\sqrt{6}} & \sqrt{\frac{2}{3}}Pk_z & 0 & 0 & -E_g - E & 0 & 0 & 0 \\ 0 & \frac{Pk_-}{\sqrt{2}} & 0 & 0 & 0 & -E_g - E & & 0 \\ \frac{Pk_-}{\sqrt{3}} & \frac{Pk_-}{\sqrt{3}} & 0 & 0 & 0 & 0 & -E_g - E - \Delta & 0 \\ & \frac{Pk_-}{\sqrt{3}} & 0 & 0 & 0 & 0 & 0 & -E_g - E - \Delta \end{bmatrix} \quad (5)$$

Here P is the Kane parameter, E_g - the band gap energy, Δ- the value of spin-orbital splitting and $k_\pm = k_x \pm i k_y$, $\vec{k} = -i\vec{\nabla}$. The zero of energy is chosen at bottom of the conduction band.

The Rashba Hamiltonian has the following nonzero elements:

$$H_{12} = -i \cdot \frac{1}{2} \cdot R_c \cdot k_- , \; H_{34} = -i \cdot \frac{\sqrt{3}}{2} \cdot R_v \cdot k_- , \; H_{45} = -i \cdot R_v \cdot k_- , \quad (6)$$

$$H_{56} = -i \cdot \frac{\sqrt{3}}{2} \cdot R_v \cdot k_- , \; H_{78} = -i \cdot \frac{1}{2} \cdot R_\Delta \cdot k_- , \quad H_{ijj} = H_{ji}^* \quad (7)$$

For Kane model putting $R_c=2R$, $R_v=R$, $R_d=2R$. The effective mass m_n at the band edge defined as [10]:

$$\frac{\hbar^2}{2m_n} = \frac{P^2}{3E_g} \cdot \frac{2\Lambda + 3E_g}{\Delta + E_g} \quad (8)$$

We are diagonalized the Kane Hamiltonian with the help of unitary transformation $H^d = U^{-1} H_\theta U$, where U is the matrix of the transformation (see Appendix) . For electron states

$$H_\theta = \begin{bmatrix} -E - \frac{P^2}{3}\left(\frac{2}{E + E_g} + \frac{1}{E + E_g + \Delta}\right)k^2 & 0 \\ 0 & -E - \frac{P^2}{3}\left(\frac{2}{E + E_g} + \frac{1}{E + E_g + \Delta}\right)k^2 \end{bmatrix} \quad (9)$$

After unitary transformation the Rashba Hamiltonian with providing the terms linear with k will be as follows for the conduction band.

$$H_R = \begin{bmatrix} 0 & -iR \cdot k_- \\ iR \cdot k_+ & 0 \end{bmatrix} \quad (10)$$

The spin splitting for electron states it increases linearly with in plane wave vector k, whereas the spin-splitting of heavy hole states can be of third order in k. These results are in agreement with [11].

Following the perturbation approach we present the Hamiltonian H as:

$$H = H_\theta + H_R \quad (11)$$

Where the Hamiltonian H_0 describes the electron states in zero Rashba spin-orbital interaction, and the Hamiltonian describes the effect of a weak Rashba spin-orbital interaction H_R.

In cylindrical coordinates the eigenfunction for unperturbed Hamiltonian H_0 is

$$\begin{bmatrix} C_1 \\ C_2 \end{bmatrix} = \begin{bmatrix} \exp i[(j-1/2)\varphi + k_z z] \cdot J_{j-1/2}(k\rho) \\ \exp i[(j+1/2)\varphi + k_z z] \cdot J_{j+1/2}(k\rho \end{bmatrix} \quad (12)$$

where φ is azimuthal angle, ρ is the distance from disk axis, and $J_j(\rho)$ the Bessel function of the l-th order.

We expand eigenfunction for perturbed Hamiltonian H in the basis of the two lowest spin-resolved eigenstates of the Hamiltonian H_0. Accordingly,

$$\Psi = d_1 \cdot \nu_1 \cdot C_1 + d_2 \cdot \nu_2 C_2 \quad (13)$$

where k, q are wave vector perpendicular and parallel to the quantum disk axis.

Equating the determinant of matrix (15) to zero, one obtains for the spectrum of electrons

Substituting this result in Eq (11), and using to the standard recurrence relations

$$\left(\frac{d}{dx} + \frac{j \pm 1/2}{x}\right) J_{j \pm 1/2}(kx) = k J_{j \mp 1/2}(kx) \quad (14)$$

we get the coefficients $d_{1,2}$ satisfy the eigenvalue equation:

$$\begin{bmatrix} \varepsilon - E & -iRk_- \\ iRk_+ & \varepsilon - E \end{bmatrix} \begin{pmatrix} d_1 \\ d_2 \end{pmatrix} = 0 \quad (15)$$

where ε is the solution of equations:

$$\varepsilon(\varepsilon + E_g)(\varepsilon + \Delta + E_g) - \frac{1}{3}(3\varepsilon + 2\Delta + 3E_g)P^2(k^2 + q^2) = 0 \quad (16)$$

$$E = \varepsilon \pm iRk \quad (17)$$

Using equations (16) and (17) found the equation for value of k

$$k^2 \pm kR\frac{3}{(2\Delta + 3E + 3E_g)^2}\left(-\frac{3E(E + E_g)(E + E + \Delta)}{(2\Delta + 3E + 3E_g)} + E(E + E_g) + (2E + E_g)(E + E + \Delta)\right)$$
$$q^2 - \frac{3E(E + E_g)(E + E + \Delta)}{(2\Delta + 3E + 3E_g)P^2} = 0 \quad (18)$$

The boundary conditions requiring the equality of radial function to zero on quantum disk boundary have the following form:

$$d_1 J_{j-1/2}(k_1 a) + d_2 J_{j-1/2}(k_2 a) = 0 \quad (19)$$

$$d_1 J_{j+1/2}(k_1 a) + d_2 J_{j+1/2}(k_2 a) = 0 \quad (20)$$

where $k_{1,2}$ are the solutions of the quadratic equation (18).

The spectrum of the electrons in quantum disk is defined from the equality to zero of a determinant of the system (19)-(20):

$$J_{j-1/2}(k_1 a)J_{j+1/2}(k_2 a) - J_{j-1/2}(k_2 a)J_{j+1/2}(k_1 a) = 0 \quad (21)$$

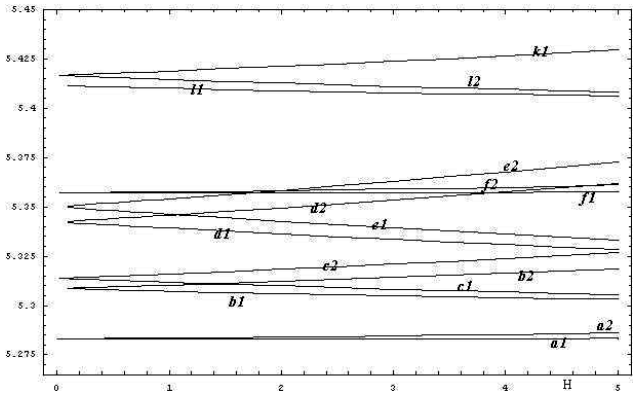

*Fig.1.*Rashba splittings. Energy as a function of γ=R/P for the states (1/2,0)(a), (3/2,0)(b), (1/2,1)(c), (5/2,0)(d), (3/2,1)(e), (1/2,2)(f), (7/2,0)(l), (5/2,1)(m), (3/2,2)(n), (1/2,3)(k)

The energy is complicated of the disk parameters and the electron angular momentum. The energy system consist of discrete levels enumerated by a set of numbers $\{n,j\}$, where n denotes to the nth solution of (21) with fixed j.

We have solved this dispersion relations for a JnSb disk for several radii ρ, several thickness d, and several R using the band structure parameters: m_0=0.014m$_0$, E_g=0.24eV, R=4.10^{-21}eV.cm [12,13].

The evolution of the first few energy levels with the parameter $\gamma=R/P$ is shown in fig.1.The energy scale is in init. of *Eg*, *Eg* is band gap energy and the curves are labelled by quantum number (n, j).

In fig.2.show Rashba splitting (Energy differences *E(1/2,1)-E(3/2,0)*) as a function of ρ for thickness of quantum disk *d=20A*.

It has been seen that the Rashba splitting are decreased with the increasing of radius. The thickness dependence of

Rashba splitting calculated for JnSb quantum disk is shown in fig.3.for ρ=200A.

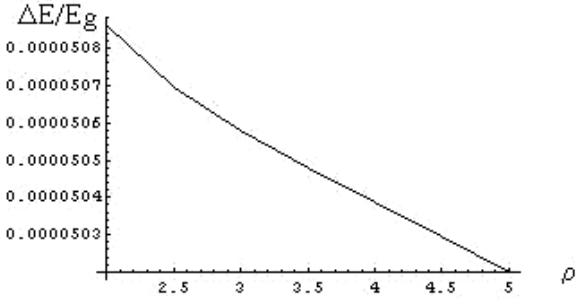

Fig.2. Energy differences (E(1/2,1)-E(3/2,0))/E_g as a function of ρ for thickness of quantum disk d=20A.

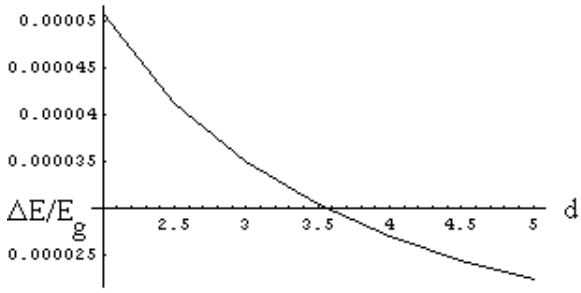

Fig.3. Energy differences (E(1/2,1)-*E*(3/2,0))/E_g as a function of d for radii of quantum disk ρ=200A.

It has been seen that the Rashba splitting decreases with the increasing of thickness.

Conclusion.

Analytic solutions of the Kane equations have been presented for a quantum disk in the presence of Rashba spin-orbit .The nonparabolicity of the spectrum of light holes, electrons and spin-orbit splitting valence band were taken into account. The spin splitting for electron states it increases linearly with in plane wave vector $k_{||}$, whereas the spin-splitting of heavy hole states can be of third order in $k_{||}$.

Appendix.

Nonzero matrix elements for transformation matrix U are:

$$U_{11} = N_1, U_{13} = -\frac{N_1 \cdot P}{\varepsilon_1 + E_g} \cdot \frac{k_-}{\sqrt{2}},$$

$$U_{14} = \frac{N_1 \cdot P}{\varepsilon_1 + E_g} \cdot \frac{\sqrt{2}q}{\sqrt{3}},$$

$$U_{15} = \frac{N_1 \cdot P}{\varepsilon_1 + E_g} \cdot \frac{k_+}{\sqrt{6}},$$

$$U_{17} = -\frac{N_1 \cdot P}{\varepsilon_1 + E_g + \Delta} \cdot \frac{q}{\sqrt{3}},$$

$$U_{18} = \frac{N_1 \cdot P}{\varepsilon_1 + E_g + \Delta} \cdot \frac{k_+}{\sqrt{3}}$$

$$U_{22} = N_1, U_{24} = -\frac{N_1 \cdot P}{\varepsilon_1 + E_g} \cdot \frac{k_-}{\sqrt{6}},$$

$$U_{25} = \frac{N_1 \cdot P}{\varepsilon_1 + E_g} \cdot \frac{\sqrt{2}q}{\sqrt{3}},$$

$$U_{26} = \frac{N_1 \cdot P}{\varepsilon_1 + E_g} \cdot \frac{k_+}{\sqrt{2}},$$

$$U_{27} = -\frac{N_1 \cdot P}{\varepsilon_1 + E_g + \Delta} \cdot \frac{k_-}{\sqrt{3}},$$

$$U_{28} = -\frac{N_1 \cdot P}{\varepsilon_1 + E_g + \Delta} \cdot \frac{q}{\sqrt{3}}$$

where $N_1^{-2} = 1 + \frac{P^2}{3} \cdot \left(k^2 + q^2\right) \cdot \left(\frac{2}{\varepsilon_1 + E_g} + \frac{1}{\varepsilon_1 + E_g + \Delta}\right)$

The expressions U_{3j}, U_{5j} are derived from U_{1j} if the corresponding substitutions $N_1 \to N_2$, $N_1 \to N_3$ and $\varepsilon_1 \to \varepsilon_2$, $\varepsilon_1 \to \varepsilon_3$ respectively. The expressions U_{4j}, U_{6j} are derived from U_{2j} if the corresponding substitutions $N_1 \to N_2$, $N_1 \to N_3$ and $\varepsilon_1 \to \varepsilon_2$, $\varepsilon_1 \to \varepsilon_3$ respectively. Where ε_1, ε_2, ε_3 are energy spectrum electrons, light hole and spin-split holes respectively.

$$U_{73} = N_4 \cdot \frac{2}{\sqrt{3}} \cdot \frac{k_-}{k_+}, \; U_{74} = N_4 \cdot \frac{k_-}{2q}, \; U_{75} = N_4$$

$$U_{86} = N_4 \cdot \frac{2}{\sqrt{3}} \cdot \frac{k_+}{k_-},\ U_{85} = -N_4 \cdot \frac{k_+}{2q},\ U_{84} = N_4$$

where

$$N_4^{-2} = 1 + \frac{k_+ k_-}{4q^2} + \frac{4}{3} \cdot \frac{k_+ k_-}{k_- k_+}$$

[1] *T. Chakraborty*. Quantum Dots, Elsevier, 1999.

[2] *D. Bimberg, M. Grundman, M. Ledentsov.* Quantum Dot Heterostructures, JOHN WILEY, 2001.

[3] *G. A. Prinz*. Sciense, 1990, 282, 1660.

[4] *Yu.A. Buchkov and E.I. Rashba*. J. Phys., 1984, C 17, 6039.

[5] *S. Datta and B. Das*. Appl. Phys. Lett. 1990, 56, 665.

[6] *E.Tsitsishvili, G.S. Lazano and A.O.Gogolin*. Preprint.cond-mat.0310024, 2003, v2.

[7] *E.N. Bulgakov, A.F. Sadreev.* Pis'ma v ZhETF, 2001, vol. 73, iss. 10, pp. 573-577.

[8] *G.L. Bir and G.E. Pikus*. Symmetry and Strain-Induced Effects in Semiconductors. Wiley, New York, 1974.

[9] *A.I. Anselm*. Introduction to Semiconductor Theory. Nauka, Moscow, 1978; Prentice-Hall, Englewood.

[10] *W. Zawadzski, S.Klahn, and U.Merkt* Phys.Rev B, 1986, 33,10,6916.

[11] *L.G. Gerchikov and A.V. Subashiev*. Sov.Phys-Semicond., 1973, 26.

[12] *E.A. de Andrada e Silva*. Phys.Rev B, 1997, vol. 55, N. 24.

[13] *C.F.Destefani*, *E. Sergio Ullao, and G.E. Marques* Preprint/cond-mat/0307027v1,2003.

F.M. Haşımzadə, A.M. Babayev

SPİN-ORBİTAL QARŞILIQLI TƏSİRİ ZƏİF OLAN KEYN NANODİSKİ

Keyn spektrinə malik yarımkeçirici nanodiskdə elektronların enerji spektrləri Raşba spin-orbital qarşılıqlı təsiri nəzərə alınmaqla hesablanmıışdır. Raşba parçalanmasının nanodiskin radiusundan və qalınlığından asılılığı öyrənilmişdir. Göstərilmişdir ki, nanodiskin radiusu və qalşnlığı artdiqca parçalanmanın qiyməti azalır.

Ф.М. Гашимзаде, А.М. Бабаев

КЕЙНОВСКИЙ КВАНТОВЫЙ ДИСК СО СЛАБОЙ СПИН-ОРБИТАЛЬНОЙ СВЯЗЬЮ

Найдены энергетический спектр носителей заряда в квантовом диске с учетом спин-орбитального взаимодействия Рашба. Найдены зависимость расщепления Рашбы от радиуса и толщины квантового диска. Показано, что при возрастании радиуса и толщины диска расщепление уменьшается.

Received: 03.06.04

RAMAN SCATTERING IN QUANTUM WIRE IN A MAGNETIC FIELD

T.G. ISMAILOV, B.H. MEHDIYEV
Institute of Physics of Azerbaijan National Academy of Sciences
Baku, Az-1143, H. Javid ave. 33

Electron Raman scattering are investigated in a parabolic semiconductor quantum wire in a transverse magnetic field neglecting phonon-assisted transitions. The ERS cross-section is calculated as a function of the frequency shift and the magnetic field strength. The process involves an interband electronic transition and an intraband transition between quantized subbands. We analyze the differential cross-section for different scattering configurations. We study selection rules for the processes. The singularities in the Raman spectra are found and interpreted. The scattering spectrum shows density-of-states peaks and interband matrix elements maximums and strong resonance when scattered frequency equals the "hybrid" frequency or confinement frequency depending on polarization. Numerical results are presented using parameters caaracteristic of GaAs/AlGaAs.

1. Introduction

Low-dimensional semiconductor systems, particularly quantum wires are attracting considerable attention recently, in part, because they exhibit novel physical properties and also because of potential applications involving them. In recent years, a number of innovative techniques have been developed to grow or to fabricate and to study experimentally a variety of quantum wire structures having different geometries and potentials.

Many recent experimental and theoretical studies have been performed on quantum wires subjected to a transverse magnetic field [1-7]. The electronic properties of quantum well wires in a transverse magnetic field have investigated in [8-9]. The subband dispersion and magnetoabsorption have been studied for rectangular QW in [10].

Magnetic field applied perpendicular to the wire axis, "free electron" direction, can change significantly the electronic states of semiconductor quantum wire structures.

Electron Raman scattering seems to be a useful technique providing direct information on the energy band structure and the optical properties of the investigated systems [11-12]. In particular, the electronic structure of semiconductor materials and nanostructures can be thoroughly investigated considering different polarizations for the incident and emitted radiation [13].

The differential cross-section in general case, usually shows singularities related to interbanda and interband transitions. This latter result strongly depends on the scattering configurations: the structure of the singularities is varied when the photon polarizations change. This feature of ERS allows to determine the subband structure of the system by direct inspection of the singularity positions in the spectra.

For bulk semiconductors ERS has been studied in the presence of external applied magnetic and electric fields[14-16]. In the case of a quantum well preliminary results were reported in [17]

Raman scattering in low-dimensional semiconductor systems has been the subject of many theoretical and experimental investigations [18, 19].

Interband ERS processes can be qualitatively described in the following way: after the absorption of an external photon from the incident radiation field a virtual electron-hole pair is created in an intermediate crystal state by means of an electron interband transition involving the crystal valence and conduction bands. The electron (hole) in the conduction (valence) band is subject to a second interband transition with the emission of secondary radiation photon. Therefore, in the final state we have a real electron-hole pair in the crystal and a photon of the secondary radiation field. The effect of external applied fields on this kind of processes for bulk semiconductors were investigated in [15, 16]. In the case of a quantum well preliminary results were reported in Ref. [17].

In this work we present a systematic study of the interband ERS in direct band gap semiconducting parabolic quantum wire in a transverse magnetic field. In these systems due to electron confinement and magnetic field the conduction (valence) band is split in a subband system and transitions between them determine the ERS processes. Numerical results for the ERS differential cross-section are presented using parameters characteristic of GaAs/AlGaAs.

This paper is organized as follows. In Section II the energy spectrum and wave functions for QW with parabolic confinement potential are given in a transverse magnetic field. In Section III we present the general relations needed for our calculations of the ERS cross-section. Section IV is devoted to the calculations of the ERS differential cross-sections. Finally Section V is concerned with the discussion of the obtained results.

2. Wave functions and energy spectrum

We consider a quantum wire aligned along the y direction with transverse magnetic field $\vec{H} = (0,0,H)$ applied along z direction. The quantum wire is characterized by parabolic confinements in the plane (x, z). The effective mass Schrodinger equation for electron in conduction band can be written as

$$\left(\frac{1}{2 \cdot m_e} \left(\vec{p} + \frac{e}{c} \vec{A} \right)^2 + \frac{1}{2} m_e \omega_{0e}^2 \left(x^2 + z^2 \right) \right) \psi_e(x, y, z) = E_e \psi_e(x, y, z) \tag{1}$$

where $\vec{A}=(0,Hx,0)$ the vector potential in the Landau gauge and ω_{0e} characterizes the parabolic potential of the QW for electron in conduction band. We look for the solution in the form $\psi_e(x,y,z)=\varphi(x)\eta(z)e^{\frac{i}{\hbar}p_{y,e}y}$ where $p_{y,e}=\hbar k_{y,e}$ is the quasi-momentum of an electron.

After trivial shifting of the origin of coordinates and separating the variables in the usual way we obtain the eigenfunctions and eigenvalues of the Schrödinger equation (1)

$$\psi_{N_{1e},N_{2e},k_{y,e}}=\varphi_{N_{1e}}\left(\frac{x-x_{0e}}{\widetilde{L}_e}\right)\eta_{N_{2e}}\left(\frac{z}{L_e}\right)e^{ik_{y,e}y} \tag{2}$$

$$E_e=\left(N_{1e}+\frac{1}{2}\right)\hbar\widetilde{\omega}_e+\left(N_{2e}+\frac{1}{2}\right)\hbar\omega_{0e}+\frac{\hbar^2k_{y,e}^2}{2m_e}\left(\frac{\omega_{0e}}{\widetilde{\omega}_e}\right)^2 \tag{2, a}$$

The wave functions and energy eigenvalues for electron in valence band can be written as

$$\psi_{N_{1h},N_{2h},k_{y,h}}=\varphi_{N1h}\left(\frac{x-x_{0h}}{\widetilde{L}_h}\right)\eta_{N_{2e}}\left(\frac{z}{L_h}\right)e^{ik_{y,h}y} \tag{3}$$

$$E_h=-E_g-\left(N_{1h}+\frac{1}{2}\right)\hbar\widetilde{\omega}_h-\left(N_{2h}+\frac{1}{2}\right)\hbar\omega_{0h}-\frac{\hbar^2k_{y,h}^2}{2m_h}\left(\frac{\omega_{0h}}{\widetilde{\omega}_h}\right)^2 \tag{3,a}$$

where E_g is the gap energy of the bottom of the conduction band in the absence of the external magnetic field, ω_{0h} oscillator frequency of the parabolic potential for electron in the valence band. In Eqs. (2) and (3)

$$\widetilde{\omega}_{e,h}=\sqrt{\omega_{0e(h)}^2+\omega_{e(h)}^2} \tag{4}$$

is "hybrid" frequency. The subscript e and h denote conduction and valence band electrons, respectively.

$$\omega_{e(h)}=\frac{eH}{m_{e(h)}c} \tag{5}$$

is the cyclotron frequency, $m_{e(h)}$ is the effective mass.

$$x_{0e(h)}=\frac{\hbar\omega_{e(h)}}{m_{e(h)}\widetilde{\omega}_{e(h)}^2}k_{ye(h)} \tag{6}$$

is oscillator centre.

The full energy spectrum in (2) and (3) is governed by quantum numbers $N_{1e(h)}$, $N_{2e(h}$ and $k_{ye(h)}$.

$$\varphi_{N_{1e(h)}}\left(\frac{x-x_{oe(h)}}{\widetilde{L}_{e(h)}}\right)=\left(\frac{1}{\pi\widetilde{L}_{e(h)}^2}\right)^{1/4}\frac{1}{\sqrt{2^{N_{1e(h)}}N_{1e(h)}!}}\exp\left(-\frac{1}{2}\frac{(x-x_{oe(h)})^2}{\widetilde{L}_{e(h)}^2}\right)H_{N_{1e(h)}}\left(\frac{x-x_{oe(h)}}{\widetilde{L}_{e(h)}}\right) \tag{7}$$

$$\eta_{N_{2e(h)}}\left(\frac{z}{L_{e(h)}}\right)=\left(\frac{1}{\pi L_{e(h)}^2}\right)^{1/4}\frac{1}{\sqrt{2^{N_{2e(h)}}N_{2e(h)}!}}\exp\left(-\frac{1}{2}\frac{z^2}{L_{e(h)}^2}\right)H_{N_{2e(h)}}\left(\frac{z}{L_{e(h)}}\right) \tag{8}$$

where parameters

$$\widetilde{L}_{e(h)}=\sqrt{\frac{\hbar}{m_{e(h)}\widetilde{\omega}_{e(h)}}};\quad L_{e(h)}=\sqrt{\frac{\hbar}{m_{e(h)}\omega_{0e(h)}}}; \tag{9}$$

are the units of length.

$$H_n(\xi)=n!\sum_{k=0}^{[\frac{n}{2}]}\frac{(-1)^k}{k!(n-2k)!}(2\xi)^{n-2k} \tag{10}$$

is the Hermitian polynomial.

3. Preliminary relations

We start with the following general expression for the scattering cross-section $\frac{d^2S}{d\Omega d\nu}$ of the scattering of incident light with frequency ν_0 and polarization $\vec{e}_0$ into light with frequency ν_1 and polarization $\vec{e}_1$:

$$\frac{d^2S}{d\Omega d\nu} = \left(\frac{e^2}{m_0c^2}\right)^2 \frac{\nu_1}{\nu_0} \sum_{i,f} \left|A_{i,f}\right|^2 \hbar\delta(\hbar\nu - E_f + E_i) \tag{11}$$

where

$$A_{i,f} = \frac{1}{m_0} \sum_r \left(\frac{\langle f|\vec{e}_1\vec{p}|r\rangle\langle r|\vec{e}_0\vec{p}|i\rangle}{E_f - E_r + \hbar\nu_0} + \frac{\langle f|\vec{e}_0\vec{p}|r\rangle\langle r|\vec{e}_1\vec{p}|i\rangle}{E_f - E_r - \hbar\nu_1} \right) \tag{12}$$

Here *i*, *r* and *f* denote the initial, intermediate, and final states, respectively, E_i, E_r and E_f- are the corresponding energies, $\vec{p}$ is the one-electron momentum operator and m_0 is the free electron mass. $\nu = \nu_0 - \nu_1$ is a frequency shift. Equations (1) and (2) are based on the electric dipole approximation. The δ-function in (1) express the energy-conservation condition

$$\hbar\nu_0 = \hbar\nu_1 + E_f - E_i \tag{13}$$

Then Raman scattering processes consist of two steps. First, an incident light quantum is absorbed creating an electron –hole pair between the state (N_{1h}, N_{2h}) in the valence band and the state (N'_{1e}, N'_{2e}) in the conduction band. Second, a scattered photon is emitted due to an electronic transition from the state (N'_{1e}, N'_{2e}) to the state (N_{1e}, N_{2e}) in conduction band. The Raman shift $\hbar\nu$ is equal to the excitation energy of the electron-hole pair created in the scattering process.

In our model we assume that the conduction band is empty and the valence band completely occupied by electrons. We neglect all the transitions assisted by phonons.

The initial, intermediate and final state energy and wave functions are:

$$\begin{aligned}
E_i &= E_h(N_{1h}, N_{2h}, k_{yh}); \quad & \left|N_{1h}, N_{2h}, k_{yh}\right\rangle &= U_v\psi(N_{1h}, N_{2h}, k_{yh}) \\
E_r &= E'_e(N'_{1e}, N'_{2e}, k'_{ye}); \quad & \left|N'_{1e}, N'_{2e}, k'_{ye}\right\rangle &= U_c\psi(N'_{1e}, N'_{2e}, k'_{ye}) \\
E_f &= E_e(N_{1e}, N_{2e}, k_{ye}); \quad & \left|N_{1e}, N_{2e}, k_{ye}\right\rangle &= U_v\psi(N_{1h}, N_{2h}, k_{yh})
\end{aligned} \tag{14}$$

4. Calculation of Raman scattering cross section

Using Eqs. (14) the DCS for ERS can be written as

$$\begin{aligned}
\frac{d^2S}{d\Omega d\nu} = \left(\frac{e^2}{m_0c^2}\right)^2 \frac{\nu_0 - \nu}{\nu_0} \sum_{N_{1e},N_{2e}} \sum_{N_{1h},N_{2h}} \sum_{k_{ye},k_{yh}} \left|A_{N_{1h},N_{2e},N_{1e},N_{2e}}\right|^2 \hbar \cdot \delta\Big(\hbar\nu - E_g - \\
- E_{N_{1h}} - E_{N_{2h}} - E_{N_{1e}} - E_{N_{2e}} - \frac{\hbar^2k_{ye}^2}{2m_e}\left(\frac{\omega_{0e}}{\tilde{\omega}_e}\right)^2 - \frac{\hbar^2k_{yh}^2}{2m_h}\left(\frac{\omega_{0h}}{\tilde{\omega}_h}\right)^2\Big)
\end{aligned} \tag{15}$$

where

$$\begin{aligned}
A_{N_{1h},N_{2e},N_{1e},N_{2e}} = \frac{1}{m_0} \sum_{N'_{1e},N'_{2e}} \Bigg(\frac{\langle N_{1e}, N_{2e}, k_{ye} \left|\vec{e}_1\vec{p}\right| N'_{1e}, N'_{2e}, k'_{ye}\rangle\langle N'_{1e}, N'_{2e}, k'_{ye} \left|\vec{e}_0\vec{p}\right| N_{1h}, N_{2h}, k_{yh}\rangle}{E_h(N_{1h}, N_{2h}, k_{yh}) + \hbar\nu_0 - E'_e(N'_{1e}, N'_{2e}, k'_{ye})} + \\
+ \frac{\langle N_{1e}, N_{2e}, k_{ye} \left|\vec{e}_0\vec{p}\right| N'_{1e}, N'_{2e}, k'_{ye}\rangle\langle N'_{1e}, N'_{2e}, k'_{ye} \left|\vec{e}_1\vec{p}\right| N_{1h}, N_{2h}, k_{yh}\rangle}{E_h(N_{1h}, N_{2h}, k_{yh}) - \hbar(\nu_0 - \nu) - E'_e(N'_{1e}, N'_{2e}, k'_{ye})}
\end{aligned} \tag{16}$$

and

$$E_{N_{1e(h)}} = \left(N_{1e(h)} + \frac{1}{2} \right) \hbar \widetilde{\omega}_{e(h)}; \qquad E_{N_{2e(h)}} = \left(N_{2e(h)} + \frac{1}{2} \right) \hbar \omega_{0e(h)}; \tag{17}$$

The matrix elements of the interband transitions can be written as

$$\begin{aligned} \left\langle N_{1e},\, N_{2e},\, k_{ye} \left| \vec{e}_j \vec{p} \right| N'_{1e},\, N'_{2e},\, k'_{ye} \right\rangle &= \left\langle N_{1e},\, N_{2e},\, k_{ye} \left| e_{jx} p_x \right| N'_{1e},\, N'_{2e},\, k'_{ye} \right\rangle + \\ \left\langle N_{1e},\, N_{2e},\, k_{ye} \left| e_{jy} p_y \right| N'_{1e},\, N'_{2e},\, k'_{ye} \right\rangle &+ \left\langle N_{1e},\, N_{2e},\, k_{ye} \left| e_{jz} p_z \right| N'_{1e},\, N'_{2e},\, k'_{ye} \right\rangle \end{aligned} \tag{18}$$

where

$$\left\langle N_{1e},\, N_{2e},\, k_{ye} \left| e_{jx} p_x \right| N'_{1e},\, N'_{2e},\, k'_{ye} \right\rangle = - \frac{i\hbar}{\widetilde{L}_e} e_{jx} \delta_{N'_{2e}, N_{2e}} \left[\sqrt{\frac{N_{1e}}{2}} \delta_{N'_{1e}, N_{1e}-1} \sqrt{\frac{N_{1e}+1}{2}} \delta_{N'_{1e}, N_{1e}+1} \right] \delta_{k_{ye}, k'_{ye}} \tag{19}$$

$$\left\langle N_{1e},\, N_{2e},\, k_{ye} \left| e_{jy} p_y \right| N'_{1e},\, N'_{2e},\, k'_{ye} \right\rangle = \hbar k'_{ye} e_{jy} \delta_{N'_{2e}, N_{2e}} \delta_{N'_{1e}, N_{1e}} \delta_{k_{ye}, k'_{ye}} \tag{20}$$

$$\left\langle N_{1e},\, N_{2e},\, k_{ye} \left| e_{jz} p_z \right| N'_{1e},\, N'_{2e},\, k'_{ye} \right\rangle = - \frac{i\hbar}{L_e} e_{jz} \delta_{N'_{1e}, N_{1e}} \left[\sqrt{\frac{N_{2e}}{2}} \delta_{N'_{2e}, N_{2e}-1} - \sqrt{\frac{N_{2e}+1}{2}} \delta_{N'_{2e}, N_{2e}+1} \right] \delta_{k_{ye}, k'_{ye}} \tag{21}$$

If we consider allowed electron transitions between conduction and valence bands, the interband matrix element in the envelope function approximation, can be written as

$$\left\langle N'_{1e},\, N'_{2e},\, k'_{ye} \left| \vec{e}_j \vec{p} \right| N_{1h},\, N_{2h},\, k_{yh} \right\rangle = \left(\vec{p}_{cv} \cdot \vec{e}_j \right) \cdot I_{N_{1h}, N'_{1e}} \left(k_y \right) \cdot I_{N_{2h}, N'_{2e}} \cdot \delta_{k_{yh}, k'_{ye}} \tag{22}$$

where $\vec{p}_{cv} = \left\langle u_c \left| \vec{p} \right| u_v \right\rangle$ - the momentum matrix element between the valence and conduction bands (evaluated at $\vec{k} = 0$)and

$$I_{N_{1h}, N'_{1e}} \left(k_y \right) = \int_{-\infty}^{+\infty} \varphi_{N_{1h}} \left(\frac{x - x_{0h}}{\widetilde{L}_h} \right) \varphi_{N'_{1e}} \left(\frac{x - x_{0e}}{\widetilde{L}_e} \right) dx \tag{23}$$

$$I_{N_{2h}, N'_{2e}} = \int_{-\infty}^{+\infty} \eta_{N_{2h}} \left(\frac{z}{L_h} \right) \eta_{N'_{2e}} \left(\frac{z}{L_e} \right) dz \tag{24}$$

We find that the matrix elements (19)-(22) vanish unless the following selection rule is obeyed

$$k_{ye} = k_{yh} = k'_{ye} = k_y \tag{25}$$

The EHP does not change its total momentum during the absorption or the emission of a photon (photon momentum is neglected).

Using (10) it can be obtained that

$$\begin{aligned} I_{N_{1h}, N'_{1e}}(k_y) = {} & \left(\frac{1}{\pi} \right)^{1/2} \left(\frac{1}{\widetilde{L}_h \widetilde{L}_e} \right)^{1/2} \frac{N'_{1e}!\, N_{1h}!}{\sqrt{2^{N_{1e}+N_{1h}} N_{1e}!\, N_{1h}!}} \sum_{k=0}^{[N_{1h}/2]} \sum_{j=0}^{[N'_{1e}/2]} \frac{(-1)^{k+j} 2^{N_{1h}+N'_{1e}-2k-2j}}{k!\, j!\, (N_{1h}-2k)!\, (N'_{1e}-2j)!} \left(\frac{1}{\widetilde{L}_e} \right)^{N'_{1e}-2j} \cdot \\ & \cdot \left(\frac{1}{\widetilde{L}_h} \right)^{N_{1h}-2k} \sum_{\mu=0}^{N_{1h}-2k} \frac{(N_{1h}-2k)!}{\mu!\, (N_{1h}-2k-\mu)!} (x_{0e} - x_{0h})^{N_{1h}-2k-\mu} \sum_{\nu=0}^{N'_{1e}-2j+\mu} \frac{(N'_{1e}-2j+\mu)!}{\nu!\, (N'_{1e}-2j+\mu-\nu)!} \cdot \\ & \cdot \left[(-1)^{\nu} + 1 \right] exp\left(- \frac{(x_{0e} - x_{0h})^2}{2(\widetilde{L}_e^2 + \widetilde{L}_h^2)} \right) \frac{1}{2} \left(\frac{\widetilde{L}_e^2 + \widetilde{L}_h^2}{2\widetilde{L}_e^2 \widetilde{L}_h^2} \right)^{-\frac{\nu+1}{2}} \Gamma\left(\frac{\nu+1}{2} \right) \left(- \frac{\widetilde{L}_e^2 (x_{0e} - x_{0h})}{\widetilde{L}_e^2 + \widetilde{L}_h^2} \right)^{N'_{1e}-2j+\mu-\nu} \end{aligned} \tag{26}$$

and

$$I_{N_{2h},N'_{2e}} = \left(\frac{1}{\pi}\right)^{1/2} \frac{1}{\sqrt{L_e L_h}} \sqrt{\frac{N_{2h}!\, N'_{2e}!}{2^{N_{3e}+N_{3h}}}} \sum_{\alpha=0}^{[N'_{2e}/2]} \sum_{\beta=0}^{[N_{3h}/2]} \frac{(-1)^{\alpha+\beta} 2^{N'_{2e}-2\alpha+N_{3h}-2\beta}}{\alpha!\,\beta!\,(N'_{2e}-2\alpha)!\,(N_{3h}-2\beta)!} \cdot$$

$$\cdot \left(\frac{1}{L_e}\right)^{N'_{2e}-2\alpha} \left(\frac{1}{L_h}\right)^{N_{3h}-2\beta} \left[(-1)^{N'_{2e}+N_{3h}-2\alpha-2\beta}+1\right] \frac{\Gamma\left(\frac{N'_{2e}+N_{3h}-2\alpha-2\beta+1}{2}\right)}{2\left(\frac{\sqrt{L_h^2+L_e^2}}{\sqrt{2}L_h L_e}\right)^{N'_{2e}+N_{3h}-2\alpha-2\beta+1}} \tag{27}$$

X-X scattering

We first consider the case where both the incident and the scattered radiation are polarized parallel to the x axis.

Performing the summation over k_y in (15) we obtain expression for DCS of the ERS process:

$$\frac{d^2S^{xx}}{d\Omega d\nu} = \sigma_0 \frac{\nu_0-\nu}{\nu_0} \sum_{N_{1h},N_{2h},N_{1e},N_{2e}} \left[\sum_{N'_{1e},N'_{2e}} I_{N_{1h},N'_{1e}}\left(k_y(\nu)\right)\cdot I_{N_{2h},N'_{2e}} \cdot \delta_{N'_{2e},N_{2e}} \cdot \left(\sqrt{\frac{N_{1e}}{2}}\cdot\delta_{N'_{1e},N_{1e}-1} -\right.\right.$$

$$\left.\left. - \sqrt{\frac{N_{1e}+1}{2}}\cdot\delta_{N'_{1e},N_{1e}+1}\right)\cdot\left(\frac{1}{A(\nu)}+\frac{1}{B(\nu)}\right)\right]^2 \cdot \frac{1}{\sqrt{\frac{\hbar\nu}{E_g}-\frac{E_{N_{1e}}}{E_g}-\frac{E_{N_{1h}}}{E_g}-\frac{E_{N_{2e}}}{E_g}-\frac{E_{N_{2h}}}{E_g}-1}} \tag{28}$$

where

$$\sigma_0 = \left(\frac{e^2}{m_0c^2}\right)^2 \frac{L_y|\vec{p}_{cv}|^2\hbar^2}{\sqrt{2}\pi\tilde{L}_e^2 m_0^2 E_g^{5/2}\sqrt{\frac{1}{m_e}\left(\frac{\omega_{0e}}{\tilde{\omega}_e}\right)^2+\frac{1}{m_h}\left(\frac{\omega_{0h}}{\tilde{\omega}_h}\right)^2}} \tag{29}$$

$$A(\nu) = \frac{\hbar}{E_g}\left(\nu_0-\nu+(N_{2e}-N'_{2e})\omega_{0e}+(N_{1e}-N'_{1e})\tilde{\omega}_e\right) \tag{30}$$

$$B(\nu) = \frac{\hbar}{E_g}\left((N_{2e}-N'_{2e})\omega_{0e}+(N_{1e}-N'_{1e})\tilde{\omega}_e-\nu_0\right) \tag{31}$$

and $k_y(\nu)$ -is the root of the delta function argument

$$|k_y(\nu)| = \frac{\sqrt{2}}{\hbar}\frac{\left(\hbar\nu-E_g-E_{N_{1e}}-E_{N_{1h}}-E_{N_{2e}}-E_{N_{2h}}\right)^{\frac{1}{2}}}{\sqrt{\frac{1}{m_e}\left(\frac{\omega_{0e}}{\tilde{\omega}_e}\right)^2+\frac{1}{m_h}\left(\frac{\omega_{0h}}{\tilde{\omega}_h}\right)^2}} \tag{32}$$

Z-Z Scattering

We next display the Raman cross section for the case where the incident and scattered light are polarized parallel to z axis:

$$\frac{d^2S^{zz}}{d\Omega d\nu} = \sigma_1 \frac{\nu_0-\nu}{\nu_0} \sum_{N_{1h},N_{2h},N_{1e},N_{2e}} \left[\sum_{N'_{1e},N'_{2e}} I_{N_{1h},N'_{1e}}\left(k_y(\nu)\right)\cdot I_{N_{2h},N'_{2e}} \cdot \delta_{N'_{1e},N_{1e}} \cdot \left(\sqrt{\frac{N_{2e}}{2}}\cdot\delta_{N'_{2e},N_{2e}-1} -\right.\right.$$

$$- \sqrt{\frac{N_{2e}+1}{2}} \cdot \delta_{N'_{2e},N_{2e}+1} \Bigg) \cdot \left(\frac{1}{A(\nu)} + \frac{1}{B(\nu)} \right) \Bigg]^2 \cdot \frac{1}{\sqrt{\frac{\hbar\nu}{E_g} - \frac{E_{N_{1e}}}{E_g} - \frac{E_{N_{1h}}}{E_g} - \frac{E_{N_{2e}}}{E_g} - \frac{E_{N_{2h}}}{E_g} - 1}} \quad (33)$$

where

$$\sigma_1 = \left(\frac{e^2}{m_0 c^2} \right)^2 \frac{L_y |\vec{p}_{cv}|^2 \hbar^2}{\sqrt{2}\pi L_e^2 m_0^2 E_g^{5/2} \sqrt{\frac{1}{m_e}\left(\frac{\omega_{0e}}{\tilde{\omega}_e}\right)^2 + \frac{1}{m_h}\left(\frac{\omega_{0h}}{\tilde{\omega}_h}\right)^2}} \quad (34)$$

Let us make some remarks concerning the above equations. From Eq.(27) it follows that $I_{N_{2h},N'_{2e}}$ vanishes unless $N'_{2e} + N_{2h} = 2n$, where n is an integer. So, transition can only take place between N_{2h} and N'_{2e} subbands with the same parity ($2m \to 2n$; and $2m+1 \to 2n+1$; m and n are integers). But for Eq. (26) quantum numbers N_{1h} and N'_{1e} can change arbitrarily.
Hence, the following selection rules are obtained for interband transitions:

$$\left| N_{1h} - N'_{1e} \right| = 0,1,2,....;$$
$$\left| N_{2h} - N'_{2e} \right| = 0,2,4...$$

As can be seen from Eqs. (28) and (33) the DCS is directly proportional to the density-of –states of carriers in the valence and conduction bands and the interband matrix elements. In this case, the scattering spectrum shows density-of-states peaks and interband matrix elements maximums. The positions of these structures are given as follows:

$$\hbar\nu = E_{N_{1h}} + E_{N_{2h}} + E_{N_{1e}} + E_{N_{2e}} + E_g \quad (35)$$

Here, the following selection rules must be fulfilled: $N'_{1e} = N_{1e} \pm 1$, $N'_{2e} = N_{2e}$ for X-X polarization and $N'_{2e} = N_{2e} \pm 1$, $N'_{1e} = N_{1e}$ for Z-Z polarization. In this case when $\left| N_{1h} - N'_{1e} \right| = 2n+1$ the spectrum shows maximums and when $\left| N_{1h} - N'_{1e} \right| = 2n$ the ERS spectrum shows singular peaks. The peaks and maximums related to these structures correspond to interband EHP transition and their position depends on the magnetic field.

Other singularities of equations (28) and (33) occur whenever $A(\nu) = 0$. In the X-X scattering configuration this singularity is

$$\hbar\nu = \hbar\nu_0 - \hbar\tilde{\omega}_e \quad (36)$$

Here the following selection rules is fulfilled: $N'_{1e} = N_{1e} + 1$, $N'_{2e} = N_{2e}$.

For Z-Z scattering configuration Raman singularity is

$$\hbar\nu = \hbar\nu_0 - \hbar\omega_{0e} \quad (37)$$

In this case the selection rules are $N'_{1e} = N_{1e}$,

$$N'_{2e} = N_{2e} + 1.$$

As can be seen from equations (36) and (37) these frequencies correspond to electron transitions connecting the subband edges for a process involving the conduction band (i.e., intraband transitions).
We can also notice that Y-Y scattering configuration is free from Raman singularity and related to selection rules $N'_{1e} = N_{1e}$, $N'_{2e} = N_{2e}$.

5. Discussion of the results

In the following we present detailed numerical calculations of DCS of GaAs/AlGaAs parabolic quantum wire in the presence of uniform magnetic field as a function $\hbar\nu / E_g$. The physical parameters used in our expressions are: $E_g = 1.5177$ eV, $m_e = 0.0665 m_0$, $m_h = 0.45 m_0$ (the heave-hole band). Taking the ratio 60:40 for the band-edge discontinuity [20, 21], the conduction and valence barrier heights are taken to be $\Delta_e = 255$ meV and $\Delta_h = 170$ meV. The oscillation frequencies ω_{0e} and ω_{0h} of the parabolic quantum wire are determined via

$$\omega_{0e(h)} = \frac{2}{d}\sqrt{\frac{2\Delta_{e(h)}}{m_{e(h)}}}$$

where d -is the quantum wire diameter.
In figure 1 (a)-1(d) we show the Raman spectra of the parabolic quantum wire in the X-X scattering configuration for different magnetic fields, such as $H = 0, 2\cdot10^4, 6.5\cdot10^4, 8.5\cdot10^4$ Gauss. The diameter d of the QWR is 2000 $\overset{o}{A}$. The incident radiation frequency was fixed as $\hbar\nu_0 = 1.82$ eV. The positions of the singularities are defined by (35) and (36).

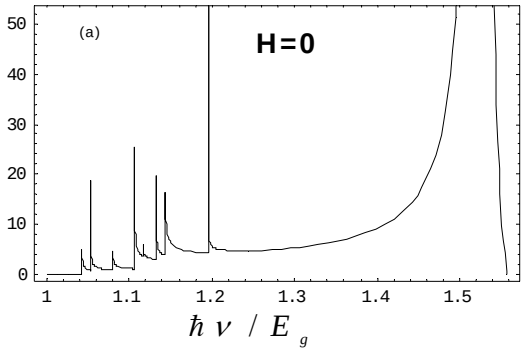

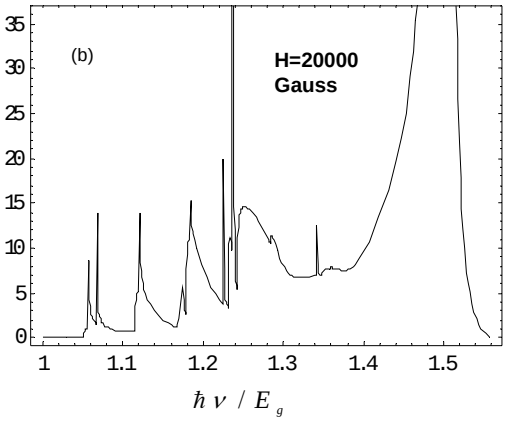

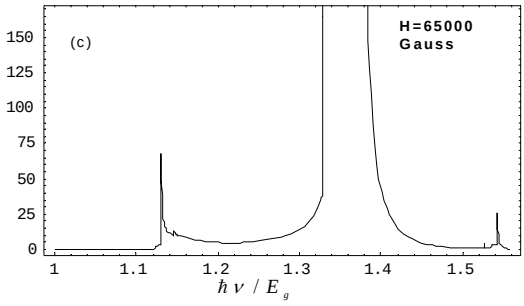

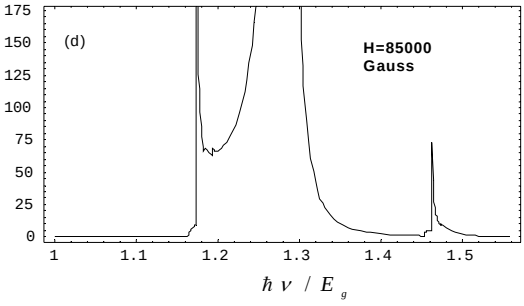

Fig. 1 (a)-(d). Calculated Raman cross section of the PQWR in the X-X scattering configuration with different transverse magnetic field.

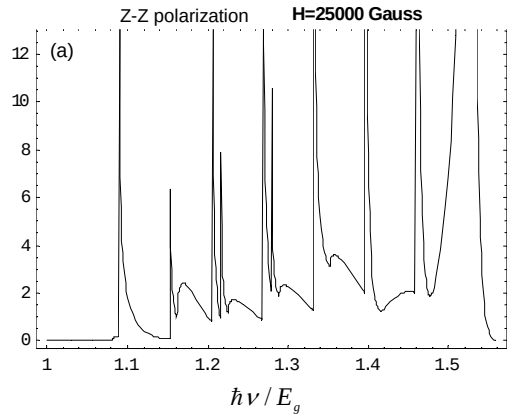

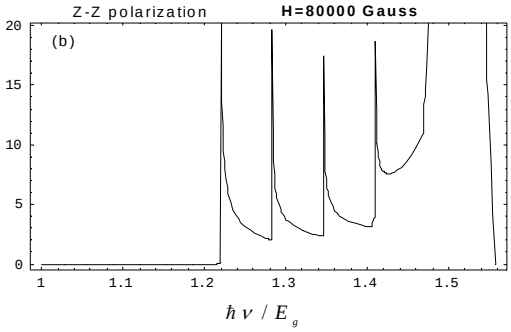

Fig.2 (a)-(b). Calculated Raman cross section of the PQWR in the Z-Z scattering configuration with different transverse magnetic field.

Fig.2(a)-2(b) shows Raman spectra for Z-Z scattering configuration for magnetic fields H=2.5·10^4, 8·10^4, Gauss. The other parameters coincide with those of figure 1.

The structure of the DCS, as given in the figures provides a transparent understanding of the energy subband structure of the parabolic quantum wire in a transverse magnetic field.

In the present work we have applied a simplified model for the electronic structure of the system. In a more realistic case we should consider multiband structure using a calculation model like that of Luttinger-Kohn or the Kane model. The above-mentioned assumptions would lead to better results but entail more complicated calculations. However, within the limit of our simple model we are able to account for the essential physical properties of the discussed problem. The fundamental features of the DCS, as described in our paper, should not change very much in real QWR case. It can be easily proved that the singular peak in the DCS will be present irrespective of the model used for the subband structure and may be determined for the values of $\hbar\nu_1$ equal to the energy difference between two subbands $\hbar\nu_1 = \hbar\nu_0 - \hbar\nu = E^e_\alpha - E^e_\beta$ where $E^e_\alpha > E^e_\beta$ are respective electron energies in the subbands. At present there is a lack of experimental work on this type of ERS. Our major aim in performing these calculations is to stimulate experimental research in this direction.

[1] *Y. Nagamune, Y. Arakawa, S. Tsukamoto, M. Nishioika, S. Sasaki and M. Miura*. Phys. Rev. Lett., 1992, 69 2963.
[2] *A.S. Plaut, H. Lage, P. Grambow, D. Heitmann, von Klitzing K. and K. Ploog. Phys. Rev. Lett.*, 1991, 67 1642.
[3] *T. Demel, D. Heitmann, P. Grambow and K. Ploog*. Phys. Rev. Lett., 1991,66 2657.
[4] *A.R. Goni, A. Pinczuk, J.S. Weiner, B.S. Dennis, L.N. Pfeifer and K.W. West*. Phys. Rev. Lett. 1991, 70 1151.
[5] *K.K. Choi, D.C. Tsui and S.C. Palmateer*. Phys. Rev., 1986, B 33 8216.
[6] *C.J.B. Ford, T.J. Thornton, R. Newbery, M. Pepper, H. Ahmed, G. Davies and D. Andrews*. Superlatt. Microstruct, 1988, 4 451.
[7] *J. Liu , K. Ismail , K.Y. Lee, J.M. Hong and S. Washburn*. Phys. Rev., 1993, B 47 13039.
[8] *J.A. Brum, G. Bastard, L.L. Chang and L. Esaki.* Superlatt. Microstruct, 1997 3 47.
[9] *G. Bastard, J.A. Brum and R. Ferreira*. Solid State Phys., 1991, 44 395.
[10] *A. Lorenzoni and L.C. Andreani*. Semicond. Sci. Technol., 1999, 14 1169.
[11] *M. Cardona and G. Güntherodt*. 1989 Light Scattering in Solids V (Topics in Applied Physics 66) (Heidelberg: Springer).
[12] *M. Cardona*. Superlatt. Microstruct, 1990, 7 183.
[13] *A. Pinczuk and E. Burstein.* 1983 Light Scattering in Solids I (Springer Topics in Applied Physics 8) ed. M. Cardona (Heidelberg: Springer).
[14] *R.F. Wallis and D.L. Mills*. Phys. Rev. B, 1970, 2 3312.
[15] *F. Comas, C. Trallero-Giner., I.G. Lang. and S.T. Pavlov.* 1985 Fiz. Tverd. Tela 27 57 (Engl.Transl. Sov. Phys. Solid State 27 32).
[16] *F. Bechstedt, R. Enderlein and K. Peuker*. Phys. Status Solidi (b), 1975, 68 43
[17] *R. Riera, F. Comas, C. Trallero-Giner and S.T. Pavlov*. Phys. Status Solidi (b), 1988, 148 533.
[18] *R. Betancourt-Riera, J.M. Bergues, R. Riera, J.L. Marin*. Physica, 2000, E 5 204.
[19] *J.H. Burnett, H.M. Cheong, R.M. Westervelt, W. Paul, P.F. Hopkins, M. Sundaram, and A.C. Cossard.* Phys. Rev. B, 1993, 47 4524.
[20] *R.C. Miller, D.A. Kleinman, and A.C. Gossard.* Phys. Rev B, 1984, 29 7085.
[21] *J. Batey, S.L. Wright, and D.J. Di Maria*. J. Appl. Phys. 1985.57 484.

T.H. İsmayılov, B.H. Mehdiyev

MAQNİT SAHƏSİNDƏ YERLƏŞMİŞ KVANT MƏFTİLİNDƏ RAMAN SƏPİLMƏSİ

Eninə magnit sahəsində yerləşmiş parabolic kvant məftilində fononun iştirakı olmadan işığın Raman səpilməsi tədqiq edilmişdir. Elektron Raman səpilməsinin effektiv en kəsiyinin tezliyin sürüşməsindən və maqnit sahəsindən asılılığı hesablanmışdır. Kvantlanmış alt səviyyələr arasında zonalararası və zonadaxili keçidlərin iştirakı ilə baş verən proseslərə baxılmışdır. Düshən və səpilən işığin polyarizasiyasından asılı olaraq secmə qaydaları məsələnin müxtəlif parametrlərinin (siklotron tezlikləri və saxlayicı potencilın tezliyi) qiymətlərində tədqiq edilmişdir. Electron Raman səpilməsinin differensial effectiv en kəsiyi hal sıxlığı ilə bağlı məxsusiyyətlərə və keçidlərin matris elementləri ilə bağlı əlavə strukturlara malikdir.

Т.Г. Исмаилов, Б.Г. Мехтиев

ЭЛЕКТРОННОЕ КОМБИНАЦИОННОЕ РАССЕЯНИЕ СВЕТА В КВАНТОВОЙ ПРОВОЛОКЕ В МАГНИТНОМ ПОЛЕ

Исследовано электронное комбинационное рассеяние света (ЭКРС), без участия фононов, в параболической квантовой проволоке ,в поперечном магнитном поле . Рассчитаны зависимости сечения ЭКРС от сдвига частоты и магнитного поля. Рассмотрены процессы с участием как межзонных, так и внутризонных преходов между квантованными подзонами. Изучены правила отбора и проведен анализ дифференциального сечения рассеяния для различных поляризаций падающего и рассеянного излучений и для различных соотношений между параметрами задачи (циклотронными частотами и частотами удерживающего потенциала электронов и дырок). Сечение ЭКРС содержит сингулярности обязанные плотности состояний и дополнительные структуры ,связанные с матричными элементами переходов.

Received: 22.06.04.

INFLUENCE OF THE SURFACE STATE TO THE THRESHOLD AND TIME PROPERTIES OF THE FERROELECTRIC LIQUID CRYSTAL

H.F. ABBASOV
Baku State University,
Baku, Az-1148, Z. Khalilov str. 23

In this work the influence of the polar and dispersive parts of the anchoring energy of the liquid crystal molecules with surfaces on the threshold voltage and the switching time of the "up-down" and "twist-down" transitions were studied by computer modeling of the ferroelectric liquid crystal electrooptic properties.

The electrooptic properties of the surface stabilized ferroelectric liquid crystal (SSFLC) depend both on the material parameters and external parameters [1-3]. The electrooptic switching with high speed and low threshold voltage occurs in this materials and widely use in the display technique.

The threshold and time characteristics of this effect strongly depend on the surface state treatment.

In the given work the influence of the polar and dispersive parts of the anchoring energy on the threshold voltage and the switching time of the electrooptic effects were studied by computer modelling of the ferroelectric liquid crystal electrooptic properties.

The considered geometry of the electrooptic cell is shown in fig.1. The director of the SSFLC, the applied electric field and the spontaneous polarization has the following component, consequently:

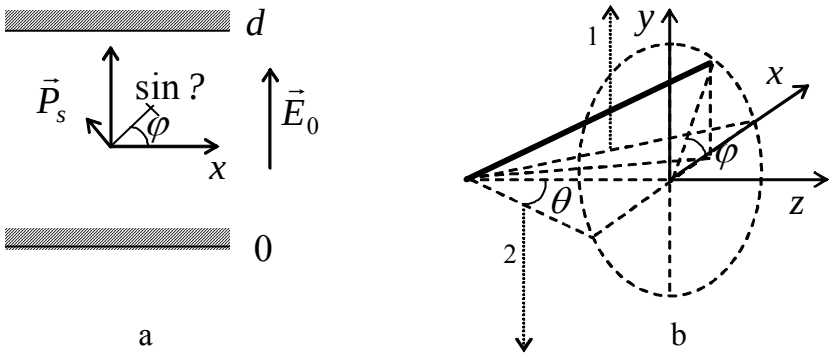

Fig.1 The cell geometry

$$\vec{n}(\sin\theta\cos\phi, \sin\theta\sin\phi, \cos\theta),\ \vec{E}(0, E_0, 0),\ P_s(P_s\sin\phi, P_s\cos\phi, 0) \quad (1)$$

were θ and Φ are tilt angle and azimuthally angle, respectively.

For considered geometry the free energy per unit area of the cell has the form:

$$F = \frac{1}{2}\int_0^d B\theta^2\left(\frac{d\phi}{dy}\right)^2 dy - \frac{1}{2}\int_0^d \varepsilon_0\Delta\varepsilon(\vec{n}\vec{E})^2 dy - \frac{1}{2}\int_0^d \vec{P}_0\vec{E}dy \mp$$

$$\mp W_1^{0,d}\cos\phi_s - W_2^{0,d}\cos^2\phi_s \quad (2)$$

where the first term is the elastic energy density (B is corresponding elastic constant), the second term relates to the electric field interaction with the dielectric anisotropy of the medium ($\Delta\varepsilon = \varepsilon_{||} - \varepsilon_{\perp}$ is the anisotropy of the dielectric permittivity, ε_0 is the electric constant) and the third term describes the electric field interaction with the spontaneous polarization. The term $W_1^{0,d}\cos\phi_s$ describes the polar interaction of FLC molecules with the surface: this term takes the minimum on the lower surface if $\phi_s = 0$ and on the upper surface if $\phi_s = \pi$. The term $W_2^{0,d}\cos^2\phi_s$ describes the dispersive interaction with the surface and takes the minimum if on the both surfaces $\phi_s = 0$ or $\phi_s = \pi$.

The minimization of the free energy density (2) gives us the dynamic Euler-Lagrange equation:

$$\theta^2\gamma\,\frac{d\phi}{dt} = B\theta^2\,\frac{d^2\phi}{dy^2} + \frac{\varepsilon_0\Delta\varepsilon\theta^2E^2}{2}\sin 2\phi - P_sE_\theta\sin\phi \qquad (3)$$

with the boundary conditions:

$$B\theta^2\left.\frac{d\phi}{dy}\right|_{0,d} = W_1^{0,d}\sin\phi_s \mp W_2^{0,d}\sin 2\phi_s \qquad (4)$$

where γ - is the rotational viscosity.

For numerical solving this problem has been used MathCad-2001 program [4] and the Johns retardation matrix method was applied for determining of the light transmittance of the FLC cell [5].

It was analyzed the dependences of the threshold voltages and the switching times of $Up(\varphi_0 = \varphi_d = \pi) - Down(\varphi_0 = \varphi_d = 0)$ and $Twist(\varphi_0 = 0,\ \varphi_d = \pi) - Down(\varphi_0 = \varphi_d = 0)$ transitions on the polar (at $y = 0 \quad W_1^0 = W_{11}$, $y = d \quad W_1^d = W_{12}$) and the dispersive parts (at $y = 0 \quad W_2^0 = W_{21}$, $y = d \quad W_2^d = W_{22}$) of the anchoring energy. The threshold voltage was determined from the voltage dependence of the cell transmittance.

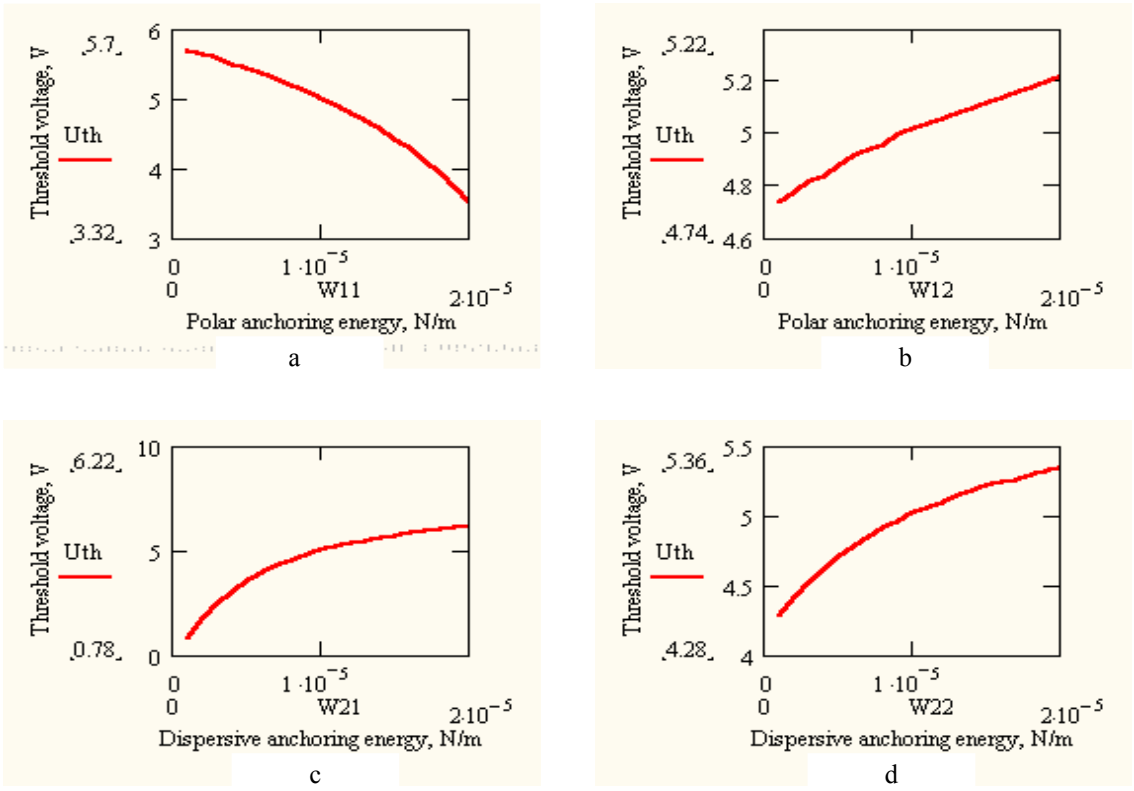

Fig.2. Dependences of the threshold voltage on the anchoring energy at lower (a, c) and upper surfaces (b, d) for the "up-down" transition.

The threshold voltage and the corresponding switching time of the "up-down" transition decrease by increasing of the polar part of the anchoring energy at the lower surface W_{11} (fig.2a, 3a) that was expected, because the rise of the polar anchoring with lower surface stimulates the "up-down" transition.

By increasing of the polar anchoring with upper surface the threshold voltage (fig.2b) and the corresponding switching time (fig.3b) of the "up-down" transition increase, because with the increasing of the polar anchoring at the upper surface the initial "up" state becomes more stable and the occurring "up-down" transition becomes more difficult.

The rising of the dispersive part of the anchoring energy both at upper and lower surfaces leads to the increasing of U_{th} and τ_{sw} (fig. 2c, 2d, 3c, 3d).

The dispersive interaction with surface is same for both surfaces and the increasing one of these leads to the rising another.

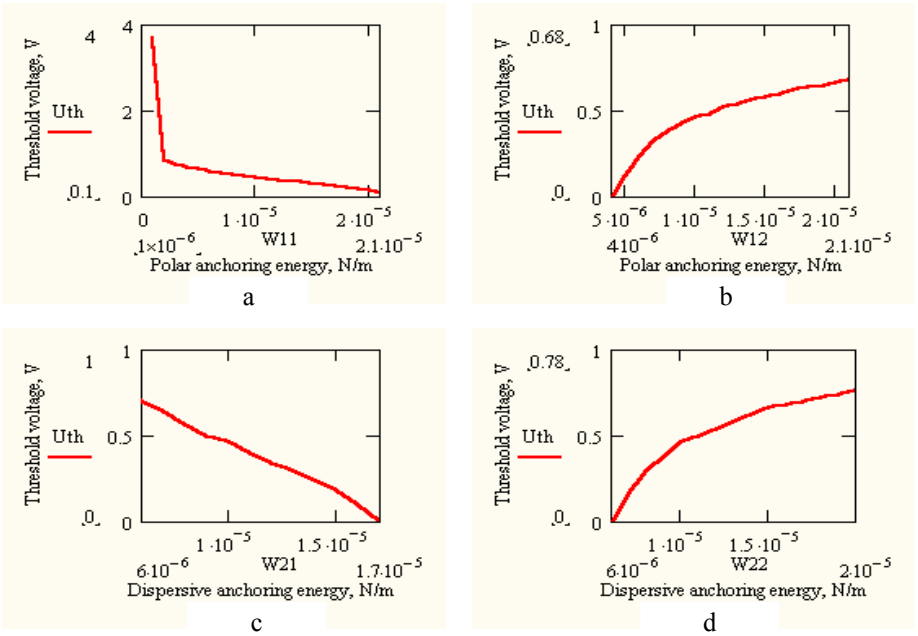

Fig.3 Dependences of the switching time on the anchoring energy at lower (a, c) and upper surfaces (b, d) for the "up-down" transition.

Some of the electro optic characteristics of the "twist-down" transition are analogously to the "up-down" transition. U_{th} decrease by increasing of the polar anchoring at the lower surface (fig.4a) and U_{th} increase too by increasing of the polar anchoring at the upper surface (fig.4b).

Note, that the rising of the dispersive anchoring at the lower surface stimulates the "twist-down" transition (fig.4c) and the increasing of the dispersive anchoring at upper surface, in contrary, resist to occurring this transition (fig.4d).

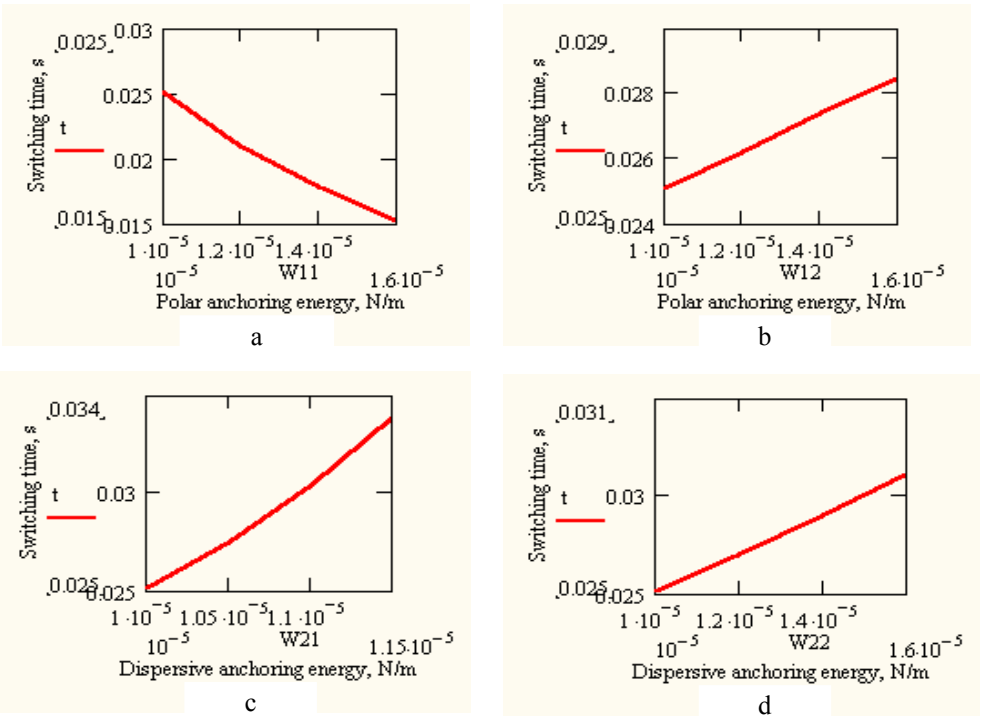

Fig.4. Dependences of the threshold voltage on the anchoring energy at lower (a, c) and upper surfaces (b, d) for the "twist-down" transition.

Therefore, for switching time and threshold voltage decreasing it is necessary to increase the polar interaction at lower surface in the "up-down" transition case and it is necessary to rise the polar and dispersive anchoring at lower surface and to decrease them at upper surface in the "twist-down" transition case.

[1] *N.A.Clark and S.T.Lagerwall.* "Appl.Phys.L", v.36 (1980), 899.
[2] *N.A.Clark, M.A.Handshy, S.T.Lagerwall.* "Mol.Cryst.Liq.Cryst", 1983, v.93, p.213
[3] *Y.Ouchi, H,Takezoe, A.Fukuda.* "Jap.P.Appl", 1987, v.26, N1, p.1
[4] *H.F.Abbasov, A.R.Imamaliev.* "Fizika", ANAS, 2003, v.9, N1, p.6
[5] *Yariv P.Yeh,* "Optical waves in crystals", 1993, 616p.

H. F. Abbasov

SEQNETOELEKTRİK MAYE KRİSTALIN ASTANA VƏ ZAMAN XASSƏLƏRİNƏ SƏTH ŞƏRAİTİNİN TƏSİRİ

Bu işdə seqnetoelektrik maye kristalın elektrooptik xassələrinin kompüter modelləşdirilməsi yolu ilə maye kristal molekullarının səthlə ilişmə enercisinin polyar və dispersiv hissələrinin «up-down» və «twist- down» keçidlərinin astana gərginliyinə və keçid müddətinə təsiri öyrənilmişdir.

Х.Ф. Аббасов

ВЛИЯНИЕ СОСТОЯНИЯ ПОВЕРХНОСТИ НА ПОРОГОВЫЕ И ВРЕМЕННЫЕ ХАРАКТЕРИСТИКИ СЕГНЕТОЭЛЕКТРИЧЕСКОГО ЖИДКОГО КРИСТАЛЛА

В данной работе было изучено влияние полярной и дисперсионной частей энергии сцепления молекул с поверхностью на пороговые напряжения и времени включения переходов «up-down» и «twist-down» компьютерным моделированием электрооптических свойств сегнетоэлектрического жидкого кристалла.

Received: 02.07.04

YÜKDAŞIYICI-FONON QARŞILIQLI SÖVQÜNÜN REKOMBİNASİYA PROSESLƏRİNƏ TƏSİRİ

Z.Ə. VƏLİYEV, N.A. QARDAŞBƏYOVA, X.Ə. HƏSƏNOV
Naxçıvan Dövlət Universiteti

İşdə, zəif və güclü elektrik sahəsində, n-tipli yarımkeçiricilərdə kənar dislokasiyalar tərəfindən qeyri-əsas yükdaşıyıcıların, yəni deşiklərin tutulması hadisəsi tədqiq olunur. Elektrik sahəsinin zəif və güclü olduğunu təyin edən $A=\varepsilon/\varepsilon_{xar}$ parametrinin qiymətindən asılı olaraq, tutulmanın effektiv kəsiyi hesablanmışdır.

Uyğun hesablamaların köməyi ilə alınan nəticələrin tətbiq olunma hüdudlarını təyin edən xarakteristik sahənin intensivliyi qiymətləndirilir.

Məlum olduğu kimi [1] güclü elektrik sahələrində yükdaşıyıcılar və akustik fononların qarşılıqlı təsiri nəticəsində onların qızması və qarşılıqlı sövqü baş verir. Bu zaman yükdaşıyıcı və akustik fonon arasındakı qarşılıqlı təsir prosesi və onu xarakterizə edən yükdaşıyıcıların impulsunun relaksasiya tezliyi həm yükdaşıyıcıların, həm də fononların dreyf sürətindən asılı olur.

$$\nu_p(\varepsilon) = \frac{W_0 kT\sqrt{2m}}{\pi^2\hbar^3 s}\,\varepsilon^{1/2}\left(1-\frac{u}{V}\,\delta\right) = \nu_{\vec{p}}^{(0)}\left(1-\frac{u}{V}\right)\delta, \qquad (1)$$

burada u - fononların, V - yükdaşıyıcıların dreyf sürətləri, s - səsin kristaldakı sürəti,

$$\delta = 3s^2/u^2(\varphi-1);\quad \varphi = \frac{s}{2u}\ln\frac{1+u/s}{1-u/s} = \frac{s}{u}\,\mathrm{arth}\,\frac{u}{s};$$

$$V = \frac{V_0}{\delta} + u;\quad \vec{V}_0 = \frac{e\vec{\varepsilon}}{m\nu_{\vec{p}}^{(0)}(\varepsilon)};\quad W_0 = 2\pi E_c^2/\hbar^2\,\rho s \qquad . \qquad (2)$$

$\nu_{\vec{p}}^{0}(\varepsilon)$ – yükdaşıyıcı və fononların qızması və qarşılıqlı sövqü olmadıqda relaksasiya tezliyi, E_c - deformasiya potensialı sabiti, $\vec{\varepsilon}$ xarici elektrik sahəsinin intensivliyi, m - yükdaşıyıcının kütləsi, T - termodinamik temperatur, k - Bolsman sabitidir. (1) və (2) ifadələrindən göründüyü kimi $u \to V \to s$ şərti ödənildikdə δ və φ kəmiyyətləri kəskin şəkildə artır, $\left(1-\frac{u}{V}\right)\to 0$ olduğundan $\nu_{\vec{p}}^{0}(\varepsilon)\to 0$ olur. Bu zaman qarşılıqlı təsirdə olan yükdaşıyıcı və akustik fononlar bağlı sistem əmələ gətirir və onlar bütöv sistem kimi hərəkət edirlər. Belə hərəkət prosesində yükdaşıyıcıların impuls və enerjiyə görə relaksasiyası aşqarsız kristallarda əsasən qəfəsin sıfırıncı rəqslərindən baş verir.

Biz n - tip yarımkeçiricilərdə yüklü qıraq dislokasiyalar tərəfindən qeyri əsas yükdaşıyıcıların tutulması məsələsini tədqiq etdiyimizdən yükdaşıyıcı dedikdə deşikləri nəzərdə tuturuq. Onların baxılan halda paylanma funksiyası

$$f_0(\varepsilon) = c\exp\left[-\frac{2u}{V(T)}\left(\frac{1}{2}\frac{\varepsilon}{kT}\right)^2 - \frac{V_0(T)u}{9s^2}\left(\frac{\varepsilon}{kT}\right)^{3/2} + \frac{V_0^2u^2}{18s^2}\frac{\varepsilon}{kT} - \right.$$
$$\left. - \left(\frac{V_0(T)u}{3s^2}\right)^3\left(\frac{\varepsilon}{kT}\right)^{1/2} + \left(\frac{V_0(T)u}{3s^2}\right)^4 \ln\left|\frac{V_0(T)}{3s^2} + \left(\frac{\varepsilon}{kT}\right)^{1/2}\right|\right] \qquad (3)$$

şəklində olur. Burada c- normallaşdırıcı vuruqdur.

$$V(T) = V(\varepsilon)\big|_{\varepsilon=kT};$$
$$V_0(T) = V_0(\varepsilon)\big|_{\varepsilon=kT}.$$

Tədqiqatların zəif və güclü elektrik sahələrində aparılması nəzərdə tutulur. Bu limit halları bir-birindən

$$A = \frac{e\varepsilon u}{3s^2 m\gamma_{ps}(T)}\left(\frac{kT}{ms^2}\right)^{1/2} = \frac{\varepsilon}{\varepsilon_{xar}}$$

parametrinin qiyməti ilə seçilirlər. $A<<1$ qiymətləri zəif elektrik sahələri, $A>>1$ qiymətləri isə güclü elektrik sahələri limit halına uyğun gəlir. (Burada $\nu_{ps}(T)$ - deşiklərin impulsunun qəfəsin sıfırıncı rəqslərindən səpilməsinin relaksasiya tezliyinin $\varepsilon=kT$ - dəki qiymətidir).

$$\nu_{ps}(\varepsilon) = \nu_{ps}^{T}\frac{\varepsilon}{kT}; \qquad \nu_{ps}(T) = \frac{64\pi m^2 kTW_0}{5}$$

zəif sahələr limit halında $A<<1$ olduqda

$$f_0(\varepsilon) = c\exp\left[-\frac{u}{2V(T)}\left(\frac{\varepsilon}{kT}\right)\right] = c_1\exp\left[-\frac{\varepsilon_{xar.1}}{\varepsilon}\left(\frac{\varepsilon}{kT}\right)^2\right]$$

$$\varepsilon_{xar.1} = um\nu_{ps}(T)/2e, \qquad c_1 = \frac{4\pi^2\hbar^3 p}{(2mkT)^{3/2}\Gamma(3/4)}\left(\frac{\varepsilon_{xar.1}}{\varepsilon}\right)^{3/4},$$

burada $\Gamma(\alpha)$ -Eylerin qamma funksiyasıdır.

Güclü elektrik sahələri limit halında

$$f_0(\varepsilon) = c_2\exp\left[-\frac{6s}{2V_0(T)V(T)}\left(\frac{\varepsilon}{kT}\right)^{5/2}\right] = c_2\exp\left[-\left(\frac{\varepsilon_{xar.2}}{\varepsilon}\right)^2\left(\frac{\varepsilon}{kT}\right)^{5/2}\right]$$

$$\varepsilon_{xar.2} = \frac{sm}{e}\sqrt{\frac{6}{5}}\gamma_{ps}(T);$$

$$c_2 = \frac{5\pi^2\hbar^3 p}{(2\pi kT_h)^{3/2}\Gamma(2/5)}.$$

Sonuncu limit halında deşik sisteminin orta kinetik enerjisi kristal qəfəsin T temperaturu ilə deyil,

$$T_h = T\left(\frac{\varepsilon}{\varepsilon_{xar.2}}\right)^{4/5}$$

ifadəsi ilə təyin edilir.

Deşiklərin yüklü qıraq dislokasiyalar tərəfindən tutulmasının effektiv kəsiyi [2-3] işlərində təklif olunan hesablama üsulu əsasında həyata keçirilmişdir. Hesablamaların detallarına varmadan tutulmanın effektiv kəsiyi üçün aşağıdakı ifadələri yaza bilərik:

$$\sigma = \frac{mE_c^2}{2\pi\hbar^4\rho_0}\begin{cases}\dfrac{\pi}{\Gamma(3/4)}\left(\dfrac{\varepsilon_{xar.1}}{\varepsilon}\right)\displaystyle\int d^3\vec{r}\left(\sqrt{\frac{2|u|}{ms^2}}-1\right)^3, & A<<1\\ \dfrac{ms^2}{12kT}\left(\dfrac{\varepsilon_{xar.2}}{\varepsilon}\right)^{2/5}\dfrac{\Gamma(2/5)}{\Gamma(2/5)}\displaystyle\int d^3\vec{r}\left(\sqrt{\frac{2|u|}{ms^2}}-1\right)^3, & A>>1\end{cases}$$

Bir faktı qeyd edək ki, zəif və güclü elektrik sahələri limit halında $\int d^3\vec{r}\left(\sqrt{\frac{2|u|}{ms^2}}-1\right)^3$ inteqralında inteqrallama sərhədləri müxtəlif fiziki şərtlərlə bağlı olduğu üçün onların mötərizədən kənara vuruq şəklində çıxarılması məqsədə uyğun hesab edilməmişdir. Beləliklə, [2-3]-ə uyğun hesablamalar aparmaqla deşiklərin qıraq dislokasiyalar tərəfindən tutulmasının effektiv kəsiyi üçün aşağıdakı münasibətləri alarıq:

$$\sigma = \frac{\sqrt{\pi} m^3 E_c^2}{4\hbar^4 \rho} \begin{cases} \frac{3\sqrt{\pi}}{\Gamma(3/4)} \left(\frac{\varepsilon_{xar.1}}{\varepsilon}\right)^{1/2} R^3 \sqrt{\frac{2|u|}{ms^2}} \left(1 - 2\gamma_0^{1/2} + 2\pi\gamma_0 - \frac{4}{3}\gamma_0^{3/2}\right), A << 1 \\ \frac{\Gamma(2/5)}{\Gamma(3/5)} \left(\frac{\varepsilon_{xar.2}}{\varepsilon}\right)^{2/5} R_0^2 \left(1 + \sqrt{\frac{3}{2}} \frac{R_0}{R}\right)^3, A >> 1 \end{cases}$$

Burada $\gamma_0 = ms/\pi u_0$, $u_0 = ef^2/4\pi\varepsilon\varepsilon_0 a$ işarə edilmişdir. (f - dislokasiyanın elektronlarla dolma əmsalı, a_0 - dislokasiyanın oxu boyunca kristal qəfəsin periodu, ε_0 - elektrik sabiti, ε - dielektrik nüfuzluğudur).

Alınan nəticələrin tətbiqolunma hüdudlarını müəyyənləşdirmək üçün A kəmiyyətinə daxil olan ε_{xar} sahəni qiymətləndirək. Parametrlərin

$$a = 5 \cdot 10^{-10} m,\ \varepsilon \sim 10,\ s \sim 3 \cdot 10^3 \frac{m}{san},\ m \sim 0{,}3 \cdot 10^{-31} kq,\ T \sim 300k,\ E_c \sim 10^{-18} c$$

qiymətlərində $\varepsilon_{xar} \sim 10^3 \frac{V}{m}$ olur; yəni $\varepsilon_{xar} < 10^3 \frac{V}{m}$ - zəif sahələr, $\varepsilon_{xar} > 10^3 \frac{V}{m}$ isə güclü sahələr limit halı reallaşacaqdır.

[1] *Z.A. Veliev, A.S. Axmedov.* Qalvanomaqnitnie effekti v poluprovodnikax s nizkoy konsentrasiyey elektronov. Materiali respublikanskoy konferenüii, Naxiçevan, 1987, s. 73-74.

[2] *V.N. Abakumov, N.N. Yassievis, V.İ. Perel.* FTP, 1978, t. 12, vip. 1, s. 3-32.

[3] *Z.A. Veliev, N.A. Kardaşbekova.* İzv. BQU, Fiz.-mat. seriya, Baku, 2000, № 4. S. 63-64.

З.А. Велиев, Н.А. Кардашбекова, Х.А. Гасанов

ВЛИЯНИЕ ВЗАИМНОГО УВЛЕЧЕНИЯ СИСТЕМЫ НОСИТЕЛЬ-ФОНОН НА РЕКОМБИНАЦИОННЫЕ ПРОЦЕССЫ

В работе исследована задача о захвате неосновных носителей заряда, т.е. дырок, в слабом и сильном электрических полях в n - типа полупроводниках, со стороны краевых дислокаций. В зависимости от значения параметра $A = \varepsilon / \varepsilon_{xar}$, который характеризует слабое или сильное электрическое поле, вычислено эффективное сечение захвата.

С помощью соответствующих вычислений оценена величина характеристического поля, которая определяет предел применимости полученных результатов.

Z.A. Veliev, N.A. Kardashbayova, Kh.A. Hasanov

THE INFLUENCE OF THE CHARGE CARRIER-PHONON MUTUAL DRAG ON THE RECOMBINATION PROCESSES

The question of the capture of the non-basic charge carriers, i.e. the holes by the edge dislocations in n-type semiconductors in the weak and strong electric fields is investigated. The effective cross section of the capture is calculated depending on the ratio $A = \varepsilon / \varepsilon_{char}$, characterizing the weakness or strongness of the electric field. The characteristic field determining the boundaries of application of the obtained results is estimated by means of corresponding calculations.

Received: 16.06.04

XARİCİ ELEKTRİK-KVANTLAYICI MAQNİT VƏ ELEKTROMAQNİT SAHƏLƏRİNDƏ REKOMBİNASİYA PROSESLƏRİ

Z.Ə. VƏLİYEV, X.Ə. HƏSƏNOV
Naxçıvan Dövlət Universiteti

İşdə cütləşmiş elektrik və kvantlayıcı maqnit sahələrində, həmçinin maqnit sahəsinə perpendikulyar müstəvidə yerləşən dəyişən elektrik sahəsində kənar dislokasiyalarla yüklənmiş n-tip yarımkeçiricilərdə deşiklərin tutulması məsələsi tədqiq olunmuşdur. Deşiklərin yaşama müddəti üçün alınan analitik ifadədən görünür ki, bu kəmiyyət kristal və temperaturun parametrlərindən asılı olduğu kimi, həm də xarici sahələri xarakterizə edən kəmiyyətlərdən asılıdır.

Kinetik əmsalların müxtəlif kombinasiyalı xarici sahələrdə ölçülməsi üsulları təkmilləşdikcə bu sahələrdə həmin kəmiyyətlərin nəzəri tədqiqi də genişlənir. Qarşılıqlı perpendikulyar statik elektrik və kvantlayıcı maqnit sahələrinə ($\vec{E} \perp \vec{H}$ və $\vec{E} \perp OX$, $\vec{H} \perp OZ$ - istiqamətlənməsi halında) maqnit sahəsində perpendikulyar müstəvi üzərində yerləşən $\vec{\varepsilon} = \vec{\varepsilon}_0 \cos \omega t$ xarici dəyişən elektrik sahəsini də əlavə etdikdə ($\vec{\varepsilon}$ vektoru xy müstəvisi üzərindədir) alınan sahələr sistemində hissəcik stasionar hallara malik olur.

$$i\hbar \frac{\partial \Psi}{\partial t} = \sum_i \left[\frac{1}{2\mu_i} \left(-i\hbar \frac{\partial}{\partial x_i} - \frac{e}{c} A_i \right)^2 - eE_i x_i \right] \Psi \qquad (1)$$

$$x_1 = x;\ x_2 = y;\ x_3 = z;$$

$$A = (A_1; A_2; A_3) = \left(-\frac{c}{\omega} \varepsilon_{ox} \sin \omega t;\ -\frac{c}{\omega} \varepsilon_{oy} \sin \omega t - Hx;\ 0 \right)$$

Dalğa tənliyinin həllindən alınan stasionar hallar

$$\varepsilon_{Nk_y k_z} = \left(N + \frac{1}{2} \right) \hbar\omega_H + \frac{\hbar^2 k_z^2}{2\mu_z} + eEa^2 k_y - \frac{(e\varepsilon)^2}{4\left(\omega_H^2 - \omega^2\right)} \left(\frac{\varepsilon_{ox}^2}{\mu_x} + \frac{\varepsilon_{oy}^2}{\mu_y} \right) \qquad (2)$$

ifadəsi ilə təyin edilir. Bu ifadədə $\omega_H = eH \Big/ \sqrt{\mu_x \mu_y}\, c$ - anizotropiya nəzərə alınmaqla tsiklotron tezliyi, $a = \left(c\hbar / eH\right)^{1/2}$ - maqnit uzunluğudur. μ_i -lər uyğun istiqamətdə hissəciyin effektiv kütləsi, c - işığın boşluqdakı sürəti, ε_{ox} və ε_{oy} - xarici dəyişən elektrik sahəsinin x və y oxları istiqamətində amplitud qiymətləridir.

Elektron keçiriciliyinə malik silisium n-Si kristalda yüklü kənar statik dislokasiyalar olduqda $\vec{E} \perp \vec{H}_{kv}$ istiqamətlənməsində rekombinasiya dalğalarının yayılması tədqiq edilmiş və təcrübi nəticələr [1,2] işlərində nəzəri təhlildən keçirilərək təcrübi faktlarla uzlaşan nəzəri nəticələr alınmışdır.

Alınan bu nəticələr sahələrin yuxarıda göstərilən daha praktik konfiqurasiyasında n-Si kristalında qeyri əsas yükdaşıyıcıların - deşiklərin qıraq disloksiyalar tərəfindən tutulması məsələsinin tədqiqinin zəruriliyini ortaya qoyur.

Sərbəst deşiklər stasionar kvant hallarına malik olduğundan onların yüklü qıraq dislokasiyalar tərəfindən tutulması, pilləvari tutulma mexanizmi vasitəsi ilə həyata keçir. Bu halda deşiklərin kristal qəfəsə enerji vermə mexanizmi akustik fononlarla qarşılıqlı təsir hesabına olur. Kvantlayıcı statik maqnit sahəsi Z oxu istiqamətində (dislokasiyanın oxu boyunca) yönəldiyindən xy müstəvisində deşiklərin hərəkəti kvatlanmış olur. $\hbar\omega_H > kT$ şərti ödənildiyi üçün deşiklərin kinetik enerjisi $\varepsilon \sim \hbar\omega_H / 2$ tərtibindədir. Ona görə də qıraq dislokasiyanın potensial sahəsində şüalandırılan fononların xarakterik enerjisi $\hbar\omega(q_H) \approx \left(2\varepsilon\mu s^2\right)^{1/2} = \left(\hbar\omega_H \mu s^2\right)^{1/2}$ tərtibində olur. Burada s - səsin kristalda yayılma sürəti, μ deşiyin effektiv kütləsidir). Bu enerji $H=0$ olduqda şüalanan fotonun $kT \cdot ms^2$ xarakterik enerjisindən çox olur. Məsələnin həlli zamanı deşiklərin akustik fononlardan səpilməsinə baxılır və bu vaxt $\varepsilon_{ox} KT >> \left(\hbar\omega_H \cdot \mu s^2\right)^{1/2}$ limit halının reallaşdığı fərz olunur.

Bu limit halında deşiklərin enejilərini kiçik paylarla itirəcək və onların tutulma prosesi tam enerjisinin müsbət qiymətlər oblastından mənfi qiymətlər oblastına kvazidiskret enerji səviyyələri ilə kəsilməz enişlə keçidi baş verəcəkdir. Deşiklər praktik olaraq tam enerjiləri $W \le -kT$ olduqda tutulmuş hesab olunurlar və onların geri qayıtma ehtimalı enerjinin bu qiymətlərində sıfra yaxındır.

Dislokasiyaların konsentrasiyası elə götürülür ki, onların R radiuslu silindrləri bir-biri ilə kəsişmirlər ($2R >> N_D^{-1}$, R dislokasiyanın radiusu, N_D -onların konsentrasiyasıdır), yəni hər bir dislokasiya mərkəzi təcridedilmiş şəkildə təsir göstərir. Onda vahid həcmdə olan tam rekombinasiya seli $J = P/\tau_h$, aşağıdakı kimi ifadə edilə bilər:

$$J = N_D \cdot j \tag{3}$$

(3) ifadəsindən deşiklərin disloksiyanın potensial sahəsində sərbəst yaşama müddəti üçün

$$\tau_h = \frac{P}{N_D \cdot j} \tag{4}$$

alarıq.

Rekombinasiya seli j [3-5] işlərinə uyğun şəkildə aparılır. [3-5]-də təklif olunan üsuldan istifadə edərək deşiklərin yaşama müddəti üçün

$$\tau_h^{-1} = kTf(0)\frac{N_D}{p}\int_{-W}^{0}\frac{exp(W/kT)}{B(W)}dW \tag{5}$$

ifadəsini alarıq. Burada $f(W)$ deşiklərin Bolsman paylanma funksiyasıdır.

$$f(W) = Ap\,exp(W/kT_h) \tag{6}$$

Bu ifadədəki A və T_h kəmiyyətləri aşağıdakı kimi təyin edilirlər:

$$A = \left(\frac{2\pi}{\mu}\right)^{3/2}\frac{\hbar^2}{\omega_H\sqrt{T_h}};\quad T_h = T\left(1+\frac{1}{2}\beta^2\right);\quad \beta = \frac{c}{s}\frac{\varepsilon^*}{H} \tag{7}$$

Enerji fəzasında $B(W)$ diffuziya əmsalı [3-5] işlərinə uyğun şəkildə hesablanmışdır:

$$B(W) = \frac{m^2E_c^2(\hbar\omega_H)^3}{2\rho_0\pi^2\hbar^7esa\varepsilon^*}R(W)\left\{exp\left(-2\frac{\hbar\omega^*(q_H)}{U_0}\right)ln\frac{\hbar\omega^*(q_H)-e\varepsilon^*a_H}{\hbar\omega^*(q_H)} - exp\left(-2\frac{e\varepsilon^*a}{U_0}\right)\times\right.$$

$$\left.\times Ei\left(\frac{\hbar\omega^*(q_H)-e\varepsilon^*a}{U_0}\right) - Ei\left(2\frac{\hbar\omega^*(q_H)}{U_0}\right)\right\} \tag{8}$$

Burada $Ei(x) = e^x\int_0^\infty e^{-y}\frac{dy}{J-x}$ inteqralıdır [6]..

R_0, U_0, $\hbar\omega^*(q_H)$ və ε^* kəmiyyətləri aşağıdakı düsturlarla müəyyən edilirlər:

$$R_0 = 2r_D\,exp(-W/U_0),\ U_0 = e^2f/2\pi\varepsilon\varepsilon_0a$$

$$\hbar\omega^*(q_H) = \hbar\omega(q_H)(1+\beta);\quad \hbar\omega(q_H) = \hbar s(q_H) = \left(\hbar\omega_H ms^2\right)^{1/2}$$

$$\varepsilon^* = E - \frac{Ee}{2\mu_x\omega_H^2a} - \frac{e}{4(\omega_H^2-\omega^2)}\left(\frac{\varepsilon_x^2}{\mu_x}+\frac{\varepsilon_y^2}{\mu_y}\right) \tag{9}$$

Əgər

$$\frac{e\varepsilon^*a}{\hbar\omega^*(q_H)} = \beta = \frac{V_{holl}}{s} << 1$$

olarsa $V_{holl} = e\varepsilon^*/H$, bu zaman $B(W)$-nin (8) düsturu ilə təyin edilən ifadəsi sadələşir və

$$B = \frac{2E_c^2 m^4 r_D^2}{\pi^2 \gamma^2 s \rho_0 \hbar^7} \left(\frac{\hbar\omega_H}{U_0}\right)^3 \ln \frac{U_0}{3\hbar\omega(q_H)} e^{\frac{2E}{U_0}} \quad (10)$$

şəklinə düşür. (10)-u (5)-də nəzərə alsaq deşiklərin yaşama müddəti üçün

$$\tau_h^{-1} \approx 0{,}3\tau_0^{-1} \ln\left(\frac{U_0}{3\hbar\omega(q_H)} + \frac{\beta^2}{2}\right)\left(\frac{\hbar\omega_H}{U_0}\right)^2$$

alınar. Burada $\tau_h^{-1} = N_D \langle V \rangle \sigma_0$

$$\sigma_0 = \frac{20 m^3 E_c^2 r_D^2}{3\sqrt{\pi}\hbar^4 \rho s}\,;\ \langle V \rangle = \left(\frac{8kT}{\pi\mu}\right)^{1/2}$$

Göründüyü kimi deşiklərin yaşama müddəti həm temperaturun, həm də xarici sahələrin amplitud və tezliyin funksiyasıdır.

Alınan ifadələrin maqnit sahəsinə nəzərən tətbiqolunma hüdudlarına baxaq: τ_h^{-1} üçün alınan ifadə maqnit sahəsinə nəzərən aşağıdan $\hbar\omega_H >> kT$, yuxarıdan isə $kT >> \left(\hbar\omega_H / ms^2\right)^{1/2}$ ifadələri ilə məhduddur. Buradan

$$1 << \frac{\hbar\omega_H}{kT} << \frac{ms^2}{kT} \text{ və ya}$$

$$1 << \frac{H}{H_{xar}} << \frac{ms^2}{kT}$$

.

[1] *Z.A. Veliev.* FTP, 1985, t.1 , v. 6, s. 1141-114.
[2] *Z.A.Veliev.* FTP, 1989, t. 23, v.8, s. 1524-1526.
[3] *Z.A. Veliev.* FTP, 1983, t.17, v.7. s. 1351-1353.
[4] *Z.A. Veliev*. FTP, 1999, t.33, v. 11, s. 1308-1302.
[5] *Z.A. Veliev.* J.Physics.1997, v.3.1, p.42-43.
[6] *E. Yanke, F. Emde, F. Lyoş.* Spesialnie funksii. M., Nauka, 1977, s. 60-61.

З.А. Велиев, Х.А. Гасанов

РЕКОМБИНАЦИОННЫЕ ПРОЦЕССЫ ВО ВНЕШНИХ ЭЛЕКТРИЧЕСКОМ, КВАНТУЮЩЕМ МАГНИТНОМ И ЭЛЕКТРОМАГНИТНОМ ПОЛЯХ

В работе исследована задача захвата дырок в полупроводниках *n* -типа с заряженными краевыми дислокациями в скрещенных электрическом и квантующем магнитном полях, а также в переменном электрическом поле, расположенном в плоскости, перпендикулярной магнитному полю. Как видно из аналитического выражения, полученного для времени жизни дырок, эта величина зависит как от параметров кристалла и температуры, так и от величин, которые характеризуют внешние поля.

Z.A. Veliev, Kh.A. Hasanov

THE RECOMBINATION PROCESSES IN THE EXTERNAL ELECTRIC, QUANTIZING MAGNETIC AND ELECTROMAGNETIC FIELDS

The question of capture of the holes in n-type semiconductors with charged edge dislocations in the mutual perpendicular static electric and quantizing magnetic fields and also in the alternating electric field located on the surface which is perpendicular to the magnetic field is investigated. It is determined that the lifetime of the holes depends on both the parameters of the crystal, temperature and the quantities characterizing the external fields.

Received: 22.07.2004

HIGH FREQUENCY PROBE MEASUREMENTS AND LOCAL BEAM-PLASMA INTERACTION NEAR DOUBLE LAYER

M. MOSLEHI-FARD
Faculty of Physics, University of Tabriz, Tabriz 51664, Islamic Republic of Iran

A.H. MURADOV
Department of Physical Electronics, Baku State University, Baku, 370148, Z.Khalilov st. 23. Azerbaijan

The spatial distributions of high and low frequency fields were measured on the anode side of double layer. Measurements show that double layer is composed of a central region with a very sharp potential gradient surrounded by regions where ions and electrons entering the layer are accelerated. Low frequency field, which appears due to double layer motion and potential drop fluctuations in the layer, has a sharp maximum in the double layer region. The high frequency field has a broad maximum around the electron plasma frequency and it is localized in the anode plasma. Its maximum is displaced from the double layer to the high potential side, where electron beam is formed.

Distribution functions measured with the help of improved pair probe method showed that electron energy distribution is consisted of two parts: thermalized trapped electrons and beam part, which is formed passing through the double layer. Though electron beam rapidly losses its energy exciting high frequency field in the anode plasma, it does not become completely thermalized and preserves its directed character up to the anode surface.

Keywords: Double layer, Beam-Plasma interaction, High frequency field, Anode plasma.

1. INTRODUCTION

In number laboratory experiments the properties of double layer (DL) have been investigated in magnetized as well as in unmagnetized plasma [1.2.3]. However, little is known about the excitation of waves and fluctuations at a DL. In addition to possible instabilities associated with the spatial inhomogenity at the layer, interaction is expected between the surrounding plasma and the particle beams that are formed as the result of acceleration. Interesting questions are whether such interactions may lead to a strong modification of the DL structure, whether the electron beam breaks up and becomes completely thermalized within the anode plasma, and what fraction of the beam energy is converted to hf energy and ultimately radiated.

If the beam were completely thermalized the anode current would have the character of a random current, reduced by a Boltzmann factor corresponding to the potential minimum near the anode. The average depth of the fluctuating potential minimum is about 4V [1]. Probe measurements in the anode plasma indicate the electron temperature about 2 eV and density $3.10^{-15}m^{-3}$. A plasma with this density and temperature could only supply an anode current of a fourth or less of the actual current. The conclusion is that the electron beam does not become completely thermalized. The majority of the beam electrons make a single transit through the anode plasma to the anode.

In this paper results of experimental investigation of a DL in a magnetized plasma column on the anode side of the layer are reported. The spatial distributions and other important properties of the fluctuating electric field are presented for the high and low frequency waves. Electron energy distribution function have been studied with the help of improved pair probe method. Measurements show that the DL is composed of a central region with a very sharp potential gradient, surrounded by regions where ions and electrons entering the layer are accelerated. Though electron beam mainly losses its energy exciting hf field in the anode plasma, it preserves its directed character up to the anode surface.

2. THE DL FORMATION

The plasma column, which is confined by a homogeneous axial magnetic field, is obtained between the hollow electrode with inner diameter of 1.5 cm and the anode. The plasma source is a DC arc discharge between the mercury pool cathode and hollow electrode. The mercury vapor pressure in the vacuum chamber is kept at 0.1 mTor, which is about one order of magnitude smaller than the pressure in the plasma source.

The electron mean free path is much longer than the plasma column whereas the ion mean free path for charge exchange is estimated to 6 cm. In the current-free column the following parameter values are typical. The axial electric field is weak about 1 V/m and directed towards the anode. The electrons have a Maxwellian distribution with a temperature of about 2 eV. The ion energy can be estimated to be of the order of 0.1 eV. For the weak magnetic fields considered here, the ion gyro radius is larger than the column diameter, and a radial field confines the ions. The electron number density is of the order of $3\ 10^{15}\ m^{-3}$. This is also the typical electron number density on the low potential side of the formed DL.

When a sufficiently large electron current is drawn to the anode, an anode sheath depleted of ions is formed. The electrons in this sheath form a negative space charge and the anode potential rises to the value necessary to draw the actual electron current to the anode. When the potential difference between the anode and plasma exceeds the ionization potential of the gas, ionization begins in a thin sheath close to the anode, and electric field at the anode surface is expected to be reduced due to the space charge of the ions. When the current is further increased, the region with steep potential gradient moves further away from the anode and forms a DL. The layer can be placed at any desired distance from the anode by varying the anode current. The DL separates the cathode plasma from the anode plasma [4].

Number of axially and radial movable Langmuir probes have been used for potential, density and electron temperature determinations. The bandwidth of these probes is limited to about 200 kHz because of their rather large capacitance's to ground (100 pF).

Special methods have been used to overcome the difficulties caused by the fluctuations in the plasma, and to compensate for the inevitable disturbance of the plasma caused by the presence of the probes. A sampling technique has been used to select moments when the layer position and the potential drop over the layer assume fixed values.

The cathode plasma is quiescent but the potential of the anode plasma fluctuates almost coherently with the fluctuating potential drop across the double layer. Within the anode plasma the signals were found to be almost identical, independent of the probe positions, and the small delays between the probe potential fluctuations are consistent with propagation velocities of the order of the thermal electron velocity (10^6m/s) or larger.

Measurements of the spatial distributions for various frequencies confirm that the low frequency field assumes its maximum values in a region at the double layer, where it typically is an order of magnitude larger than in the surrounding plasmas. This is shown in figure 1a for a frequency of 50 kHz (bandwidth 8 kHz), and single- humped distributions like this one were found for frequencies larger than some tens of kHz. This suggests that the fluctuations in the layer profile are the dominating source for the electric field at these frequencies and that the axial layer motion manifests itself only in the width of the hump, which is a rough measure of the amplitude in the motion.

The radial electric field is directed inward in the cathode plasma but directed outward in the anode plasma. The equipotential lines, which are transverse to the magnetic field at the symmetry axis, tend to become parallel with the magnetic field at the plasma boundary. There is a radial expansion of the plasma column towards the anode. Most of this expansion seems to occur in a region at the DL.

The cathode plasma, which is maintained by the plasma source, provides the layer with reflected ions and free electrons, and random electron flux at the potential minimum ($x \approx x_0$, figure 1) determines the electron flux towards the layer and the discharge current.

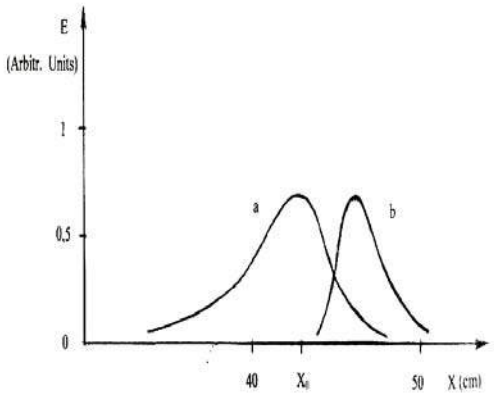

Fig.1. a) The spatial distribution of low frequency field for a frequency 50 kHz (bandwidth 8 kHz).
b) The spatial distribution of high frequency field, measured by a twin probe for a frequency of 500 MHz (bandwidth 3 MHz).

The acceleration of these electrons in the layer increases the probability of impact ionization by several orders of magnitude, and this process is the only source for positive ions in the anode plasma. The potential in the anode plasma assumes a flat maximum so that a potential well is formed for the electrons. Probe measurements show that the depth of the well, which is determined by the potential minimum in front of the anode, is at least 4 V, but it may be deeper. Although the electron mean free path is much longer than the length of the plasma column, elastic and inelastic collisions between electrons and atoms can accordingly build up a trapped electron population, which gives reflected electrons at the layer. Thus both free and reflected ions and electrons are present at the layer.

It can also be argued that the DL is strong, that is, the particle energies gained by accelerating in the layer (18 V) are much larger than the energies of the particles when they enter the layer. Electrons in the cathode plasma are Maxwellian-distributed with a temperature of 2eV. Accordingly the distribution function of the electrons, that enter the layer at the potential minimum, can be approximated by a half-Maxwellian distribution with this temperature. The fast ions, that have been accelerated in the DL, are lost in the cathode plasma by charge transfer collisions. The energy of ions moving towards the layer in the cathode plasma is therefore determined mainly by the mean free path for charge transfer collisions and the weak axial field there, which is directed towards the layer for $x<x_0$. The average energy can be estimated to be about 0-5 eV. In the anode plasma the initial energy of the ions, when they are formed by impact ionization, is negligible, and the maximum ion energy is limited by the passed potential difference. The energy of the trapped electrons in the anode plasma is limited by the depth of the potential well there; that is, the potential difference between this point and the point at the potential minimum in front of the anode.

3. HIGH FREQUENCY FIELDS AND BEAM – PLASMA INTERACTION

The electron distribution function on the high potential side of the double layer may be strongly modified due to beam-plasma interaction. A first evidence of this interaction is a high frequency field with frequencies of the order of the plasma frequency. The conditions on the high potential side of the DL are similar to those prevailing in front of the cathode sheath in hot-cathode, low pressure discharges, and in that case a large number of investigations of the high frequency field and the energy dispersion of electron beam have been presented [5]. Here the high frequency field existence on the high potential side of the DL and its properties with earlier investigations were demonstrated. Accordingly the same group of problems appearing in beam-plasma interaction should also be of importance for the understanding of a DL phenomenon.

Specially developed twin probes were used in the measurements for the following reasons. A single coaxial cable with the inner conductor as a probe tip would measure the difference between the potential of the tip and badly defined potential of the outer conductor, because this has usually to be grounded at some point several wavelengths from the plasma volume. In particular, this potential would depend on the way in which the cable enters the plasma, and

correlation measurements with two probes would become erroneous. The twin probe consists of two thin parallel cables with the inner conductor protruding 2 mm into the plasma. The outer conductors are carefully joined near the probe tips, and therefore have a common potential. This unknown potential is eliminated by forming the difference of the signals in a hybrid tee. All cables are carefully terminated in the receiving end to avoid standing waves. The HF power is measured with a spectrum analyzer with 3 MHz HF bandwidth and 3 Hz LF bandwidth. All measurements are thus time-averages over periods that are long compared with the periods of the low frequency fluctuations.

The spatial distribution of the power level associated with the HF field, measured by a twin probe, is shown in figure 1b for a frequency of 500 MHz. It is a single hump in the anode plasma with a remarkably sharp maximum displaced about 100 Debye lengths from the DL. Similar distributions were found for frequencies between 300 and 700 MHz.

The power spectrum, shown in figure 1b, has a maximum in the vicinity of the plasma frequency. However, since the diagram represents time-averaged values, any possible fine structure is probably wiped out by the low frequency fluctuations. Errors due to the frequency-dependent coupling between the probe and the plasma also distort such diagrams.

Improved sampling and signal averaging technique has allowed refined probe measurements. Pairs of thin rod-shaped probes (Ø 0.2mm, ℓ =5mm), one rod parallel to the beam, the other transverse, have been used. The parallel probe exhibits only its small end surface to a parallel flow while the perpendicular one shows a hulf – cylindrical. Total areas of two probes were equal and currents of thermal electrons of both probes should be identical. Difference of currents $J_{\perp} - J_{II}$ provides a rough method to distinguish beam electrons. Thus $\frac{d}{dV}(J_{\perp} - J_{II})$ represents directed part of electron energy distribution function. In fig 2 is shown $\frac{d}{dV}(J_{\perp} - J_{II})$ versus V measured at different distances of DL. To eliminate hysteresis the curve 2a is measured in both direction of change of ramping potential. Near the DL (fig 2a) $\frac{d}{dV}(J_{\perp} - J_{II})$ shows a sharp peak according to the beam electrons accelerated in DL. This is an unstable situation and leads to hf – generation. Further downstream this peak diminishes and gradually disappears, though directed character of distribution function preserves in the course of whole anode plasmas.

Pair collisions cannot explain the strong energy exchange, obtained from the comparison of curves a, b, c, d in fig 2, as the mean free path of electrons is much longer than the plasma column length. The rapid loss of energy of electrons, accelerated through the DL can be explained by the conversion of this energy to the *hf* field generation. These oscillations having noise character with the wide spectrum exists in the measured curves. It should be noted that in this method the errors connected with the plasma potential oscillations eliminated since potentials of both probes change identically.

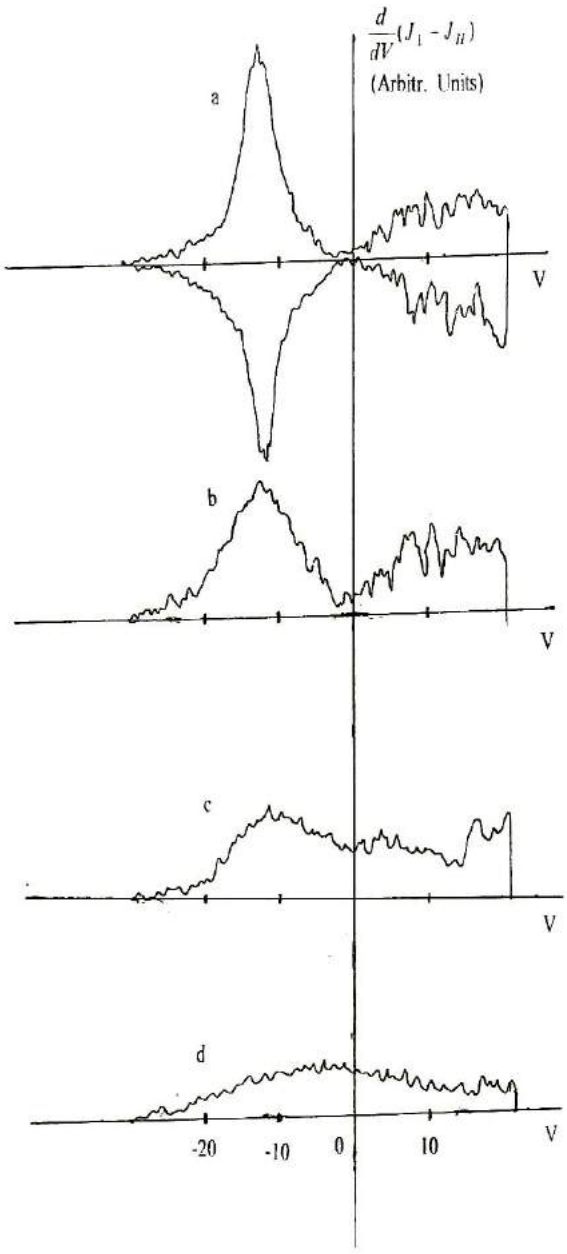

Fig.2. Measured $\frac{d}{dV}(J_{\perp} - J_{II})$ at different distances from the DL: a) 0,5 cm; b) 2 cm; c) 6 cm; d) 12 cm.

4. CONCLUSIONS

The double layer investigated is associated with low frequency and high frequency field fluctuations. Low frequency field is partly due to an axial layer motion back and forth and partly due to potential fluctuations in the layer. It has a sharp maximum in the double layer region. The high frequency field, which has a broad maximum around the electron plasma frequency, is also sharply localized in space. It has its maximum displaced from the double layer on the high potential side where an electron beam is formed. It is associated with axially propagating waves with a phase velocity that is nearly constant over a wide range of frequencies and rather smaller than the electron beam velocity.

Electron energy distribution is consisted of sum of thermalized trapped part and beam part, which is formed passing through the double layer. The measurements performed with the help of twin probes showed that beam electrons rapidly loss their energy exciting high frequency field. If the beam were completely thermalized, plasma with actual density and temperate could not supply an anode current. Consequently though electron beam mainly losses its energy exciting *hf* field in the anode plasma, it does not become completely thermalized and preserves its directed character up to the anode surface. The majority of the beam electrons make a single transit through the anode plasma to the anode.

[1] *S. Torven, L. Lindberg*. J.Phys.D. Appl. Phys. 1980, v.11, p.2285. Properties of a fluctuating double layer in a magnetised plasma column.
[2] *M.V. Nezlin* Plasma Physics 1981. v.7, p.1048.
[3] *T. Gyergyek* Plasma Phys. and Controlled Fusion 1999, v.41. p.175. Experimental study of the nonlinear dynamics of a harmonically forced double layer.
[4] *A.H. Muradov* Plasma Physics 1985, v.11.N.11.p.1385.
[5] *V.L. Granovskiy* Elektric current in gases, v.2. 1971. M. "Nauka" Pbl. Co.

M. Moslehi-Fard, Ə.X.Muradov

İKİQAT TƏBƏQƏ YAXINLIĞINDA YÜKSƏK TEZLİKLİ ZOND ÖLÇMƏLƏRİ VƏ DƏSTƏ-PLAZMA QARŞILIQLI TƏSİRİ

Plazmada ikiqat elektrik təbəqəsindən anod tərəfdə yüksək- və alçaq tezlikli elektrik sahələrinin intensivliklərinin fəzada paylanması ölçülmüşdür. Ölçmələr göstərdi ki, ikiqat təbəqə potensialın çox kəskin dəyişdiyi mərkəzi hissədən və onu əhatə edən, elektron və ionların ilkin sürətləndiyi, ətraf oblastlardan təşkil olunub. Alçaq tezlikli sahənin amplitudu ikiqat təbəqə oblastında kəskin maksimuma malikdir. Bu sahə əsasən ikiqat təbəqənin bütövlükdə fluktuasiya xarakterli hərəkəti və potensialın profilinin dəyişməsi ilə əlaqədardır. Yüksək tezlikli sahə plazmanın elektron tezliyi yaxınlığında geniş maksimuma malikdir və ikiqat təbəqədən yüksək potensial tərəfdə, elektron dəstəsinin formalaşdığı oblastda, lokallaşmışdır.

Paylanma funksiyasının təkmilləşmiş iki zond üsulu ilə ölçülməsi göstərdi ki, elektronların enerciyə görə paylanma funksiyası iki hissədən təşkil olunub:

1. Demək olar ki, izotrop paylanmış istilik elektronlarına uyğun hissə; 2. İkiqat təbəqədən keçərkən sürətlənərək dəstə təşkil edən istiqamətlənmiş hissə. Elektron dəstəsinin anod plazmasında yüksək tezlikli rəqslər həyəjanlaşdırması hesabına öz enercisini sürətlə itirməsinə baxmayaraq paylanma funksiyası tam izotrop olmur, və özünün istiqamətlənmiş xarakterini bütün anod plazması boyunja saxlayır.

М.Мослехи-Фард, А.Х.Мурадов

ВЫСОКОЧАСТОТНЫЕ ЗОНДОВЫЕ ИЗМЕРЕНИЯ И ЛОКАЛЬНОЕ ПУЧКОВО-ПЛАЗМЕННОЕ ВЗАИМОДЕЙСТВИЕ ВБЛИЗИ ДВОЙНОГО СЛОЯ

Измерены пространственные распределения высоко- и низкочастотных полей на анодной стороне от двойного электрического слоя. Измерения показали, что двойной слой состоит из центральной части с очень резким скачком потенциала, окруженной областями в которых электроны и ионы предварительно ускоряются. Амплитуда низкочастотного поля, возникающего в результате продольных флуктуационных перемещений двойного слоя и изменений профиля потенциала, имеет резкий максимум в области слоев. Высокочастотное поле имеет широк ий максимум вблизи электронной плазменной частоты и локализовано в анодной плазме. Его максимум несколько смещен от двойного слоя в сторону высокого потенциала, где формируется электронный пучок.

Измерения функции распределения усовершенствованным методом двух зондов показали, что функция распределения электронов состоит из двух частей: 1. Соответствующая запертым тепловым электронам и 2. Пучковой части, формирующейся при прохождении пролетных электронов через двойной слой. Хотя электронный пучок быстро теряет энергию в анодной плазме на возбуждение высокочастотного поля, распределение электронов полностью не термализуется, и сохраняет направленный характер вплоть до поверхности анода.

Received: 22.06.04

BULK SPIN WAVES PROPAGATION IN DIRECTION PERPENDICULAR TO THE (110) PLANE FOR FERROMAGNETIC SUPERLATTICE

V.A.TANRIVERDIYEV, V.S. TAGIYEV, S.M. SEYID-RZAYEVA
Institute of Physics of Academy of Sciences of Azerbaijan
Baku - 1143, H.Javid av. 33

A superlattice consisting of alternating layers of two-simple Heizenberg ferromagnetic is considered. Using Green function method the dispersion equations of bulk spin waves propagation in direction perpendicular to the plane (110) are derived for this systems. The numerical results are shown graphically.

During the past decade, there has been considerable effort devoted to the synthesis and study of composite materials, and of superlattices formed from alternating layers of different materials [1-3]. The study of spin waves is very useful in determining the fundamental parameters that characterize magnetic superlattice. In magnetic superlattices, elementary excitations have properties distinctly different from the modes associated with any one constituent. Bulk spin waves of periodic structure or magnetic superlattices have been analyzed theoretically in many special cases [4-6]. In the short-wavelength limit, where the exchange coupling is dominant, comparatively fewer studies have been done. Some qua1itative features of superlattice are most easily explained for the simple – cubic structure in terms of modified single - film properties. The bulk spin-wave regions in simple-cubic Heisenberg ferromagnetic material are derived in Ref.[4] The aim of this paper is to study by the Green function method [7,8] properties of an ferromagnetic superlattice with quantum Heisenberg spins at finite temperature and this theoretical studies are analogous to one from the Ref.[9], where bulk spin waves propagation in direction perpendicular to the plane (001) in ferromagnetic superlattice is considered.

As indicated in fig. 1 we consider in this paper a simple cubic ferromagnetic superlattice model in which the atomic planes of material 1 alternate with atomic planes of material 2. The materials are taken to be simple – cubic Heisenberg ferromagnetic, having exchange constant J_1 and J_2 and lattice constant a.

We consider here the following Heisenberg Hamiltonian:

$$H = -\frac{1}{2}\sum_{i,j} J_{ij}\left(S_i S_j\right) - \sum_i g\mu_\beta\left(H_0 + H_i^{(A)}\right)S_i^z \quad (1)$$

where J_{ij} -represents the exchange between the spins S_i and S_j of the nearest neighbors. H_0 is an applied magnetic field in the superlattice z direction, and $H_i^{(A)}$ (i =1,2) anisotropy field for a ferromagnetic with simple unaxial anisotropy along the z axis. We define a double – time Green function in real space $G_{ij}(t,t') = << S_i^+(t); S_j^-(t') >>$.

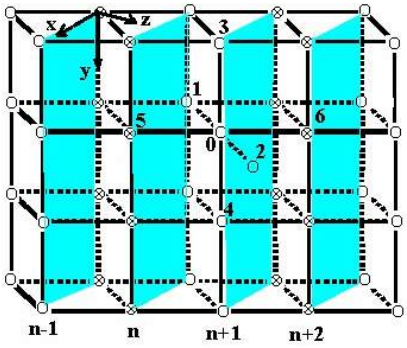

Fig. 1 A simple cubic ferromagnetic superlattice model in which the atomic planes of material 1 alternate with atomic planes of material 2. The same lattice parameter a is assumed for all materials.

We consider here the following Heisenberg Hamiltonian:

$$H = -\frac{1}{2}\sum_{i,j} J_{ij}\left(S_i S_j\right) - \sum_i g\mu_\beta\left(H_0 + H_i^{(A)}\right)S_i^z \quad (1)$$

where J_{ij} -represents the exchange between the spins S_i and S_j of the nearest neighbors. H_0 is an applied magnetic field in the superlattice z direction, and $H_i^{(A)}$ (i =1,2) anisotropy field for a ferromagnetic with simple unaxial anisotropy along the z axis. We define a double – time Green function in real space $G_{ij}(t,t') = << S_i^+(t); S_j^-(t') >>$. Writing the equation of motion for Green function and employing the random-phase approximation one obtains a set of equations. Furthermore, to emphasize the layered structure we shal1 use the following the frequency and two-dimensional. Fourier transformation [6,10]

$$G_{i,j}(t,t') = \frac{1}{\pi^2}\int dk_{||}\, exp[ik_{||}(r_i - r_j)]\,\frac{1}{2\pi}\int d\omega G_{nn'}(\omega,k_{||})\, exp[-i\omega(t-t')] \quad (2)$$

where $k_{||}$ is two-dimensional wave vector, ω is spin-wave frequency, n and n' indices of the layers to which r_i and r_j and belong, respectively.

$$\begin{cases}(\omega - A_1)G^{(1)}_{n,n'} + J_1\langle S^z_1\rangle tG^{(1)}_{n+1,n'} + J\langle S^z_1\rangle t^*G^{(2)}_{n+1,n'} + J_1\langle S^z_1\rangle t^*G^{(1)}_{n-1,n'} + J\langle S^z_1\rangle tG^{(2)}_{n-1,n'} = 2\langle S^z_1\rangle\delta_{n,n'} \\ (\omega - A_2)G^{(2)}_{n,n'} + J_2\langle S^z_2\rangle tG^{(2)}_{n+1,n'} + J\langle S^z_2\rangle t^*G^{(1)}_{n+1,n'} + J_2\langle S^z_2\rangle t^*G^{(2)}_{n-1,n'} + J\langle S^z_2\rangle tG^{(1)}_{n-1,n'} = 2\langle S^z_2\rangle\delta_{n,n'}\end{cases} \quad (3)$$

where

$$A_{1(2)} = g\mu_B\left(H_0 + H^{(A)}_{1(2)}\right) + 4J_{1(2)}\langle S^z_{1(2)}\rangle + 2J\langle S^z_{2(1)}\rangle - 2J_{1(2)}\langle S^z_{1(2)}\rangle\cos\left(k_y a\right),$$
$$t = exp\left(ik_x a/\sqrt{2}\right),\ t^* = exp\left(-ik_x a/\sqrt{2}\right)$$

The system is also periodic in z direction which lattice constant is $a/\sqrt{2}$. According Bloch's theorem we can write

$$G^{(1),(2)}_{n+1,n'} = exp\left(ik_z a/\sqrt{2}\right)G^{(1),(2)}_{n,n'} = TG^{(1),(2)}_{n,n'} \quad (4)$$

Using (4) the system of equation of (3) can be written the following matrix form

$$\begin{pmatrix}\omega - A_1 + J_1\langle S^z_1\rangle\left(tT + t^*T^*\right) & J\langle S^z_1\rangle\left(t^*T + tT^*\right) \\ J\langle S^z_2\rangle\left(t^*T + tT^*\right) & \omega - A_2 + J_2\langle S^z_2\rangle\left(tT + t^*T^*\right)\end{pmatrix}\cdot\begin{pmatrix}G^{(1)}_{n,n'} \\ G^{(2)}_{n,n'}\end{pmatrix} = \begin{pmatrix}2\langle S^z_1\rangle\delta_{n,n'} \\ 2\langle S^z_2\rangle\delta_{n,n'}\end{pmatrix} \quad (5)$$

The dispersion of equation for the bulk spin waves propagating in direction perpendicular to the plane (110) for the superlattice under consideration is derived by the equation (5) as following form:

$$\omega^2 + \omega\left\{2\cos\left(a\left(k_x + k_z\right)/\sqrt{2}\right)\left(J_1\langle S^z_1\rangle + J_2\langle S^z_2\rangle\right) - A_1 - A_2\right\} + \left(2J_1\langle S^z_1\rangle\cos\left(a\left(k_x + k_z\right)/\sqrt{2}\right) - B_1\right)\times$$
$$\times\left(2J_2\langle S^z_2\rangle\cos\left(a\left(k_x + k_z\right)/\sqrt{2}\right) - B_2\right) - 4J^2\langle S^z_1\rangle\langle S^z_2\rangle\left(\cos\left(a\left(k_x - k_z\right)/\sqrt{2}\right)\right)^2 = 0 \quad (6)$$

The equation (6) is the main results of this paper. It can be verified from equation (6) that when both media are identical it reduces to dispersion equation of bulk spin waves propagation in direction perpendicular to the plane (110) for ferromagnetic constituents [4,5].

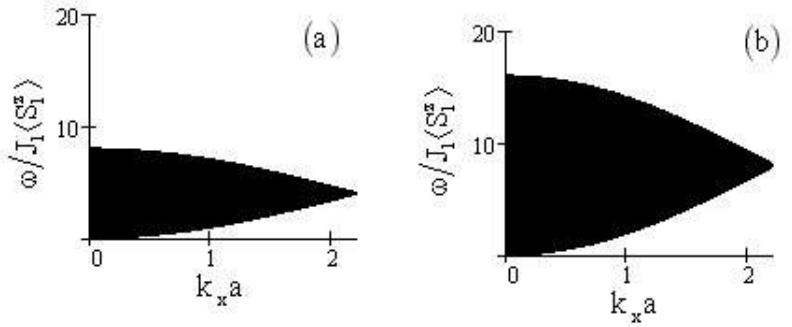

Fig 2 Bulk spin-wave regions for (a) the constituents 1 and (b) constituents 2 with the parameters $J_2/J_1 = 2$; $g_1 = g_2$; $g_1\mu_B H_0/J_1\langle S^z_1\rangle = 0.05$, $g_1\mu_B H^{(A)}_1/J_1\langle S^z_1\rangle = 0.01$; $g_2\mu_B H^{(A)}_2/J_1\langle S^z_1\rangle = 0.03$.

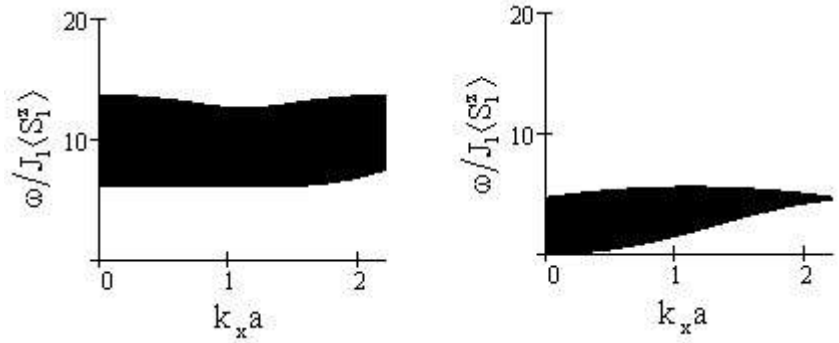

Fig. 3 Bulk spin–wave regions for superlattice, when $J/J_1 = 1.5$ and the other parameters are chosen as Fig. 1.

In Fig.2, 3 the results numerically illustrated for particular choice of parameters. Fig. 3 shows the bulk spin-wave regions for the superlattice as a function of the quantity $k_x a$, while fig. 2 shows those for the components 2 and 3. The analysis of the results shows that the width of the bulk-spin wave regions in ferromagnetic superlattice is depended on wave vectors and exchange interaction.

[1] *Ed. By M.Cottam.* "Linear and Nonlinear Spin Waves in Magnetic Films and Superlattices", World Scientific, 1994.

[2] *Feng Chen and H.K.Sy.* J. Phys. Condens. Matter. 1995, 7, 6591

[3] *R.E.Camley and R.L.Stamps.* J.Phys. Condens. Matter. 1993, 5, 3727.

[4] *T.Wolfram and R.E.DeWames,* Prog. Surf. Sci. 1972, 2, 233.

[5] *R.E.DeWames and T. Wolfram.* Phys. Rev. 1969, 185, 720

[6] *V.A.Tanriverdiyev, V.S.Tagiyev, M.B.Guseynov.* Transactions, Azerbaijan Academy of Sciences, 2000, 2, 20.

[7] *V.L. Bonc-Bruyevic, S.V. Tyablikov.* Metodi funkcii Grina statisticeskoy mexanike. M.: FM literature, (1961)

[8] *Yi-Fang Zhou.* Tsung-han Lin. Physics Lett. A. v.134, N.4, p.1989, 257-259.

[9] *V.S. Tagiyev, V.A.Tanriverdiyev, S.M.Seyid-Rzayeva, M.B.Guseynov*. Fizika, 6, N. 1, 2000 p.33-35.

[10] *H.T.Diep.* Physics Lett.A 1989 138, 69

V.Ə. Tanrıverdiyev, V.S. Tağıyev, S.M. Seyid Rzayeva

FERROMAGNİT İFRAT QƏFƏSDƏ (110) MÜSTƏVİSİNƏ PERPENDİKULYAR İSTİQAMƏTDƏ YAYILAN HƏCM SPİN DALĞALARI

İki müxtəlif sadə kubik Heyzenberq ferromaqnitin atom laylarının növbələşməsindən alınan ifrat qəfəs tədqiq olunub. Qrin funksiyası metodu ilə ifrat qəfəsin oxu boyunca yayılan həcm spin dalğaları üçün dispersiya tənliyi tapılıb. Alınan nəticələr parametrlərin seçilmiş qiymətləri üçün kəmiyyətcə təsvir olunub.

В.А . Танрывердиев, В.С. Тагиев, С.М. Сеид-Рзаева

ОБЪЕМНЫЕ СПИНОВЫЕ ВОЛНЫ, РАСПРОСТРАНЯЮЩИЕСЯ В НАПРАВЛЕНИИ ПЕРПЕНДИКУЛЯРНОМ К ПЛОСКОСТИ (110) В ФЕРРОМАГНИТНОЙ СВЕРХРЕШЕТКЕ

Рассматривается сверхрешетка, состоящая из чередующихся слоев двух различных типов Гейзенберговских ферромагнетиков. Используя метод функции Грина получены дисперсионные уравнения для объемных спиновых волн, распространяющихся в направлении перпендикулярном к плоскости (110). Численные результаты представлены графически.

Received: 24.07.04

THE EFFECT OF THE THERMAL INFLUNCE ON THE MICROHARDNESS AND THE CRYSTAL EXPANSION OF BaF_2

O. DAVARASHVILI, M. ENUKASHVILI, N. KEKELIDZE
The Tbilisi State University name of Javakhishvili,
380128б Tbilisi, Chavchavadze ave., 1

G. DARSAVELIDZE, L. GABRICHIDZE
Institute of metallurgy and materiology name of A.Tavadze, AS of Georgia,
380060, Tbilisi, Kazbegi str., 15

T. MAMEDOV, N. AHMEDZADE
Institute of Physics of Academy of Sciences of Azerbaijan
Baku - 1143, H.Javid av. 33

L.TECER
Karaelmaz University, Zonguldak, Turkey

It was revealed, in BaF_2 crystals with grain-structure thermal influence is the reason of unstrengthening and hysteresis of the coefficient of thermal expansion.

It is observed that in the BaF_2 crystals, differing by the unit structure, the thermal influence leads to the disorder and the hysteresis character of the change of thermal expansion coefficient.

The crystals of barium ftoride are widely used in the capacity of the substrates for the epitaxial growth of compounds IV-VI seeing that of the uniqueness of the types of their crystal lattices and the nearness of the lattice constants. The epitaxy from the gas and liquid phases is usually carried out at the temperatures 300-500°C [1]. The activation of the structure-sensitive properties at such temperatures can influence on the perfection of the epitaxial layers and the state of the heteroboundary between them in the result of the borrowing of the defects from the substrates of BaF_2. The similar situation can appear at the use of BaF_2 in the capacity of buffer layers at the creation of the multi-layered structures also.

In the present paper the influence of the temperature factor on the structure-sensitive properties at the investigation of the microhardness and the thermal expansion of BaF_2 crystals has been studied.

The microhardness of the BaF_2 samples in the initial state was studying at the room temperature and after the heating till 450°C in the vacuum ~10-3mm.m.c., and the temperature dependence of the elongation ratio in the cycle heating-cooling till 600°C have been studied.

The measurements of the microhardness by Knoop were carried out on the device PMT-3 at the load ~20G. The measurement accuracy of the microhardness is <30%. The results of the microhardness measurements on the samples of the different form are presented in the table 1. From the table 1 it is seen, that sample of the prism form differs by the most microhardness. Its value is close to the literature value of the microhardness, which is equal to 82 kg/mm^2 [2]. The cycle of heating cooling in the temperature interval from room till 450°C, carried out with the velocity of he temperature change ~3gr/min, increases significantly the microhardness of the BaF_2 crystals. It is easy to propose, that given mode of the thermal influence leads to the crystal disorder the difference of the microhardness values in the samples of the different thickness connects with the forming character of the prolonged defects.

Table 1

The microhardness of the barium ftoride samples

Crystal form	Thickness, mm	Microhardness by Knoop, kg/mm^2	
		Initial state	After heating till 450ºC
1. Round plane	1	75	60
2. Beam	3	80	65
3. Rod	1	75	65

The thermal expansion of the samples of sizes 3x5x12mm^3 was investigated in the temperature interval 20-600ºC on the vacuum dilatometer with the inductive gauge. The heating of the samples was carried out with the velocity 3grad/min. The measurement accuracy of elongation ratio was 3%. The results of the measurements are given in the fig.1.

From the figure it is seen, that values of the relative aspect ratio, defined at the similar heating and cooling temperatures strongly differ, essentially in the temperature

interval 20-400ºC. At the repeating of the cycle heating-cooling, the difference of the values of the elongation ratio decreases. In the given temperature interval the decrease was 30% approximately. When the measurements are carried out in the mode of the continuous heating and cooling, this difference becomes more significant. If the crystals will be subjected to the additional following annealing at 450ºC during 30 minutes, the difference of the values of the elongation ratio would be decrease on 50%.

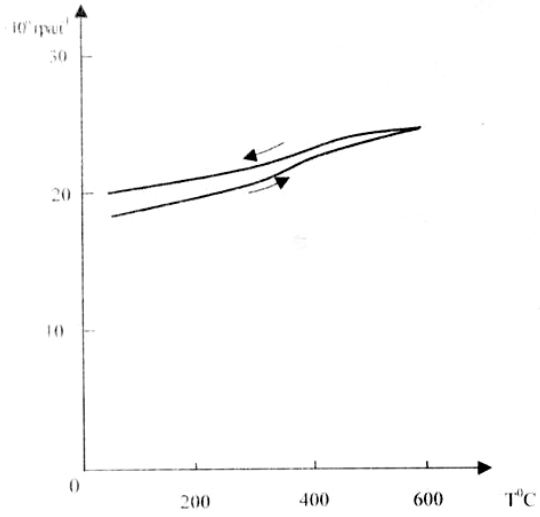

Fig.1. The dependence of the aspect ratio in the BaF_2 crystals in the cycle heating-cooling.

On the basis of the obtained results from the known ratio $\alpha=\Delta l/l\Delta T$, the values of the thermal expansion coefficient were defined. The results of the definition at the different temperatures are presented in the fig.2. From the fig.2, it is seen, that thermal expansion coefficient has the hysteresis character in the cycle heating-cooling also, and is equal to $18\cdot10^{-6}$ grad^{-1} in the initial state and after the cycle heating-cooling has the values $20\cdot10^{-6}$ grad^{-1}.

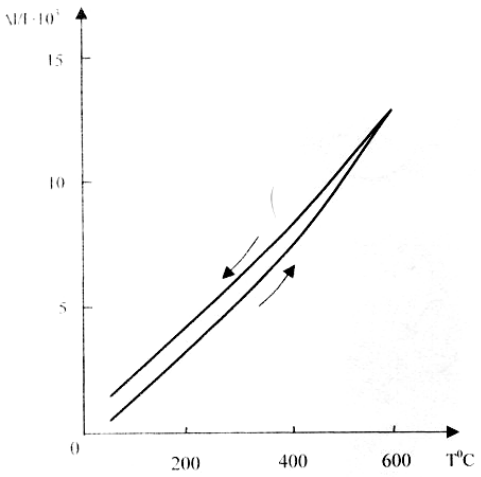

Fig.2. The temperature dependence of thermal expansion coefficient of BaF_2 crystals.

Thus, crystals of barium ftoride heating till 600ºC or the short-term extract at the temperatures ~400ºC becomes disordered, and at the same time appears the hysteresis character of the change of thermal expansion coefficient, essentially in the temperature interval from room till 450ºC. The last circumstance leads to the presence of permanent elongation ratio after cooling.

The above mentioned peculiarities, probably, connect with the relaxation of the nonhomogeneous interval stresses, leading to the creation and motion of the dislocations, essentially near block boundaries and consequently, to the crystal disorder. Such anomalies in the behaviour of thermal expansion coefficient were observed in the boron and calcite [3,4] and explained by the role of the twins and packing defects, interacting actively with he residual impurities at the thermal influence.

The paper partly is supposed by grand of NATO. PST.980089.

[1] *L.P. Bichkova, G.G. Gegiadze, O.I. Davarashvili I dr.* Jidkofazovaya epitaksiya groznikh I chetvernikh tverdikh rastvorov soedineniy IV-VI. Tbilisi, TGU, 1994, 96 str. (in Russian).

[2] *E.M. Voronkova, B.N. Grechushkina I dr.* Opticheskiye materiali dlya infrakrasnoy tekhniki, "Nauka", Moskow, 1965, 179 str. (in Russian).

[3] *G.V.Tsagareishvili, F.V.Tavadze*, etc.Boron, v.3, Warszawa, PWN, 1970, 295p.

[4] *M.B.Klassen* neklyudova. Mekhanicheskoye dvoynikovaniye kristallov. "Nauka", Moskow, 1960, 279str. (in Russian).

O.İ. Davaraşvili, M.İ. Enukaşvili, N.P. Kekelidze, Q.Ş. Darsavelidze, L.L. Qabriçidze, T.S. Məmmədov, N.D. Əhmədzade, L.N.Teser

BaF_2 KRİSTALLARININ MİKROBƏRKLİYİNƏ VƏ GENİŞLƏNMƏSİNƏ TERMİK HƏRƏKƏTİN TƏSİRİ

Blok quruluşu ilə fərqlənən kristallarında müəyyən edilmişdir ki, istilik təsiri termik genişlənmə əmsalının gisterezis xarakterli dəyişməsinə və möhkəmliyinin azalmasına gətirir.

О.И. Даварашвили, М.И. Енукашвили, Н.П. Кекелидзе, Г.Ш. Дарсавелидзе, Л.Л. Габричидзе, Т.С. Мамедов, Н.Д. Ахмедзаде, Л.Н.Тесер

ВЛИЯНИЕ ТЕРМИЧЕСКОГО ВОЗДЕЙСТВИЯ НА МИКРОТВЕРДОСТЬ И РАСШИРЕНИЕ КРИСТАЛЛОВ BaF_2

Обнаружено, что в кристаллах BaF_2, отличающихся блочной структурой, температурное воздействие приводит к разупрочнению и гистерезисному характеру изменения коэффициента термического расширения .

Received: 21.05.2004

SOLUTION OF THE PRINCIPAL CHIRAL FIELD PROBLEM AS "MATHEMATICA" ALGORITHM

M.A. MUKHTAROV
Institute of Mathematics and Mechanics
370602, Baku, F.Agaev str. 9, Azerbaijan

Solutions of the principal chiral field problem are constructed by means of Mathematica software.

1. The problem of constructing of the solutions of self-dual Yang-Mills (SDYM) model and its dimensional reductions, the principal chiral field problem in our case, in the explicit form for semisimple Lie algebra, rank of which is greater than two, remains important for the present time. The interest arises from the fact that almost all integrable models in one, two and (1+2)-dimensions are symmetry reductions of SDYM or they can be obtained from it by imposing the constraints on Yang-Mills potentials [1-12].

This work is a direct continuation of [13-15], where the exact solutions of the principal chiral field problem have been derived, and it shows how to obtain the further results using determined Mathematica algorithm. The discrete symmetry transformation method [12] applied here allows to generate new solutions from the old ones in much more easier way than applying methods from [11], and the case of SL(3,C) algebra gives us a key to construct solutions for an arbitrary semisimple algebra.

2. Equations of the principal chiral field problem are the systems of equations for the element f, taking values in the semisimple algebra,

$$\left(\theta_i - \theta_j\right)\frac{\partial^2 f}{\partial x_i \partial x_j} = \left[\frac{\partial f}{\partial x_i}, \frac{\partial f}{\partial x_j}\right] \tag{1}$$

In the case of two-dimensional space: θ_1=1, θ_2=-1, $x_1 = \xi$, $x_2 = \nu$.

Following [12], for the case of a semisimple Lie algebra and for an element f being a solution of (1), the following statement takes place:

There exists such an element S taking values in a gauge group that

$$S^{-1}\frac{\partial S}{\partial x_i} = \frac{1}{\tilde{f}_-}\left[\frac{\partial \tilde{f}}{\partial x_i}, X_M^+\right] - \theta_i \frac{\partial}{\partial x_i}\frac{1}{\tilde{f}_-} X_M^+ \tag{2}$$

Here X_M^+ is the element of the algebra corresponding to its maximal root divided by its norm, i.e.,

$$\left[X_M^+, X^-\right] = H, \left[H, X^\pm\right] = \pm 2X^\pm \quad ,$$

$\tilde{f}_-$ - is the coefficient function in the decomposition of $\tilde{f}$ of the element corresponding to the minimal root of the algebra, $\tilde{f} = \sigma f \sigma^{-1}$ and where σ is an automorfism of the algebra, changing the positive and negative roots.

In the case of algebra SL(3,C) we'll consider the case of three dimensional representation of algebra and the following form of $\sigma = \begin{pmatrix} 0 & 0 & 1 \\ 0 & 1 & 0 \\ -1 & 0 & 0 \end{pmatrix}$.

The discrete symmetry transformation, producing new solutions from the known ones, is as follows:

$$\frac{\partial F}{\partial x_i} = S\frac{\partial \tilde{f}}{\partial x_i}S^{-1} + \theta_i \frac{\partial S}{\partial x_i}S^{-1} \tag{3}$$

3. Let's represent the explicit formulae for transformation in the case of SL(3,C) algebra

$$f = \alpha_1 X_1^+ + \alpha_2 X_2^+ + \alpha_{1,2} X_{1,2}^+ + \tau_1 h_1 + \tau_2 h_2 + a_1 X_1^- + a_2 X_2^- + a_{1,2} X_{1,2}^- \quad , \tag{4}$$

In connection with the general scheme, first of all, it is necessary to find the solution of the equations (2) for the SL(3,C) valued function S for given f, solution of equations (1).

From (2) it is clear that S is upper triangular matrix and can be represented in the following form:

$$S = \exp \beta_1 X_1^+ \exp \beta_{1,2} X_{1,2}^+ \exp \beta_2 X_2^+ \exp \beta_0 H \quad , \tag{5}$$

where $H=h_1+h_2$.

After substitution of the last representation of S into (2) and taking into account (4), we have at every step of the recurrent procedure the following relations

$$\begin{gathered} \beta_0 = \ln \alpha_{1,2}, \quad \beta_1 = \alpha_2, \quad \beta_2 = \alpha_1 \\ (\beta_{1,2})_{x_i} = (\alpha_{1,2})_{zx_i} - (\delta_1 + \delta_2)_{x_i} \alpha_{1,2} - (\alpha_1)_{x_i} \alpha_2 \end{gathered} \tag{6}$$

As the initial solution we'll take the explicit solution f belonging to the algebra of upper triangular matrixes:

$$f = \alpha_1 X_1^+ + \alpha_2 X_2^+ + \alpha_{1,2} X_{1,2}^+ + \tau_1 h_1 + \tau_2 h_2 \tag{7}$$

The component form of self-duality equations for this case is following

$$\begin{gathered} \frac{\partial^2 \tau_\nu}{\partial x_i \partial x_j} = 0, \\ \frac{\partial^2 a_\nu}{\partial x_i \partial x_j} = \{\delta_\nu, \alpha_\nu\}_{x_i, x_j} \quad , \quad i=1,2, \\ \frac{\partial^2 a_{1,2}}{\partial x_i \partial x_j} = \{\delta_1 + \delta_2, \alpha_{1,2}\}_{x_i, x_j} \quad , \end{gathered} \tag{8}$$

where $\delta_1 = 2\tau_1 - \tau_2$, $\delta_2 = 2\tau_2 - \tau_1$ and figure brackets of two functions g_1 and g_2 denotes :

$$\{g_1, g_2\}_{x_i, x_j} = \frac{\partial g_1}{\partial x_i} \frac{\partial g_2}{\partial x_j} - \frac{\partial g_2}{\partial x_j} \frac{\partial g_1}{\partial x_i} .$$

The general solution of system (8) takes the form

$$\begin{gathered} \tau_i = \sum_{s=1} \tau_i^s (x_s) \ , \ \alpha_i = \oint_c \alpha_i(\lambda) \exp(-\bar{\delta}_i(\lambda)) d\lambda , \\ \bar{\delta}_i(\lambda) = \sum_{s=1} \frac{\tau_i^s (x_s)}{\lambda + \theta_s} , \\ \alpha_{1,2} = \oint_c \alpha_{1,2}(\lambda) \exp(-\bar{\delta}_1(\lambda) - \bar{\delta}_2(\lambda)) d\lambda + \\ + \oint_c \alpha_1(\lambda) \exp(-\bar{\delta}_1(\lambda)) d\lambda \oint_c \frac{d\lambda' \alpha_2(\lambda') \exp(-\bar{\delta}_2(\lambda'))}{\lambda - \lambda'} \end{gathered} \tag{9}$$

Here the circle integration goes over the complex parameter λ.

By the direct check one can be convinced that (9) are the solutions of equations (8). The formulae (9) can also be obtained as a solution of homogeneous Riemann problem in the case of the solvable algebra [11].

Let's represent two types of Backlund transformation by means of which one can construct new types of solutions of equations (8) from the known solution (9). For solutions of first two equations of (8) this two Backlund transformations are the same:

$$\theta_s (\alpha_i^k)_{x_s} - (\delta_i)_{x_s} \alpha_i^k = (\alpha_i^{k+1})_{x_s} \ , i = 1,2 \tag{10}$$

For solutions of the third equation of the system (8) they are different:

$$\theta_s (\alpha_{1,2}^{0,k})_{x_s} - (\delta_1 + \delta_2)_{x_s} \alpha_{1,2}^{0,k} - (\alpha_1^k)_{x_s} \alpha_2^k = (\alpha_{1,2}^{0,k+1})_{x_s} \tag{11}$$

and

$$\theta_s(\alpha_{1,2}^{k,0})_{x_s} - (\delta_1 + \delta_2)_{x_s}\alpha_{1,2}^{k,0} - \alpha_1^k(\alpha_2^k)_{x_s} = (\alpha_{1,2}^{k+1,0})_{x_s} \tag{12}$$

Note that starting, zero step of upper transformations procedure coincides with initial solutions (9).
Let's return to the solution of the equation (7) at the first step of the recurrent procedure.
Comparing (6) and (12) we came to the conclusion that $\beta_{1,2} = \alpha_{1,2}^{0,1}$.
Finally, knowing all components of matrix S and using (3) we can express the solution

$$F = F_1^+X_1^+ + F_2^+X_2^+ + F_{1,2}^+X_{1,2}^+ + F_1^0h_1 + F_2^0h_2 + F_1^-X_1^- + F_2^-X_2^- + F_{1,2}^-X_{1,2}^-$$

of self-duality equations at the first step of the recurrent procedure in terms of chains (10)-(12):

$$F_1^0 = \tau_1 + \frac{\alpha_{1,2}^{1,0}}{\alpha_{1,2}^{0,0}},\ F_2^0 = \tau_2 + \frac{\alpha_{1,2}^{0,1}}{\alpha_{1,2}^{0,0}}$$

$$F_{1,2}^- = \frac{1}{\alpha_{1,2}^{0,0}},\ F_1^- = \frac{\alpha_2^0}{\alpha_{1,2}^{0,0}},\ F_2^- = -\frac{\alpha_1^0}{\alpha_{1,2}^{0,0}}$$

$$F_1^+ = -\frac{1}{\alpha_{1,2}^{0,0}}\begin{vmatrix}\alpha_1^0 & \alpha_1^1\\ \alpha_{1,2}^{0,0} & \alpha_{1,2}^{1,0}\end{vmatrix},\ F_2^+ = -\frac{1}{\alpha_{1,2}^{0,0}}\begin{vmatrix}\alpha_2^0 & \alpha_2^1\\ \alpha_{1,2}^{0,0} & \alpha_{1,2}^{0,1}\end{vmatrix} \tag{13}$$

$$F_{1,2}^+ = \frac{1}{\alpha_{1,2}^{0,0}}\begin{vmatrix}\alpha_{1,2}^{0,0} & \alpha_{1,2}^{0,1}\\ \alpha_{1,2}^{1,0} & \alpha_{1,2}^{1,1}\end{vmatrix}$$

Using the equations of the principal chiral field problem for the group-valued element

$$\theta_i(g)_{x_i}\, g^{-1} = (f)_{x_i}$$

the relations (3) can be rewritten as

$$\theta_i(S_n\sigma g_n)_{x_i}(S_n\sigma g_n)^{-1} = (f_{n+1})_{x_i} \quad ,$$

So we see that the group valued elements g_{n+1} and g_n are connected by the relation

$$g_{n+1} = S_n\sigma g_n \tag{14}$$

Let's represent the explicit formulae of the recurrent procedure of obtaining the group-valued element solutions.
At every step, as it shown in [5], S is upper triangular matrix and can be represented in the following form:

$$S_n = exp(\beta_1)_nX_1^+\ exp(\beta_{1,2})_nX_{1,2}^+\ exp(\beta_2)_nX_2^+\ exp(\beta_0)_nH \quad , \tag{15}$$

where $H=h_1+h_2$ and for g_n we use the following parameterization:

$$\begin{aligned} g_n = {} & exp(\eta_1^+)_nX_1^+\ exp(\eta_{1,2}^+)_nX_{1,2}^+\ exp(\eta_2^+)_nX_2^+\ exp((t_1)_nh_1 + (t_2)_nh_2)\times \\ & \times exp(\eta_2^-)_nX_2^-\ exp(\eta_{1,2}^-)_nX_{1,2}^-\ exp(\eta_1^-)_nX_1^- \end{aligned} \tag{16}$$

with

$$g_0 = exp(\eta_1^+)_0X_1^+\ exp(\eta_{1,2}^+)_0X_{1,2}^+\ exp(\eta_2^+)_0X_2^+\ exp((t_1)_0h_1 + (t_2)_0h_2)$$

as an initial solution.

Hereafter, $X_1^\pm$, $X_2^\pm$, $X_{1,2}^\pm$, h_1, h_2 are the generators of SL(3,C) algebra.

Following the general scheme from [5] we have at
(0)-step:

$$(t_i)_0 = \tau_i^{-1} \equiv \nu_i \,, (\eta_i^+)_0 = \alpha_i^{-1}, i = 1,2 \,, (\eta_{1,2}^+)_0 = \alpha_{1,2}^{-1,0} \quad ;$$

The further calculation we deliver to Mathematica program:

$$(t_i)_0 = \tau_i^{-1} \equiv \nu_i \,, (\eta_i^+)_0 = \alpha_i^{-1}, i = 1,2 \,, (\eta_{1,2}^+)_0 = \alpha_{1,2}^{-1,0} \quad ;$$

The further calculation we deliver to Mathematica program:

$$X_1^+ = \begin{pmatrix} 0 & 1 & 0 \\ 0 & 0 & 0 \\ 0 & 0 & 0 \end{pmatrix}; \quad X_2^+ = \begin{pmatrix} 0 & 0 & 0 \\ 0 & 0 & 1 \\ 0 & 0 & 0 \end{pmatrix}; \quad X_{1,2}^+ = \begin{pmatrix} 0 & 0 & 1 \\ 0 & 0 & 0 \\ 0 & 0 & 0 \end{pmatrix};$$

$$X_1^- = \begin{pmatrix} 0 & 0 & 0 \\ 1 & 0 & 0 \\ 0 & 0 & 0 \end{pmatrix}; \quad X_2^- = \begin{pmatrix} 0 & 0 & 0 \\ 0 & 0 & 0 \\ 0 & 1 & 0 \end{pmatrix}; \quad X_{1,2}^- = \begin{pmatrix} 0 & 0 & 0 \\ 0 & 0 & 0 \\ 1 & 0 & 0 \end{pmatrix};$$

$$h_1 = \begin{pmatrix} 1 & 0 & 0 \\ 0 & -1 & 0 \\ 0 & 0 & 0 \end{pmatrix}; \quad h_2 = \begin{pmatrix} 0 & 0 & 0 \\ 0 & 1 & 0 \\ 0 & 0 & -1 \end{pmatrix}; \quad w = \begin{pmatrix} 0 & 0 & 1 \\ 0 & 1 & 0 \\ -1 & 0 & 0 \end{pmatrix};$$

```
G0 = MatrixExp[n1 X1+].MatrixExp[n1,2 X1,2+].MatrixExp[n2 X2+].MatrixExp[r1 h1].
     MatrixExp[r2 h2];
S1 = MatrixExp[b1 X1+].MatrixExp[b1,2 X1,2+].MatrixExp[b2 X2+].MatrixExp[b0 (h1 + h2)];
G1 = S1.w.G0;
MatrixForm[G1]
```

Null[4]

$$\begin{pmatrix} -e^{-b_0+r_1}(b_1 b_2 + b_{1,2}) & e^{-r_1+r_2} b_1 - e^{-b_0-r_1+r_2} n_1 (b_1 b_2 + b_{1,2}) & e^{b_0-r_2} + e^{-r_2} b_1 n_2 - e^{-b_0-r_2}(b_1 b_2 + b_{1,2})(n_1 n_2 + n_{1,2}) \\ -e^{-b_0+r_1} b_2 & e^{-r_1+r_2} - e^{-b_0-r_1+r_2} b_2 n_1 & e^{-r_2} n_2 - e^{-b_0-r_2} b_2 (n_1 n_2 + n_{1,2}) \\ -e^{-b_0+r_1} & -e^{-b_0-r_1+r_2} n_1 & -e^{-b_0-r_2}(n_1 n_2 + n_{1,2}) \end{pmatrix}$$

```
G1 /. (b1 b2 + b1,2) → a1,2[1, 0] /. n1 n2 + n1,2 → a1,2[0, -1] /. b0 → Log[a1,2[0, 0]] /.
      b1 → a1[0]
     /. b2 → a2[0] /. n1 → a1[-1] /. n2 → a2[-1]
```

$$\{\{-e^{-\text{Log}[a_{1,2}[0,0]]+r_1} a_{1,2}[1,0], e^{-r_1+r_2} a_1[0] - e^{-\text{Log}[a_{1,2}[0,0]]-r_1+r_2} a_1[-1] a_{1,2}[1,0],$$
$$e^{\text{Log}[a_{1,2}[0,0]]-r_2} + e^{-r_2} a_1[0] a_2[-1] - e^{-\text{Log}[a_{1,2}[0,0]]-r_2} a_{1,2}[0,-1] a_{1,2}[1,0]\},$$
$$\{-e^{-\text{Log}[a_{1,2}[0,0]]+r_1} a_2[0], e^{-r_1+r_2} - e^{-\text{Log}[a_{1,2}[0,0]]-r_1+r_2} a_1[-1] a_2[0],$$
$$e^{-r_2} a_2[-1] - e^{-\text{Log}[a_{1,2}[0,0]]-r_2} a_2[0] a_{1,2}[0,-1]\},$$
$$\{-e^{-\text{Log}[a_{1,2}[0,0]]+r_1}, -e^{-\text{Log}[a_{1,2}[0,0]]-r_1+r_2} a_1[-1], -e^{-\text{Log}[a_{1,2}[0,0]]-r_2} a_{1,2}[0,-1]\}\}$$

```
G1 = FullSimplify[%]
```

$$\left\{\left\{-\frac{e^{r_1} a_{1,2}[1,0]}{a_{1,2}[0,0]}, \frac{e^{-r_1+r_2}(a_1[0] a_{1,2}[0,0] - a_1[-1] a_{1,2}[1,0])}{a_{1,2}[0,0]},\right.\right.$$
$$\left.\frac{e^{-r_2}(a_1[0] a_2[-1] a_{1,2}[0,0] + a_{1,2}[0,0]^2 - a_{1,2}[0,-1] a_{1,2}[1,0])}{a_{1,2}[0,0]}\right\}, \left\{-\frac{e^{r_1} a_2[0]}{a_{1,2}[0,0]},\right.$$
$$\left.\frac{e^{-r_1+r_2}(-a_1[-1] a_2[0] + a_{1,2}[0,0])}{a_{1,2}[0,0]}, \frac{e^{-r_2}(-a_2[0] a_{1,2}[0,-1] + a_2[-1] a_{1,2}[0,0])}{a_{1,2}[0,0]}\right\},$$
$$\left.\left\{-\frac{e^{r_1}}{a_{1,2}[0,0]}, -\frac{e^{-r_1+r_2} a_1[-1]}{a_{1,2}[0,0]}, -\frac{e^{-r_2} a_{1,2}[0,-1]}{a_{1,2}[0,0]}\right\}\right\}$$

```
G1 = FullSimplify[% /. a1[0] a2[-1] → a1,2[1, -1] - a1,2[0, 0]
     /. a1[-1] a2[0] → a1,2[0, 0] - a1,2[-1, 1]]
```

$$\left\{\left\{-\frac{e^{r_1}\, a_{1,2}[1,0]}{a_{1,2}[0,0]},\ \frac{e^{-r_1+r_2}\,(a_1[0]\, a_{1,2}[0,0]-a_1[-1]\, a_{1,2}[1,0])}{a_{1,2}[0,0]},\right.\right.$$

$$\left.\frac{e^{-r_2}\,(a_{1,2}[0,0]\, a_{1,2}[1,-1]-a_{1,2}[0,-1]\, a_{1,2}[1,0])}{a_{1,2}[0,0]}\right\},$$

$$\left\{-\frac{e^{r_1}\, a_2[0]}{a_{1,2}[0,0]},\ \frac{e^{-r_1+r_2}\, a_{1,2}[-1,1]}{a_{1,2}[0,0]},\ \frac{e^{-r_2}\,(-a_2[0]\, a_{1,2}[0,-1]+a_2[-1]\, a_{1,2}[0,0])}{a_{1,2}[0,0]}\right\},$$

$$\left.\left\{-\frac{e^{r_1}}{a_{1,2}[0,0]},\ -\frac{e^{-r_1+r_2}\, a_1[-1]}{a_{1,2}[0,0]},\ -\frac{e^{-r_2}\, a_{1,2}[0,-1]}{a_{1,2}[0,0]}\right\}\right\}$$

```
T2[1] = G1[[3, 3]];
T1[1] = Minors[G1][[3, 3]];
α2[1] = G1[[2, 3]]/T2[1];
β2[1] = G1[[3, 2]]/T2[1];
β1[1] = Minors [G1][[3, 2]]/T1[1];
α1[1] = Minors [G1][[2, 3]]/T1[1];
α1,2[1] = −Minors [G1][[1, 3]]/ T1[1];
β1,2[1] = −Minors [G1][[3, 1]]/ T1[1];
FullSimplify[T2[1]]
```

$$-\frac{e^{-r_2}\, a_{1,2}[0,-1]}{a_{1,2}[0,0]}$$

```
FullSimplify[T1[1]]
```

$$\frac{e^{-r_1}\,(-(a_1[-1]\, a_2[0]+a_{1,2}[-1,1])\, a_{1,2}[0,-1]+a_1[-1]\, a_2[-1]\, a_{1,2}[0,0])}{a_{1,2}[0,0]^2}$$

```
T1[1] = FullSimplify[% /. a1[−1] a2[0] → a1,2[0, 0] − a1,2[−1, 1]
      /. a1[−1] a2[−1] → a1,2[0, −1] − a1,2[−1, 0]]
```

$$-\frac{e^{-r_1}\, a_{1,2}[-1,0]}{a_{1,2}[0,0]}$$

```
FullSimplify[β1[1]]
```

$$\frac{e^{2r_1-r_2}\, a_2[-1]\, a_{1,2}[0,0]}{-(a_1[-1]\, a_2[0]+a_{1,2}[-1,1])\, a_{1,2}[0,-1]+a_1[-1]\, a_2[-1]\, a_{1,2}[0,0]}$$

```
β1[1] = FullSimplify[% /. a1[−1] a2[0] → a1,2[0, 0] − a1,2[−1, 1]
      /. a1[−1] a2[−1] → a1,2[0, −1] − a1,2[−1, 0]]
```

$$-\frac{e^{2r_1-r_2}\, a_2[-1]}{a_{1,2}[-1,0]}$$

```
FullSimplify[β1,2[1]]
```

$$\frac{e^{r_1+r_2}\,(a_1[-1]\, a_2[0]+a_{1,2}[-1,1])}{(a_1[-1]\, a_2[0]+a_{1,2}[-1,1])\, a_{1,2}[0,-1]-a_1[-1]\, a_2[-1]\, a_{1,2}[0,0]}$$

```
β1,2[1] = FullSimplify[% /. a1[−1] a2[0] → a1,2[0, 0] − a1,2[−1, 1]
      /. a1[−1] a2[−1] → a1,2[0, −1] − a1,2[−1, 0]]
```

$$\frac{e^{r_1+r_2}}{a_{1,2}[-1,0]}$$

```
FullSimplify[β2[1]]
```

$$\frac{e^{-r_1+2r_2}\, a_1[-1]}{a_{1,2}[0,-1]}$$

```
FullSimplify[α1[1]]
```

$$\frac{a_{1,2}[0,0]\,(-a_1[0]\,a_{1,2}[0,-1]+a_1[-1]\,a_{1,2}[1,-1])}{-(a_1[-1]\,a_2[0]+a_{1,2}[-1,1])\,a_{1,2}[0,-1]+a_1[-1]\,a_2[-1]\,a_{1,2}[0,0]}$$

```
α1[1] = FullSimplify[% /. a1[-1] a2[0] → a1,2[0, 0] - a1,2[-1, 1]
      /. a1[-1] a2[-1] → a1,2[0, -1] - a1,2[-1, 0]]
```

$$\frac{a_1[0]\,a_{1,2}[0,-1]-a_1[-1]\,a_{1,2}[1,-1]}{a_{1,2}[-1,0]}$$

```
FullSimplify[α2[1]]
```

$$a_2[0]-\frac{a_2[-1]\,a_{1,2}[0,0]}{a_{1,2}[0,-1]}$$

```
FullSimplify[α1,2[1]]
```

$$\frac{a_{1,2}[0,0]\,(a_1[0]\,(a_2[0]\,a_{1,2}[0,-1]-a_2[-1]\,a_{1,2}[0,0])+a_{1,2}[-1,1]\,a_{1,2}[1,-1])}{-(a_1[-1]\,a_2[0]+a_{1,2}[-1,1])\,a_{1,2}[0,-1]+a_1[-1]\,a_2[-1]\,a_{1,2}[0,0]}+a_{1,2}[1,0]$$

```
α1,2[1] = FullSimplify[% /. a1[-1] a2[0] → a1,2[0, 0] - a1,2[-1, 1]
      /. a1[-1] a2[-1] → a1,2[0, -1] - a1,2[-1, 0]]
```

$$\frac{a_1[0]\,(-a_2[0]\,a_{1,2}[0,-1]+a_2[-1]\,a_{1,2}[0,0])-a_{1,2}[-1,1]\,a_{1,2}[1,-1]}{a_{1,2}[-1,0]}+a_{1,2}[1,0]$$

```
Expand[%]
```

$$-\frac{a_1[0]\,a_2[0]\,a_{1,2}[0,-1]}{a_{1,2}[-1,0]}+\frac{a_1[0]\,a_2[-1]\,a_{1,2}[0,0]}{a_{1,2}[-1,0]}-\frac{a_{1,2}[-1,1]\,a_{1,2}[1,-1]}{a_{1,2}[-1,0]}+a_{1,2}[1,0]$$

```
α1,2[1] = FullSimplify[% /. a1,2[1, 0] → a1[0] a2[0] + a1,2[0, 1] /
      .a1,2[1, -1] → a1[0] a2[-1] + a1,2[0, 0] /. a1,2[0, -1] → a1[-1] a2[-1] + a1,2[-1, 0]]
```

$$\frac{1}{a_{1,2}[-1,0]}(-a_1[0]\,a_2[-1]\,(a_1[-1]\,a_2[0]+a_{1,2}[-1,1])+$$

$$(a_1[0]\,a_2[-1]-a_{1,2}[-1,1])\,a_{1,2}[0,0]+a_{1,2}[-1,0]\,a_{1,2}[0,1])$$

```
α1,2[1] = FullSimplify[% /. a1[-1] a2[0] → a1,2[0, 0] - a1,2[-1, 1]]
```

$$-\frac{a_{1,2}[-1,1]\,a_{1,2}[0,0]}{a_{1,2}[-1,0]}+a_{1,2}[0,1]$$

The second step.

$$B_1=\frac{-a_1[0]\,a_{1,2}[1,0]+a_1[1]\,a_{1,2}[0,0]}{a_{1,2}[0,0]};\quad B_2=\frac{-a_2[0]\,a_{1,2}[0,1]+a_2[1]\,a_{1,2}[0,0]}{a_{1,2}[0,0]};$$

$$B_0=\mathrm{Log}\left[\frac{-a_{1,2}[1,1]\,a_{1,2}[0,0]+a_{1,2}[1,0]\,a_{1,2}[0,1]}{a_{1,2}[0,0]}\right];$$

$$B_{1,2}=\frac{1}{(a_{1,2}[0,0])\text{^}2}\,a_{1,2}[0,0]\,(a_{1,2}[1,2]\,a_{1,2}[0,0]-a_{1,2}[1,1]\,a_{1,2}[0,1])\,a_{1,2}[0,1]$$

$$(a_{1,2}[1,1]\,a_{1,2}[0,0]-a_{1,2}[1,0]\,a_{1,2}[0,1]);$$

```
S2 = MatrixExp[B1 X1†].MatrixExp[B1,2 X1,2†].MatrixExp[B2 X2†].MatrixExp[B0 (h1 + h2)];
G2 = S2.w.G1; T2[2] = G2[[3, 3]]; T1[2] = Minors[G2][[3, 3]];
α2[2] = G2[[2, 3]]/T2[2]; β2[2] = G2[[3, 2]] /T2[2]; β1[2] = Minors [G2][[3, 2]]/T1[2];
α1[2] = Minors [G2][[2, 3]]/T1[2]; α1,2[2] = -Minors [G2][[1, 3]]/T1[2];
β1,2[2] = -Minors [G2][[3, 1]]/ T1[2] FullSimplify[T2[2]]
```

$$\frac{e^{-r2}\,(a_{1,2}[0,0]\,a_{1,2}[1,-1]-a_{1,2}[0,-1]\,a_{1,2}[1,0])}{-a_{1,2}[0,1]\,a_{1,2}[1,0]+a_{1,2}[0,0]\,a_{1,2}[1,1]}$$

```
FullSimplify[T1[2]]
```

M.A. MUKHTAROV

$$(e^{-r_1}(a_{1,2}[0,0](a_1[0](a_2[0]a_{1,2}[0,-1]-a_2[-1]a_{1,2}[0,0])+a_{1,2}[-1,1]a_{1,2}[1,-1])-$$
$$((a_1[-1]a_2[0]+a_{1,2}[-1,1])a_{1,2}[0,-1]-a_1[-1]a_2[-1]a_{1,2}[0,0])a_{1,2}[1,0]))/$$
$$(a_{1,2}[0,0](-a_{1,2}[0,1]a_{1,2}[1,0]+a_{1,2}[0,0]a_{1,2}[1,1]))$$

```
T1[1] = FullSimplify[%44 /. a1,2[1, -1] → a1,2[0, 0] + a1[0] a2[-1]
        /. a1,2[0, -1] → a1,2[-1, 0] + a1[-1] a2[-1] /. a1[-1] a2[0] → a1,2[0, 0] - a1,2[-1, 1]]
```

$$(e^{-r_1}(a_1[-1]a_1[0]a_2[-1]a_2[0]+a_1[0](a_2[0]a_{1,2}[-1,0]+a_2[-1](a_{1,2}[-1,1]-a_{1,2}[0,0]))+$$
$$a_{1,2}[-1,1]a_{1,2}[0,0]-a_{1,2}[-1,0]a_{1,2}[1,0]))/(-a_{1,2}[0,1]a_{1,2}[1,0]+a_{1,2}[0,0]a_{1,2}[1,1])$$

```
ch1 = (a1[-1] a1[0] a2[-1] a2[0] + a1[0] (a2[0] a1,2[-1, 0] + a2[-1] (a1,2[-1, 1] - a1,2[0, 0])) +
      a1,2[-1, 1] a1,2[0, 0] - a1,2[-1, 0] a1,2[1, 0]);
FullSimplify[ch1 /. a1,2[1, 0] → a1,2[0, 1] + a1[0] a2[0] /. a1[-1] a2[0] → a1,2[0, 0] - a1,2[-1, 1]]
```

$$a_{1,2}[-1,1]a_{1,2}[0,0]-a_{1,2}[-1,0]a_{1,2}[0,1]$$

```
T2[2] =
  e^-r1 (a1,2[-1, 1] a1,2[0, 0] - a1,2[-1, 0] a1,2[0, 1])/
    (-a1,2[0, 1] a1,2[1, 0] + a1,2[0, 0] a1,2[1, 1])
```

$$\frac{e^{-r_1}(a_{1,2}[-1,1]a_{1,2}[0,0]-a_{1,2}[-1,0]a_{1,2}[0,1])}{-a_{1,2}[0,1]a_{1,2}[1,0]+a_{1,2}[0,0]a_{1,2}[1,1]}$$

```
FullSimplify[β1[2]]
```

$$(e^{2r_1-r_2}a_{1,2}[0,0](a_2[0]a_{1,2}[1,-1]-a_2[-1]a_{1,2}[1,0]))/$$
$$(a_{1,2}[0,0](a_1[0](-a_2[0]a_{1,2}[0,-1]+a_2[-1]a_{1,2}[0,0])-a_{1,2}[-1,1]a_{1,2}[1,-1])+$$
$$((a_1[-1]a_2[0]+a_{1,2}[-1,1])a_{1,2}[0,-1]-a_1[-1]a_2[-1]a_{1,2}[0,0])a_{1,2}[1,0])$$

```
Zn1 = (a1,2[0, 0] (a1[0] (-a2[0] a1,2[0, -1] + a2[-1] a1,2[0, 0]) - a1,2[-1, 1] a1,2[1, -1]) +
      ((a1[-1] a2[0] + a1,2[-1, 1]) a1,2[0, -1] - a1[-1] a2[-1] a1,2[0, 0]) a1,2[1, 0]);
FullSimplify[
  Zn1 /. a1,2[1, -1] → a1,2[0, 0] + a1[0] a2[-1]
      /. a1,2[0, -1] → a1,2[-1, 0] + a1[-1] a2[-1] /. a1[-1] a2[0] → a1,2[0, 0] - a1,2[-1, 1] /.
    a1,2[1, 0] → a1,2[0, 1] + a1[0] a2[0]]
```

$$a_{1,2}[0,0](-a_1[0]a_2[-1](a_1[-1]a_2[0]+a_{1,2}[-1,1])+$$
$$(a_1[0]a_2[-1]-a_{1,2}[-1,1])a_{1,2}[0,0]+a_{1,2}[-1,0]a_{1,2}[0,1])$$

```
FullSimplify[% /. a1[-1] a2[0] → a1,2[0, 0] - a1,2[-1, 1]]
```

$$a_{1,2}[0,0](-a_{1,2}[-1,1]a_{1,2}[0,0]+a_{1,2}[-1,0]a_{1,2}[0,1])$$

```
β1[2] = e^(2 r1 - r2) (a2[0] a1,2[1, -1] - a2[-1] a1,2[1, 0])/
        (-a1,2[-1, 1] a1,2[0, 0] + a1,2[-1, 0] a1,2[0, 1]);

FullSimplify[β2[2]]
```

$$\frac{e^{-r_1+2r_2}(a_1[0]a_{1,2}[0,0]-a_1[-1]a_{1,2}[1,0])}{a_{1,2}[0,0]a_{1,2}[1,-1]-a_{1,2}[0,-1]a_{1,2}[1,0]}$$

```
FullSimplify[β1,2[2]]
```

$$(e^{r_1+r_2}(a_1[0]a_2[0]a_{1,2}[0,0]-(a_1[-1]a_2[0]+a_{1,2}[-1,1])a_{1,2}[1,0]))/$$
$$(a_{1,2}[0,0](a_1[0](a_2[0]a_{1,2}[0,-1]-a_2[-1]a_{1,2}[0,0])+a_{1,2}[-1,1]a_{1,2}[1,-1])-$$
$$((a_1[-1]a_2[0]+a_{1,2}[-1,1])a_{1,2}[0,-1]-a_1[-1]a_2[-1]a_{1,2}[0,0])a_{1,2}[1,0])$$

```
FullSimplify[% /. a1,2[1, -1] → a1,2[0, 0] + a1[0] a2[-1]
      /. a1,2[0, -1] → a1,2[-1, 0] + a1[-1] a2[-1] /. a1,2[1, 0] → a1,2[0, 1] + a1[0] a2[0]
    /. a1[-1] a2[0] → a1,2[0, 0] - a1,2[-1, 1]]
```

$$(e^{r_1+r_2}a_{1,2}[0,1])/(-a_1[0]a_2[-1](a_1[-1]a_2[0]+a_{1,2}[-1,1])+$$
$$(a_1[0]a_2[-1]-a_{1,2}[-1,1])a_{1,2}[0,0]+a_{1,2}[-1,0]a_{1,2}[0,1])$$

$$\text{FullSimplify}\left[\%/.\, a_1[-1]\, a_2[0] \to a_{1,2}[0,0] - a_{1,2}[-1,1]\right]$$

$$\beta_{1,2}[2] = \frac{\dfrac{e^{r_1+r_2}\, a_{1,2}[0,1]}{-a_{1,2}[-1,1]\, a_{1,2}[0,0] + a_{1,2}[-1,0]\, a_{1,2}[0,1]}}{-a_{1,2}[-1,1]\, a_{1,2}[0,0] + a_{1,2}[-1,0]\, a_{1,2}[0,1]} \Bigg/ \frac{e^{r_1+r_2}\, a_{1,2}[0,1]}{-a_{1,2}[-1,1]\, a_{1,2}[0,0] + a_{1,2}[-1,0]\, a_{1,2}[0,1]}$$

At that point we stop the procedure, but it is obvious that it can easily be continued for any step and the resulting formulas correspond to those from [15].

As it is seen from formulas (11-12) for algebras of the rank higher than two, the number of corresponding Backlund transformations of the initial problem solutions will be equal to the rank of the algebra. Thus, it is necessary only to overcome the routine calculations using Mathematica 4-0 software.

[1] *R.S. Ward, Phil. Trans.* R. Soc. Lond.A315, 451 (1985); Lect. Notes Phys., 1987, 280, 106; Lond. Math. Soc. Lect. Notes Ser., 1990, 156, 246.

[2] *L.J. Mason and G.A. J.Sparling.* Phys. Lett., 1989, A137, 29; J. Geom. and Phys., 1992, 8, 243.

[3] *S. Chakravarty, M.J. Ablowitz and P.A. Clarkson.* Phys. Rev. Lett., 1990, 1085.

[4] *I. Bakas and D.A. Depireux.* Mod. Phys. Lett., 1991, A6, 399.

[5] *M.J. Ablowitz, S. Chakravarty and L.A. Takhtajan.* Comm. Math. Phys., 1993, 158, 1289.

[6] *T.A. Ivanova and A.D. Popov.* Phys. Lett., 1992, A170, 293.

[7] *L.J. Mason and N.M.J. Woodhouse.* Nonlinearity 1, 1988, 73; 1993, 6, 569.

[8] *M. Kovalyov, M. Legare and L. Gagnon.* J. Math. Phys., 1993, 34, 3425.

[9] *M. Legare and A.D. Popov.* Pis'ma Zh. Eksp. Teor. Fiz., 1994, 59, 845.

[10] *A.A. Belavin and V.E. Zakharov.* Phys. Lett., 1978, B73, 53.

[11] *A.N. Leznov and M.A. Mukhtarov.* J. Math. Phys., 1987, 28 (11), 2574; Prepr. IHEP, 1987, 87-90. Prepr. ICTP 163, Trieste, Italy, 1990; J. Sov. Lazer Research, 13 (4), 284, 1992.

[12] *A.N. Leznov.* IHEP preprint-92/87, 1990.

[13] *A.N. Leznov, M.A.Mukhtarov and W.J.Zakrzewski.* Tr. J. of Physics 1995, 19, 416.

[14] *M.A.Mukhtarov.* Fizika, 2002, v. 5, N 2, 38

[15] *M.A.Mukhtarov.* Fizika, 2002, v. 5, N 3, 3

M.A. Muxtarov

ƏSAS KİRAL SAHƏ MƏSƏLƏSİNİN «MATEMATİKA» ALQORİTMİ KİMİ HƏLLİ

Əsas kiral sahə tənliyinin həlli «Matematika» proqramı alqoritminin koməyi ilə qurulmuşdur.

М.А. Мухтаров

РЕШЕНИЕ ЗАДАЧИ ГЛАВНОГО КИРАЛЬНОГО ПОЛЯ КАК "МАТЕМАТИКА" АЛГОРИТМ

Решения уравнений главного кирального поля построены посредством алгоритма на программе Математика.

Received: 22.09.04

THE INFLUENCE OF THE ELECTRIC FIELD ON THE POZISTOR PROPERTIES OF THE ELECTROTECHNICAL GLASSYPLASTIC ON THE BASE OF THE EPOXIDO-CASE RESIN

M.N. BAYRAMOV, A.M. MAGERRAMOV
Institute of the Radiational Problems of NAS of Azerbaycan
Baku c., Av. G.Javid, 31a, e-mail: arifm 50@ rambler.ru.

The peculiarities of the pozistor effect in the electrotechnical pressmaterial of PET type have been investigated. The influence of the electrical discharges on the pozistor characteristics of the epoxido-case pressmaterial has been studied, the coefficients of PTCR, PTK_{ε}, T_n, ΔT_n and their stability have been defined. It is shown, that at the moderate modes of influence (9kV, 5h), the values of PTCR and PTK_{ε} increase, but values of T_n and ΔT_n decrease, and in the mode of 11kV, 5h the two regions of $\varepsilon_k(T)$ are observed on the dependence ε_k at the temperatures from 360-390K and 395-425K. It is proposed, that the first dispersion region $\varepsilon_k(T)$ connects with the before hardness processes, and second region probably is caused by the different oxygenocontaining groups, appearing at the influence of the electric discharges and their interaction with fillers in the PET samples.

The results of the investigation show, that the probability of the regulation of pozistor properties of elements, prepared from the pressmaterial of PET type by the way of influence of electric discharges and γ-radiations, and change of content and type of fillers, takes place.

INTRODUCTION

The glassyplastic materials (GM) on the base of fenoloformaldegide and epoxido-case resins, fulfilled by fiber and dispersion fillers are widely used in the electrotechnical devices, in radioelectronic equipments and e.t.c. The GM structure introduces the heterogeneous systems from fillers and polymer matrix (binding) with special building of the division boundaries between them and character structural defects [1]. For the directed change of the structure and electrophysical properties, they are often subjected to the electrodischarge modification [2,3]. At the influnce of the electric field on the GM the anomaly temperature dependency of the specific electric resistance ρ_v of pressmaterial of PET type in the temperature interval 373-500K [3] was observed. On the dependence $\rho_v(T)$ the val4ues ρ_v increase on 2-3 orders at the temperature growth till 500K, beginning from T=363K. However, the reasons, regularity and mechanism of the observable high value of the positive temperature coefficient of resistance (PTCR) of the samples of PET type haven't been investigated. It is shown, that materials with high value of PTCR are called pozistor [3]. The distinctive peculiarities of the pozistor properties of materials are the temperature interval ΔT_n, at which the high values of PTCR and reversible change of ρ_v stay without change. In the dependence on the material composition, the pozistors should have the big sensitivity, small innertionness and cost. The ceramics on the base of $BaTiO_3$ with the addition of glass in the quantity 1-5 mass.% [5] correspond to these demands. However, the pozistor properties i.e. the increase of ρ_v at the increase of T slowly depends on the applied voltage. The polymer composites have pozistor properties also, for example, on the base of polypropilen and CTS-19 [4], but the moderation of the reversibility ρ_v in the wide temperature interval is character for them.

It is need to note, that the creation of phase-boundary potential barrier, controlled by the composite dielectric constant ε_k [4,5] is the main reason of acquisition of pozistor effect by heterogeneous system.

In the case of the epoxidal glassyplastics, the value ε_k will be depended on the type of hardener and character of the influence of the electric field and discharges. On our opinion, these questions did not describe enough. Moreover, in the set of cases, the pozistor application in its capacity of the thermoregulators, fire netificators and thermogauges and e.t.c. demands the definite security at their detail geometrical sizes. These demands are possible for the compositional GM after the electrofield influences or the modification of their structure by the change of the ratio of the fillers and binding in them.

The aim of the given paper is the studying of the peculiarities of the influence of electric field and discharges (ED) on the pozistor properties of glassyplastic materials.

EXPERIMENTAL PART

The samples from GM by the thickness of 500 mkm had been obtained by the thermopressing of two marks of pressmaterial – PET and MFE-1. The samples have been prepared from the pressmaterial of PET mark on the base of the epoxido-case resin UP-643, fillers – glassifiber and caoline. In the capacity of the accelerator of the hardness process was used the accelerator A-30-1,5. The second type of the samples had been prepared from the pressmaterial of MFE-1 mark on the base of melaninoformaldegide resin with the aminosilaxan AM-2 and fillers are glassyfiber and talc [3]. The pressing temperature at the pressure 150MPa for PET and MFE-1 was 423 and 453K, correspondingly. The degree of dispersion of the powder fillers wasn't higher than 10-15 mkm, and diameter of glassyfiber – 13 mkm.

The hardness of resin was under the external pressure action. Further the GM samples were subjected to the influence of the electric discharges on the technique [6] at the effective value of voltage on the electrodes – 9kV and 11kV during 5 hours. The dielectric measurements (ε, $tg\delta$) were carried out on the device E7-8 at the frequency 1kHc. The specific electric volume resistance of ρ_v was measured with the help of the teraohmeter EK6-13 at the direct-current voltage 100V. After the sample's standing under the voltage during 1 minute, the temperature dependencies of $\rho_v(T)$ have been fixed.

The PTCR and the temperature interval ΔT_n of existence of pozistor material properties were defined on the inclination of the dependencies of $\rho_v(T)$. The value of PTCR, i.e. the sensitivity coefficient to the temperature change of the sample is defined by the formulae:

$$PTCR = lg(\rho_v^1 - \rho_v^2) / T_2 - T_1 \qquad (1)$$

where ρ_v^1 and ρ_v^2 are specific electric resistances of the sample at the temperatures T_1 and T_2, correspondingly. From the dependency $\varepsilon_k(T)$ the degree of dispersion coefficient of pozistor was defined by the formulae:

$$PTK_{\varepsilon} = \varepsilon_k^2 - \varepsilon_k^1 / T_2 - T_1 \qquad (2)$$

where ε_k^1 and ε_k^2 are values of dielectric constant at T_1 and T_2, correspondingly. In the given case the value T_1 corresponds to the temperature of the increase beginning of ρ_v and ε_k, i.e. to the temperature of appearing of pozistor properties of T_n of PET type.

THE RESULTS AND THEIR DISCUSSION

The temperature dependences of $\rho_v(T)$ of PET samples before (curve1) and after the influence of the discharges at the voltage on the cell U_p=9kV (curve2) and 11kV (curve3) are given in the fig.1. It is seen, that with the temperature increase, ρ_v of all samples firstly decrease, going through the minimum at 373-383K, and further again begin to increase. Thus, till the temperature 440-450K, the PET samples have pozistor properties. From the fig.1 it is a followed, that the influence of the electric discharges in the air leads to the increase of the inclination on the line area of $\rho_v(T)$ dependence at the temperature interval of pozistor effect appearing. Moreover, this inclination becomes more significant (curve3) with the increase of the discharge power (U_p increase). The decrease of ρ_v of the initial state parts of the dependence $\rho_v(T)$ connect with the increase of the number of current carriers and the reason of the resistance increase probably can be as the before hardness processes, i.e. the additional structuring, so the formation of the potential barrier with the depth $\Delta\varphi$.

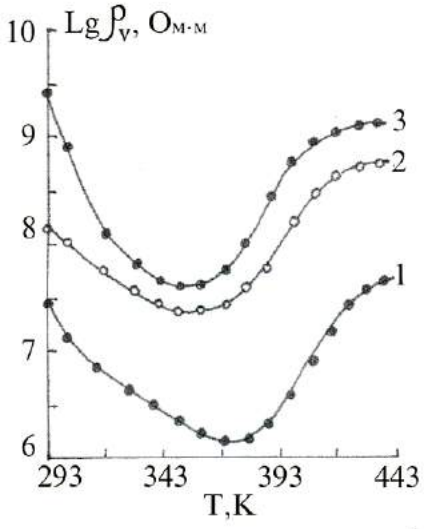

Fig.1. Temperature dependences of specific volume electric resistance ρ_v of PET pressmaterial samples; 1-initial, 2 and 3 after influence of discharges in the mode U_p=9kV, t=5 hours, U_p=11kV, t=5 hours, correspondingly.

About the going of the before hardness processes testify the data on ε_k measurement and its temperature dependencies (fig.2). As it is seen from the fig.2 the ε_k values of PET samples significantly increase in the region of the pozistor effect appearing.

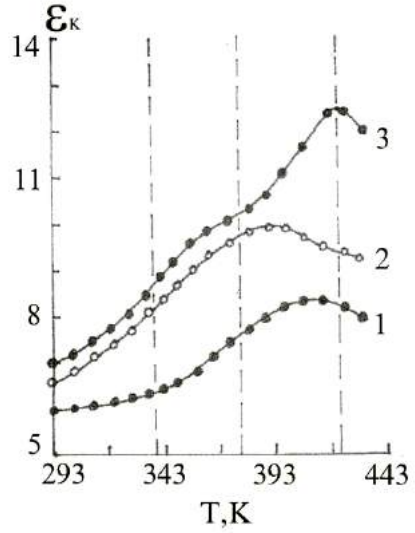

Fig.2. Temperature dependences of dielectric constant ε_k of PET pressmaterial samples: 1-initial, 2 and 3 after influence of discharges in the mode U_p=9kV, t=5 hours, U_p=11kV, t=5 hours, correspondingly.

The significant increase of ε_k takes place at the discharge influence (curve3), where the increase of the dielectric constant $\Delta\varepsilon_k$ is 5÷6. Moreover, it is need to note, that the increase of ε_k values with the temperature stops and the some decreases of ε_k, beginning from the temperature 420-430K, which testifies about the stop of the before hardness processes, are observed. As it is seen from the fig.2, the influence of the electric discharges leads to the increase of the temperature interval of the ε_k increase (curve3). The creations of the different oxygenocontaining groups can influence also on the electrophysical properties of PET at the stronger mode of discharge influence (U_p). These and other structural changes cause the increase of the value of the potential barrier $\Delta\varphi$ between matrix and PET pressmaterial fillers, which are the main reason of the pozistor effect appearing in them. Comparative studying of the $\rho_0(T)$ dependencies for MFE-1 samples before and after discharge influence shows that nonlinear dependence $\rho_v(T)$ in MFE-1 doesn't observed. This can be connected with the different composition of fillers in these glassymaterials MFE-1 has 40-50 mass.% of talc and calcium steorat. Thus, the properties mainly are caused by the presence of caoline in PET pressmaterial. At the preparation of PET the surface treated caoline of the following composition: SiO_2(45,4%), Al_2O(3)(38,8%), Ti_2O_3(1,5%) with the specific volume resistance $\rho_v=10^{15}$ Om·m and dielectric constant ε=2,6, was used. The values T_n, ΔT_n, PTCR and PTK_{ε}, changed under the influence of ED at 10-time cyclic heating-cooling of PET samples are presented in the table.

From the table it is followed, that PET pressmaterial has pozistor properties and ε_k dispersion also in the temperature interval 277-327K. At the moderate influence modes (9kV, 5h) the PTCR and PTK_{ε} values increase, but T_n and ΔT_n values decrease.

Moreover, in the mode 11kV, 5h, two region of ε_k at the temperatures from 360-390K and 395-425K (fig. 2, curve 3) are observed on the $\varepsilon_k(T)$ dependence.

Table

Pozistor characteristics	Before ED influence	After ED influence	
		9kV, 5h	11kV, 5h
T_n,K	377	363	353
ΔT_n, K	50	40	45
PTCR, (Om·m·K^{-1})	$2\cdot10^{-3}$	$5\cdot10^{-3}$	$2{,}7\cdot10^{-3}$
PTK$_\varepsilon$, K^{-1}	$3{,}3\cdot10^{-2}$	$3{,}5\cdot10^{-2}$	$4{,}7\cdot10^{-2}$

If the first dispersion region $\varepsilon_k(T)$ connects especially with before hardness processes, then the second region is caused by different oxygenocontaining groups, forming at the ED influence and their interaction with fillers in PET samples. The comparison of the values, given in the table with the values of these values for the semiconductor and ceramic materials [5,9] shows, that some pozistor characteristics (T_n and PTK$_\varepsilon$) for PET is some worth in the comparison of the corresponding parameters of these materials. However, the PET is less energy capacious, the probabilities of pozistor properties by the way of ED and γ-radiations influence, change of content and type of fillers, takes place.

[1] *I.G. Gurtovnik, V.N. Sportsmen.* Stekloplastiki radiotekhnicheskogo naznacheniya. M. Khimiya, 1987.

[2] *G.A.Abdullayev, Ch.G.Agayev, Yu.V.Gorin, F.Kh. Kulakhmedov.* Sposob izgotovleniya elektroizolyasionnikh stekloplastikovikh izdeliy. Poloj. Resheniepo zayavke №4953370/05 ot 03.01.92 g. (FIAN Azerb. Respubliki).

[3] *M.N. Bayramov, M.A. Bagirov, A.M. Magerramov.* Preprint №475, Sector RI AN Azerb., Mingechaurskoe NIO Stekloplastikov, Baku, 1992, s. 16.

[4] *M.G. Shakhtakhtinskiy, A.I.Mamedov, M.A. Ramazanov.* Dok. AN Azerb. SSR, 1986, t.57, №8, s. 34-36.

[5] *V.V. Belozerov, Yu.I. Goltsov, A.E. Panich, L.A. Shpak.* V sb. Pyezotekhnika-99, t.2, Rostov-na-Donu, Payk, 1999, s.27-33.

[6] *M.A. Bagirov, V.P. Malin.* Elektricheskoe starenie polimernikh dielektrikov. Baku, Azerneshr, 1987, s. 204.

[7] Napolniteli dlya polimernikh kompozisionnikh materialov. Per. s angl. Pod red. *P.G. Babaevskogo.* M. Khimiya, 1981, s. 154-157.

[8] *A.I. Mamedov, M.A. Kurbanov, M.G. Shakhtakhtinskiy, A.A. Garagashov.* Preprint №2, IFAN OKB "Registr", Baku,1987, s. 109.

[9] *V.V.Belozerov, Yu.I.Goltsov, L.A. Shpak, V.E.Yurkevich.* Izv. RAN, ser. fiz., t. 57, №6, s. 155-158.

[10] *A.M. Magerramov, A.M. Lobanov, M.A. Bagirov i dr.* Plasticheskie massi, 1993, №5, s.19-21.

M.N. Bayramov, A.M. Məhərrəmov

EPOKSİD QƏTRAN ƏSASLI ELEKTROTEXNİKİ ŞÜŞƏ PLASTİKİN POZİSTOR XASSƏLƏRİNƏ ELEKTRİK SAHƏSİNİN TƏSİRİ

PET presmaterialında pozistor effektinin xüsusiyyətləri tədqiq edilmişdir.

Epoksid-novalak presmaterialının pozistor xarakteristikalarına elektrik boşalmalarının təsiri oyrənilmiş, PTKS, PTK$_\varepsilon$, T_n, ΔT_n əmsalları və onların stabilliyi təyin edilmisdir. Göstərilmişdir ki, mülayim təsir rejimlərində (9 kV, 5 saat) PTKS və PTK$_\varepsilon$ qiymətləri artır, T_n və ΔT_n qiymətləri isə azalır, 11 k, 5 saat rejimində isə $\varepsilon_k(T)$ asılılığında ε_k-nın 360-390 K və 395-425 K temperaturlarında iki oblastı müşahidə olunur. Fərz edilir ki, $\varepsilon_k(T)$ dispersiyasının birinci oblastı bərkimə prosesinin davam etməsi ilə bağlıdır, ikinci oblast isə çox güman ki, elektrik boşalmalarının təsiri zamanı müxtəlif oksigenli qrupların yaranması və onların PET nümunələrindəki doldurujularla qarşılıqlı təsirləri ilə əlaqədardır. Tədqiqatların nəticələri göstərir ki, PET presmaterialından hazırlanmış elementlərin pozistor xassələrini elektrik boşalmaları və γ-şüalanma ilə təsir etməklə, həmçinin doldurucuların miqdarlarını və tiplərini dəyişməklə nizamlamaq imkanı mövcuddur.

М.Н. Байрамов, А.М. Магеррамов

ДЕЙСТВИЕ ЭЛЕКТРИЧЕСКОГО ПОЛЯ НА ПОЗИСТОРНЫЕ СВОЙСТВА СТЕКЛОПЛАСТИКА НА ОСНОВЕ ЭПОКСИДНО-НОВОЛАЧНОЙ СМОЛЫ

Исследованы особенности позисторного эффекта в электротехническом ПЭТ. Изучено влияние электрических разрядов на позисторные характеристики эпоксидно-новолачного прессматериала, определены коэффициенты ПТКС, ПТК$_\varepsilon$, T_n, ΔT_n и их стабильность. Показано,что при умеренных режимах воздействия (9 кВ, 5 ч) значения ПТКС и ПТК$_\varepsilon$ возрастают, а значения T_n и ΔT_n уменьшаются, а в режиме 11 кВ, 5 ч. на зависимости $\varepsilon_k(T)$ наблюдаются две области ε_k при температурах от 360-390 К и 395-425 К. Предполагается, что первая область дисперсии $\varepsilon_k(T)$ связана с процессами доотверждения, а вторая область, по-видимому, обусловлена различными кислородсодержащими группами, образующимися при воздействии электрических разрядов, и их взаимодействием с наполнителями в образцах ПЭТ. Результаты исследования показывают, что имеется возможность регулирования позисторных свойств элементов, изготовленных из прессматериала ПЭТ путем воздействия электрических разрядов и γ-излучений, а также изменением содержания и типа наполнителей.

Received: 23.07.04

THE STUDING OF PHOTOCONDUCTION MECHANISM OF THE PHOTOSENSITIVE CRYSTALS BY THE TYPE OF $PbGa_2S_4(Se_4)$

N.N. MUSAYEVA, O.B. TAGIYEV, R.B. JABBAROV
The Institute of Physics of NAS of Azerbaijan,
Baku-1143, H. Javid, 33

I.I. ALIYEV
The Institute of Chemical Problems of NAS of Azerbaijan

The photosensitive structures of $In/PbGaS_4$ and $In/pbGaSe_4$ have been created and investigated. the spectral dependencies of photocurrent at the different temperatures and applied voltages, show the presence of the local centers inside the forbidden band width, connected with the self-doping and appearing crystals in the process of the obtaining.

The numerous class of the triple compounds $II\text{-}III_2\text{-}IV_4$ (where II two-valent cations are Mn, Pb, Hg, Zn; III three-valent are chalcogens S, Se), belong to the number of multicomponent semiconductors, the initial investigations of which have already led to new besides them, which are perspective for the applying of the materials in the optoelectronics [1,2].

The compounds $PbGaS_4(Se_4)$, belonging to the given class, are the photosensitive ones in the visible region of the spectrum. Some parameters of crystals (the forbidden band width, the nature of the optical transitions, phonon energy, dielectric constant, photoconduction mechanism and e.t.c.) were identified by the investigations of their physical properties, in the same way as the electric and optical ones (absorption and Romanov spectrums) [3-5].

In the present paper the results of the investigations for the studying of the photoconduction nature in $PbGaS_4(Se_4)$ are presented.

On the basis of the experimental and literature data, we can note, that $II\text{-}III_2\text{-}VI_4$ belong to the defective crystal group. The wide application of the semiconductors $II\text{-}III_2\text{-}VI_4$ in the microelectronics during long time was strongly limited by fact, that in these semiconductors always many prolonged defects, such as boundaries of grains and dislocation. It is known, that such defects are responsible not only for the significant decrease of the motion of majority carriers and the life time of the minority carriers, but can be as the centers of the creation of the secondary phases and segregation of impurities in the process of the crystal growth [6].

Thus, the significant change of these material properties can be achieved by the way of the controlled doping, i.e. that in the process of the crystal growth the degree of their inclination from stoichiometric can be controlled or influenced on the segregation impurity mechanism.

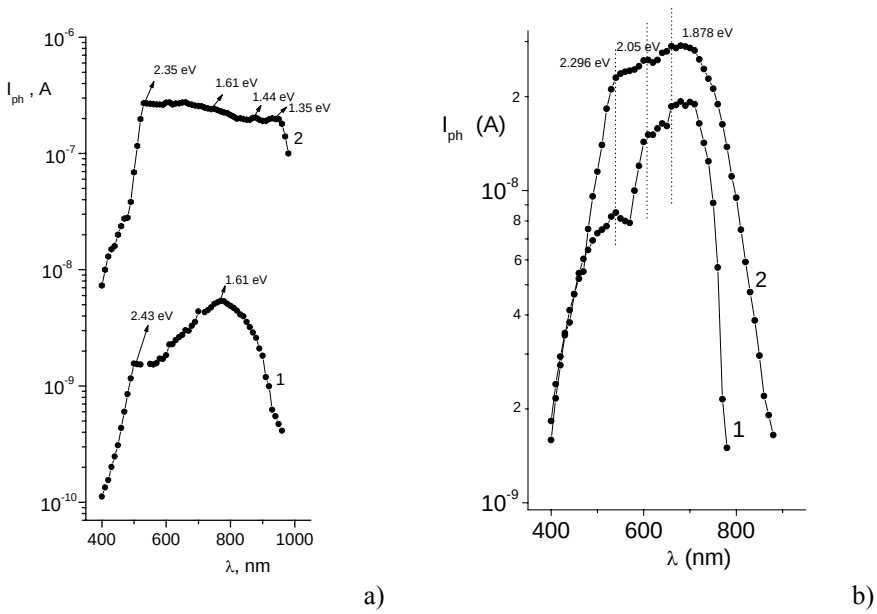

Fig.1. a) The photoconduction spectrum for the structures $In/PbGaSe_4$ at the temperatures T=110(1), 306K(2).
b) The photoconduction spectrum of $In/PbGaS_4$ at the temperatures $In/PbGaS_4$ at the temperatures T=100(1), 290K(2).

The obtaining of the detailed know ledges about local disorder, as in the elementary semiconductors, so in the compounds, is the open problem, as disordered mass impurities or point defects in some crystal region difficultly differ from the prolonged ones. The prolonged defects are the sources of the electric fields and fields of the high voltage, appearing near them, that significantly differs their electronic states from the electronic states of the local mass of

impurities. It can be proposed, that photoconduction in the crystals PbGaS4 and PbGaSe4connects with such prolonged defects, which manage to store the big enough charge for the illumination time. It is hardly to believe, that the permanent impurities, being in the substitution state or the intrinsic point defects can influence on the band structure so significantly, i.e. lead to the appearance of the local electronic stats inside the conduction band. In this case in the photoconduction band the maximums would be appeared behind the intrinsic absorption edge (fig.1a and 1b).

From the figures it is seen, energetic value of short-wave maximum on the photoconduction spectrum samples of $PbGa_2Se_4$ coincides to the value, defined from the measurements of the optical absorption (E_g=2,35eV) [4], but on the photoconduction spectrums of $PbGa_2Se_4$ samples the intrinsic conduction band isn't observed. However, the optical absorption edge for the direct allowed transitions shows that E_g=2,78eV [7].

At the low temperatures the spectrum narrower and the impurity maximum at 1,61eV becomes more intensive than the short-wave one, but the other maximums disappear. This fact probably connects with the insufficient influence of such kinds of defects on the conduction at the low temperatures. In the samples PbGa2S4 the temperature decrease doesn't lead to the decrease of the action of the similar kinds of defects that probably connects with the decrease of the defect number, taking part in the conduction.

For the observation of the effects, which go on the crystal volume of $PbGa_2Se_4$, the samples were lightened from the opposite side of contact (fig.2). It is seen, that at this the intrinsic photoconduction band becomes almost invisible on the phone of the impurity conduction bands. This fact and moreover, the difference of the energetic positions of the maximums, by our opinion connects with the quantity and different volume impurity distribution.

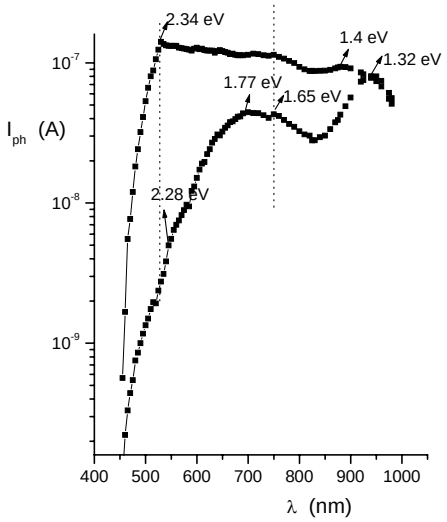

Fig.2. The photoconduction spectrum of $PbGaSe_4$ at T=300K. The illumination geometry: from the side of indium contact – 1; from the side of $PbGaSe_4$ crystal – 2.

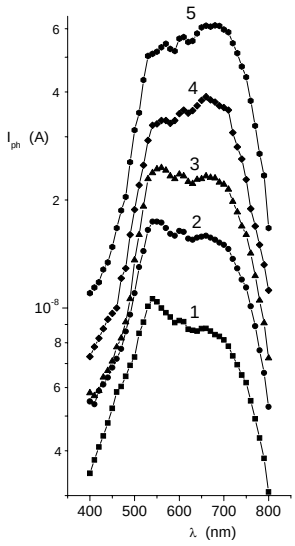

Fig.3. The photoconduction spectrums of In/$PbGaS_4$ at 300K and applied voltage U=50(1), 100(2), 250(4), 400(5).

The analysis of the obtained experimental data shows that energetic position of the maximums on the photoconduction spectrum for the sample In/$PbGaS_4$ doesn't depend on the external electric field and temperature (fig.3).

The observation of these defects connects with the realization in the base region of the structures of the complex (multicentral) recombinative model, including the *s*-channel of the intensive recombination, *r*-centers of photosensitivity, *t*-centers of majority carrier attachment [8].

As the *r*-centers are the photoactive, so they cause the more slow temp of electron recombination, and consequently the most time of their life

$$\tau_n = \frac{g_r}{C_{nr} P_r}$$

where $g_r \sim C_{pr} N_r$ realizes between regions of the temperature extinction of photocurrent (TEPh) and temperature activation (TAPh) and depends on the yield of the recombinative flux on *r*-channel ($g_r \leq 1$); C_{nr} and C_{pr} are the coefficients of the electron and hole capture by slow *r*-recombinative centers, N_r and P_r are concentrations of electrons and holes on *r*-levels at the illumination.

The intensity of the impurity band (fig.4), connected with *r*-centers is proportional to the value $\tau_n(3)$ under the condition $g_r=1$. They depend on the technology of crystal obtaining.

The regions of TAPh (100÷131K) and TEPh (131÷250K) are observed on the temperature dependence at the impurity excitation of monocrystal sample $PbGaS_4$.

At the temperature (131K), according to the photocurrent maximum, the main recombinative flux goes through r-centers. The further temperature decrease leads to the generation of the minority carriers from *r*-centers and promotes to the transition of these charges on *s*-centers, with the connection of which, the life time of the free electrons decreases and TEPh is observed.

Using the method, described in the ref [9], based on the experimental data, the energetic state of the *r*-centers of recombination, which is equal to 0,24eV, has been defined.

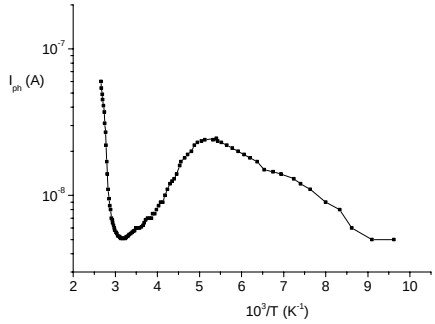

Fig.4. The dependence on the photocurrent temperature for $In/PbGaS_4$.

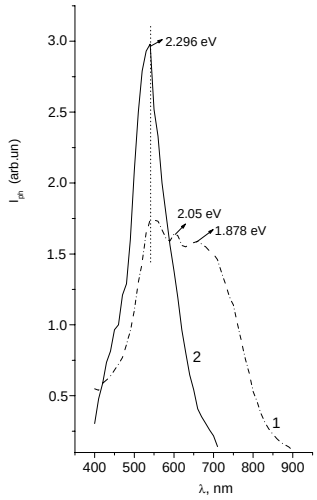

Fig.5. The photoconduction spectrums of $In/PbGaS_4$ before (1) and after annealing (2).

On the fig.5 the photoconduction spectrums before and after crystal annealing with and without sulfur atmosphere are presented. It is seen, that annealing leads to the disappearance of the another types of th defects besides the one. This proves the presence of the defective structure and in spite of the quantity of the defects this doesn't lead to the appearance of the secondary phase that is proved by differential-thermal (thermographical) analysis (fig.6).

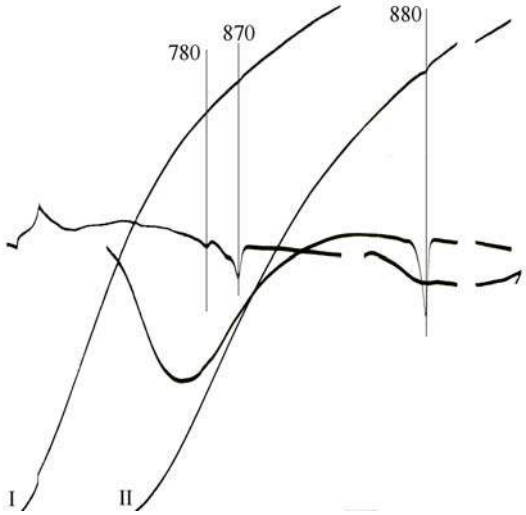

Fig.6. The thermographical spectrum of $PbGaS_4$ crystal before (I) and after annealing (II).

In the conclusion we can note, that photoelectrical active centers in $PbGa_2S_4$ and $PbGa_2Se_4$ can be intrinsic defects – vacancies of atoms of sulfur and selenium, correspondingly, appearing in the result of these atoms from the composition in the synthesis process. Quantity of these defects is correlated by the technological modes of crystal obtaining.

[1] *A.N.Georgobiani, S.I.Radautsan, N.M. Tiginyanu.* FTP, 1985 19, 193.

[2] *R.N. Bekimbetov, Yu.V. Rud, M.A. Tairov.* FTP, 1987 21, 1051.

[3] *B.G.Tagiev, O.B.Tagiev, R.B.Jabbarov, N.N.Musayeva.* Inorganic Materials, 1999, v.35, n.1, pp.33-35.

[4] *B.G.Tagiev, N.N.Musayeva, R.B.Jabbarov.* Semiconductors, 1999, v.33, n.1, pp34-36.

[5] *C.Charter, R.Jabbarov, M.Jouanne, J.Morhange, P.Benalloul, C.Barthou, J.Frigerio, B.Tagiev, E.Gambarov.* J.Phys.: Condens. Matter 14(2002)13693-13703.

[6] *S.Rizzini, N.Butta, M.Acciary, M.Acciari.* Springer Proc. in Phys., 1991 54, 178.

[7] *V.M. Golovey, L.A. Ivanchenko, A.S. Knyazev, V.A. Obolonchik, E.I. Troyan*. UFJ, 1981 т.26, №6, 1037-1039.

[8] *V.E. Lashkaryov, A.V. Lyubchenko, M.K. Sheykman.* Neravnovesnie protsessi v fotoprovodnikakh. Kiev, «Naukova Dumka», 1981, 264 c.

[9] *R. Byub.* Photoprovodimost tverdikh tel. M.: Izd-vo inostr. lit., 1962, 560 c.

N.N. Musayeva, O.B. Tağıyev, R.B. Cabbarov, İ.İ. Əliyev

$PbGa_2S_4$ (Se_4) TİPLİ FOTOHƏSSAS KRİSTALLARDA FOTOKEÇİRİCİLİYİN MEXANİZMİNİN ARAŞDIRILMASI

$In/PbGa_2S_4$ və $In/PbGa_2Se_4$ structurları yaradılmış və tədqiq edilmişdir. Müxtəlif temperaturlarda və tətbiq olunan gərginliklərdə spektral asılılıqlar qadağan olunmuş zolağın üzərində kristalın alınması zamanı əmələ gələn və özü-aşqarlama ilə əlaqədar olan lokal mərkəzlərin mövcudluğunu göstərir.

Н.Н. Мусаева, О.Б. Тагиев, Р.Б. Джаббаров, И.И. Алиев

ВЫЯСНЕНИЕ МЕХАНИЗМА ФОТОПРОВОДИМОСТИ У ФОТОЧУВСТВИТЕЛЬНЫХ КРИСТАЛЛОВ ТИПА $PbGa_2S_4(Se_4)$

Созданы и исследованы фоточувствительные структуры $In/PbGaS_4$ и $In/PbGaSe_4$. Спектральные зависимости фототока при разных температурах и приложенных напряжениях указывают на наличие локальных центров внутри ширины запрещенной зоны, связанных с самолегированием и возникающих в процессе получения кристаллов.

Received: 16.04.04

PLANT WITH THE ROTATING HEAT TRANSMITTING DISK ELECTRODE FOR ELECTROPHYSICAL INVESTIGATIONS OF THE CORROSIVE AND ELECTROCHEMICAL BEHAVIOR OF METALS

A.F. ALIYEV
Azerbaijan Power Research and Design Institute
Baku, G. Zardabi av.,94

Keywords: power engineering, electrophysics, electrochemical corrosion, heat transmission, cooling system, temperature, speed, simulation.

The laboratory plant has been worked out for electrophysical investigations of the electrochemical corrosion of metals under heat transfer and different movement speeds of electrolytes.

The plant simulates the operation conditions for the heat-exchangers` pipes and enables to elicit the heat transfer parameters` and the movement of the liquid`s impact to the corrosive and electrochemical behavior of metals in the electrolyte solutions.

Heat exchangers, in particular, used in cooling systems of the fuel and energy industry (condensers, compressors, etc.) are operating in conditions where metal and water are in contact under the heat transfer and the different speeds of movement of liquids.

As a rule, the heat exchanger pipes metals corrosive and electrochemical behavior is studied in static (no movement of liquid) and dynamic (liquid is mixed up) conditions under the thermal equilibrium, i.e. when the metal – electrode and the solution – electrolyte temperatures are the same.

However, the heat transfer surface (metal) temperature differs from the cooling (or warmed) liquid temperature in the heat transfer systems i.e. the metal - liquid interaction process is going on under the heat transfer. Mixing up of the liquid may not also correspond to the actual movement speeds observed in the heat exchangers.

To investigate the heat transfer and the liquid`s movement speed impact on electro- chemical behavior of metals, the plant with rotating heat transmitting disk electrode (fig.1) equipped with electronic speed governor and tacho-generator has been developed in the physico-chemical Institute named after L.Y. Karpov (Moscow) under the guidance of L.I. Freyman with collaboration of the author. Truncated cone (6^o) shape, 7 mm diameter and 6 mm height disk electrodes (fig.2) are used at this plant. The disks are pressed into the teflon shells with screw thread; aluminum washers are put into the shells to ensure sealing and electrical contact.

The shell with the heat transmitting disk electrode 1 is screwed on the lower hollow shaft 2 of the plant (Fig.1). Then the working surface of the disk is grinded by rotating the plant`s shaft according to the procedure [1].

Electrical contact of electrode with the shaft 2 through the aluminum washer, housing 3, brass rings 5 and copper-graphite brushes is used for polarization and measurement of the electrode potential.

Heat transfer is provided by hot glycerol from the double pump thermostat fed into the hollow shaft 2 through the coaxial double pipe 9 fixed immovably. Heat carrier is forced into the elongated inner pipe through the branch pipe 8 and is sucked off through the shorter outer pipe and branch pipe 7. Speed of suction exceeds speed of forcing in the thermostat thus preventing leakage of the heat carrier through the unsealed void between the double pipe 9 and the shaft 2.

Hollow shaft 2 together with the disk electrode 1 is put in motion by electric motor 4. Rotation is stabilized by tacho-generator 6.

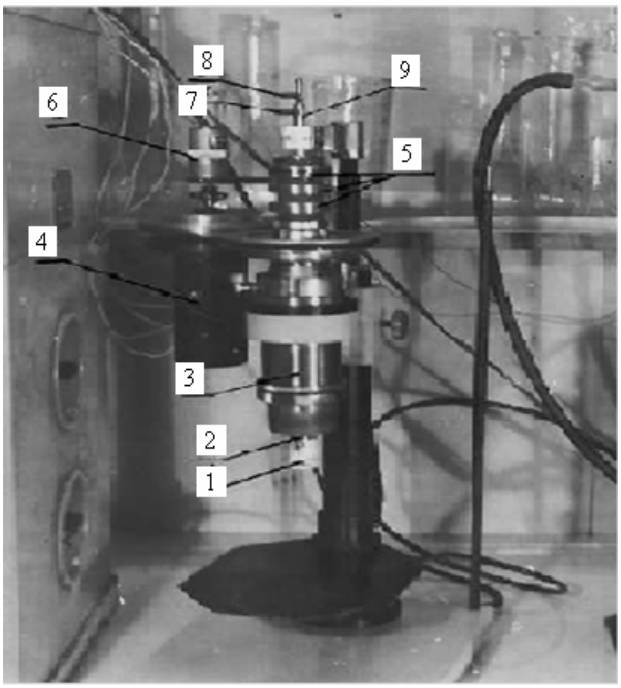

Fig.1. Plant with rotating heat transmitting disk electrode (without cell)

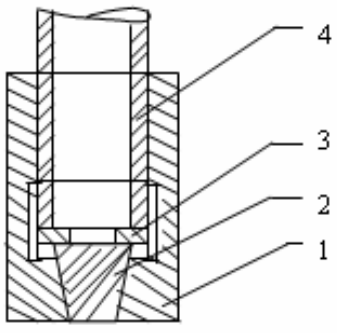

Fig.2. Heat transmitting disk electrode:
1 - teflon shell; 2 – disk electrode;
3 – aluminum washer; 4 – plant`s shaft

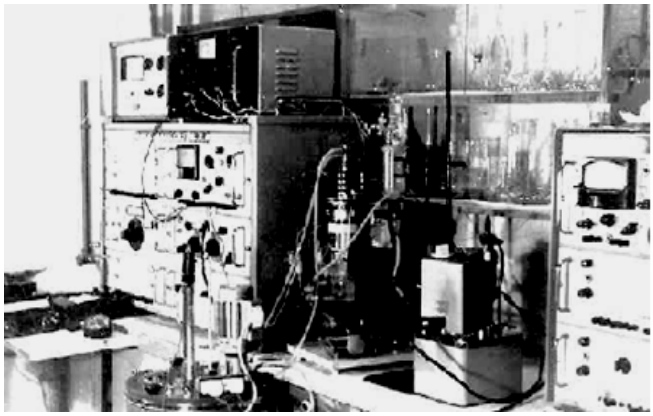

Fig.3. The plant for potentio-statical polarization measurement under the heat transfer and the rotation of the disk electrode with potentiostat, electronic speed governor, rotating heat transferring disk electrode unit, electro-chemical cell, the double pump thermostat forcing the heat carrier and the thermostat for heating of the cell.

To measure the heat carrier (glycerol) temperature directly at the warmed side of the disk electrode, a chrome-copper thermocouple is fixed inside the teflon shell (without strict contact with the electrode). The electrolyte`s temperature in the cell is maintained by the second thermostat with one pump. General view of the plant is shown on the fig.3. According to the laboratory simulation of the internal pipelines` corrosion [2], the diffusion layers on the viscously streamlined disk rotating with n rpm and at the inner side of the pipe (far enough from the inlet) have the same thickness under the average speed of the turbulent flow *U*, *m/s* if

$$U = 0{,}26\, Pr^{1/12}\, (\nu n)^{1/2},$$

where: ν is a kinematic viscosity in St; $Pr = \nu/D$ - the Prandtl criterion; D – diffusion coefficient (cm^2/s).

For example: $D \approx 1{,}0 \times 10^{-5}$ cm^2/s, $\nu = 3{,}8 \times 10^{-3}$ cm^2/s for Caspian sea water under 90^0C [3]. It appears in this case that 1000; 2000; 3000 and 4000 rpm of the disk angular speeds are corresponding to the 0,84; 1,19; 1,45 and 1,68 m/s of linear speeds of the liquid`s movement inside the pipes. Similar speeds are corresponding to the average speed of movement in the film evaporator of the Sea water [4].

The described Plant enabled electrophysical investigations of corrosive and electrochemical behavior of aluminum alloys in actual conditions of thermal desalination of the Caspian Sea water under the speeds of water movement and the temperature drops in dozens centigrade degrees in the metal – liquid system observed at practice.

[1] *L.I. Freyman, V.A. Makarov, I.E. Bryksin,* Potentiostatic methods in the corrosion investigations and electrochemical protection, Publishing House "Chimiya", Leningrad, 1972.

[2] *V.M. Novakovski*, Laboratory simulation of the pipelines` inner corrosion, "Metals protection", 1965, №2, p.224.

[3] *A.F. Aliyev.* Some problems of the Sea water film movement hydrodynamic parameters impact on the heat transfer, The 1st All-Union scientific and technical conference Reports on "Heat transfer and thermal and physical characteristics of the Sea and saltish waters used in steam-generators and water-distillers", Baku 1973, p.152.

[4] *A.F. Aliyev*. Heat transfer investigation on the Sea water film evaporator, Transactions of the A-URI "VODGEO", Moscow, 1970, 25 edition, p.41.

A.F. Əliyev

ELEKTROFİZİKİ TƏDQİQATLARI APARMAQ ÜÇÜN FIRLANAN İSTİLİK ÖTÜRÜCÜ DİSK ŞƏKİLLİ ELEKTRODLU QURĞU

İstilik ötürmə və mayelərin müxtəlif sürətləri şəraitində metalların elektro-kimyəvi korroziyasının elektro-fiziki tədqiqat işlərini aparmaq üçün laboratoriya qurğusu işlənib hazırlanıb.

Bu qurğu istilik mübadiləsi aparatların borularının istismar şəraitini modelləşdirir və elektrolit məhlullarda istilik ötürülməsinin parametrlərinin və mayenin hərəkətinə metalların elektro-kimyəvi korroziyasının özünü aparmasının təsirini aşkar etməyə imkan verir.

А.Ф. Алиев

УСТАНОВКА С ВРАЩАЮЩИМСЯ ТЕПЛОПЕРЕДАЮЩИМ ДИСКОВЫМ ЭЛЕКТРОДОМ ДЛЯ ПРОВЕДЕНИЯ ЭЛЕКТРОФИЗИЧЕСКИХ ИССЛЕДОВАНИЙ

Разработана лабораторная установка для проведения электрофизических исследований электрохимической коррозии металлов в условиях теплопередачи и различных скоростях движения жидкостей.

Установка моделирует условия эксплуатации труб теплообменных аппаратов и позволяет выявить влияние параметров теплопередачи и движения жидкости на коррозионно-электрохимическое поведение металлов в растворах электролитов.

Received: 14.05.04

THE CONDITIONS OF THE FULL ABSORPTION OF THE ELECTROMAGNETIC RADIATION OF THE TWO-LAYERED SYSTEM DIELECTRIC-METAL AT THE PRESENCE OF THE RESISTANCE TRANSFORMER

M.A. SADIKHOV, S.T. AZIZOV
Institute of Physics, Azerbaijan National Academy of Sciences
Baku, Az-1143, H. Javid ave., 33

Equations describing conditions of preferential non-reflecting (full) absorption of electromagnetic radiation into dielectric-metal system with covered arbitrary number of quarter-wave none-absorbing layers on it has been obtained. The Influence of such multilayer resistance transformer on band of preferential absorption of radiation is shown.

In the refs [1,2] the existence of the non-reflecting (full) absorption of the electromagnetic radiation in the plane two-layered system polar dielectric-metal had been theoretically predicted and experimentally proved. This effect appears in the dispersion region of the material of the dielectric covering at the discrete values of incident radiation wavelength λ_0, thickness l_0 of the reflecting layer of the covering. The obtained spectrum λ_0 and l_0 has a resonance character, it is individual for the covering substance and defined by its static and dynamical properties. The spectral values λ_0 and l_0 correspond to the appearing once so-called zero minimums of the dependence of the module of wave reflection coefficient ρ on the thickness l of composition layer. Moreover, the obtained values l_0 are close, but don't equal to the values, which are multiple once to the quarter - wave length λ_g in the dielectric covering. The specified theoretical and practical interest is the investigation of this phenomenon at the presence of the additional plane quarter-wave layers from the non-reflecting materials, which situate upper than the absorption dielectric of the two-layered system dielectric-metal [1,2]. The presence of such additional layers can influence on the selective absorption band of wave in the same way, as it is in the tasks of the optic's antireflection.

Let's consider the general task of the reflection of the plane-reflected wave, falling normally on the plane multi-layered system, which can be presented in the capacity of the two-layered absorption system dielectric-metal, connected with the air part of the radiation space with the help of resistance transformer, which in the general case presents by itself the m successively covered quarter-wave layers from the non-reflecting dielectrics. The transformation ratio of such layered resistance transformer is equal to

$$k = \left[\frac{Z_2, Z_4, Z_6 \ldots}{Z_1, Z_3, Z_5 \ldots}\right]^2 \qquad (1)$$

where Z_1, Z_2, ... Z_n are wave resistances of the direction system, filled by the materials of m successively applied layers of resistance transformer, accordingly.

The complex value of the wave reflection coefficient of the system, absorbing the dielectric-metal, taking into consideration the resistance transformer, is equal to

$$\rho = \frac{Zkth\ \gamma l - Z_0}{Zkth\ \gamma l + Z_0} \qquad (2)$$

where $\gamma = i\frac{2\pi}{\lambda}\sqrt{\varepsilon - p}$; Z, Z_0 are the wave propagation constant and the wave resistance of the directing system, filled by the material of the main absorbing layer; $\varepsilon=\varepsilon' - i\varepsilon''$; ε', ε'' -are values of the dielectric constant and dielectric loss of the material of the absorbing layer, accordingly; l is the thickness of the layer of the absorbing dielectric, $\rho = (\lambda/\lambda_{cr})^2$; λ-is the wavelength; λ_{cr} is the critical wavelength, defined by the measures of the directing system.

The values ε^I and ε^{II} of the absorbing coefficient, including in the equation (2), connect with its wave refraction coefficient n and factor of dielectric loss with the known ratios

$$\varepsilon^I = n^2 (1-y^2) ; \qquad \varepsilon^{II} = 2 n^2 y \qquad (3)$$

For the convenience of the later considering, let's introduce the mention of the given values of wave refraction coefficients n and factor of the dielectric loss y, which are differ from n and y in the case of the usage of the direction system, when value p differs from 0.

From the expressions for n, taking into consideration (3), it follows, that

$$n = \frac{n}{\sqrt{1 - p}} ; \quad y = tg\ \Delta/2 ; \quad \Delta = arctg\ \varepsilon'' /(\varepsilon' - p) \qquad (4)$$

where $n = \lambda_в/\lambda_g$; $\lambda_в = \lambda / \sqrt{1 - p}$ is the wavelength in the empty directing system and direction one, filled by the absorbing dielectric, accordingly.

Applying such output process that was in the ref [4] we obtain the following equations, defining the conditions of the full non-reflecting wave absorption in the considered multi-layered system.

$$\left.\begin{aligned}\pi(2N-1)+\operatorname{arcng}\frac{2nyk}{n^2(1+y^2)-k^2} &= \frac{1}{2y}\ln\frac{(k+n)^2+n^2\tilde{y}^2}{(k-n)^2+n^2y^2}\\ \frac{l}{\lambda_b} &= \frac{1}{kn}\left(\frac{2N-1}{4}+\frac{1}{4\pi}\operatorname{arctg}\frac{2nyk}{n^2(1+y^2)-k^2}\right.\end{aligned}\right\} \quad (5)$$

where N is the number of the zero minimum of dependence of ρ on l.

The equations (5) establish the connection between values n, y, N, at which in the considered multi-layered system the full non-reflecting wave absorption appears. At $p=0$ and $k=1$, they are equal by form with the analogical equations, obtained at the consideration of the conditions of the non-reflecting wave absorption in the two-layered system dielectric-metal in the free space.

The equation (5) doesn't take into consideration the change character with the frequencies ε', ε'' of dielectric material, which is the absorbing layer of the considered multi-layered system. For the concretization of the appearing conditions of the non-reflecting wave absorption for the real polar compositions, let's take into consideration, that their dielectric properties in the region of wave dispersion are well enough described by Debye equation

$$\varepsilon = \varepsilon' - i\varepsilon'' = \varepsilon_\infty + \frac{\varepsilon_0 - \varepsilon_\infty}{1 + i\omega\tau} \quad (6)$$

where ε_0, ε_∞ are extra dispersion statistic and high-frequency dielectric constants of composition; ω is circular frequency; τ is the relaxation time[3].

The combine solution of the equations(5) allows to find the functional connection between ε_0, ε_∞ and τ of material of the covering absorbing layer, wavelength λ_0, thickness l_0 of the covering absorption layer, transformation coefficient k, at which the non-reflecting wave-absorption in the multi-layered system will take place. For the finding of this connection the iterating process of the solution of the initial equations has been applied.

The results of the carried out calculations for the case of the first five zero minimums of function ρ(l) are given on the figure 1 in the generalized coordinate planes $\left[lg\ \omega\tau,\ \frac{l}{\lambda}\right]$ and $\left[lg\ \omega\tau,\ \varepsilon_0\right]$. Taking into consideration, that ε_∞ of the more polar compositions within 2-3 units, was equal to 2 at the carrying out of the given calculations. The obtained dependences ε_0 on $lg\omega\tau$ at different N of the zero minimum of the function $\rho(l)$, and their vertexes achieve to the value $\omega\tau=1$, according to the center of the dielectric dispersion region. The value l_0/λ_B increases with the increase of lg $\omega\tau$ and stabilizes at $\omega\tau>1$.

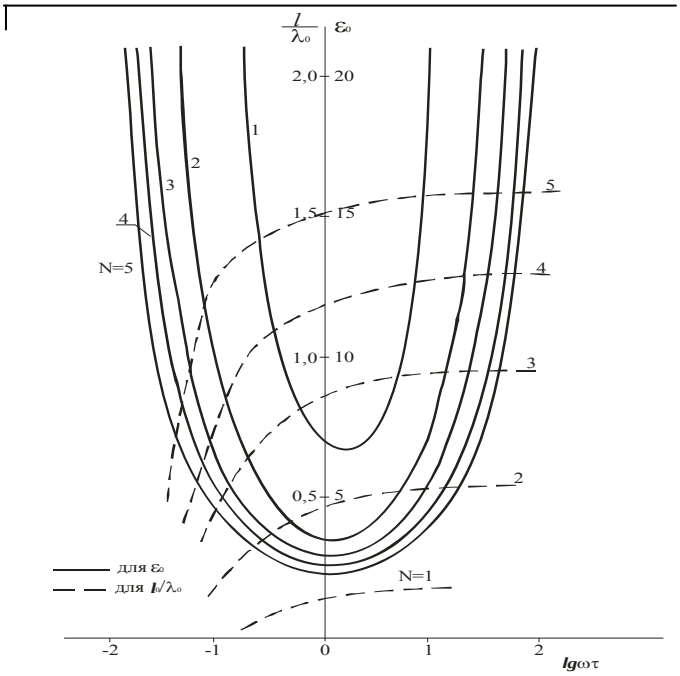

Fig.1. The dependence ε_0,ε_∞ and relaxational τ,ω characteristics of the selective wave absorption for the different numbers N of zero minimum of function $\rho(l)$.

As it follows from the fig.1, at the given N, ε_0, ε_∞ and τ can be two couples of values λ_0 and l_0, at which the conditions of non-reflecting wave absorption in the system dielectric-metal is carried out. The analysis of behaviour of functions ε_0, l_0/λ_0 on $lg\omega\tau$ shows, that in the dispersion region of composition should be the spectrum of wavelength and the spectrum of the thickness of reflecting composition layer, corresponding to it. The character of these spectrums is strongly individual for every composition and is defined by its statistic and dynamic dielectric properties. The spectrums consist on two branches: low-frequency and high-frequency, differing by only change character of values of spectral wavelengths with the increase of the thickness of covering composition layer, corresponding to it. For the low-frequency spectrum arm the increase of λ_0 with he increase of N accompanies by the increase of l_0. It is characterized, that dielectrics with small values ε_0 may have the degeneration of absorption spectrums because of the disappearance of their spectral lines, corresponding to first zero minimums of the function $\rho(l)$.

[1] *R.M. Kasimov.* Injenerno-Fizicheskiy jurnal, 1994, t.66, N 5-6.
[2] *R.M. Kasimov, M.A. Kalafi, E.R. Kasimov,Ch.O.Kadjar, E. Yu. Salaev*. Jurnal Texnicheskoy Fiziki, 1996, t.67, 2.s.167.
[3] *A.F. Xarvey.* Texnika Sverxvisokix Chactot. M.,1965.

M.A.Sadıxov,S.T.Əzizov

TƏRKİBİNDƏ MÜGAVİMƏT TRANSFORMATORU JERLƏŞƏN DİELEKTRİK-METAL İKİLAYLİ SİSTEMİNDƏ ELEKTROMAGNİT ŞÜALANMASININ ŞƏRTLƏRİ

İki laylı dielektrik-metal sisteminin üzərinə dörtdəbir dalğa layı olan əks etdirməyən layları çəkilmiş əks etdirməyən (tam) udulmasının şərtlərinin tənlikləri alınıb. Bu çox laylı mügavimət transformatorun seçilmiş udulma zolağına tə'siri qöstərilib.

М.А. Садыхов,С.Т.Азизов

УСЛОВИЯ ПОЛНОГО ПОГЛОЩЕНИЯ ЭЛЕКТРОМАГНИТНОГО ИЗЛУЧЕНИЯ ДВУХСЛОЙНОЙ СИСТЕМЫ ДИЕЛЕКТРИК-МЕТАЛЛ ПРИ НАЛИЧИИ ТРАНСФОРМАТОРА СОПРОТИВЛЕНИЯ

Получены уравнения, описывающие условия избирательного безотражательного (полного) поглощения электромагнитного излучения в системе диэлектрик - металл с нанесенным на него произвольным числом четвертьволновых непоглощающих слоев. Показано влияние такого многослойного трансформатора сопротивления на полосу избирательного поглощения излучения.

Received: 21.06.04

INVESTIGATION OF THE Al-Mn ALLOY ELECTROCHEMICAL BEHAVIOUR IN THE CASPIAN SEA WATER UNDER DIFFERENT MOVEMENT SPEEDS AND HEAT TRANSFER CONDITIONS

A.F. ALIYEV
Azerbaijan Power Research and Design Institute
Baku, G. Zardabi av., 94

Key words: power engineering, electrophysics, electrochemical corrosion, aluminum alloys, sea water, heat transfer, cooling system, desalination of water.

Different speeds of movement and heat transfer parameters impact on electrochemical behaviour of aluminium alloy in the Caspian Sea water has been investigated including also methods used to prevent scaling by acidification of water and injection of anionic surfactants. It was found that increase in speed up to 2 m/s is the favourable stability factor against the pitting corrosion and the heat transfer through the surface under the temperature drop up to 90°C / 140°C at the metal-liquid system doesn't lead to dangerous contraction of passive area, i.e. is safe from the rise of the pointed-pitting corrosion standpoint.

Caspian Sea water is often used in the Fuel and Energy and Oil and Gas extractive industry Units' cooling systems due to deficiency of fresh water in the Caspian regions of Azerbaijan, Kazakhstan and Turkmenistan. Moreover, heat transfer surfaces, as a rule, are made of costly alloys on the base of copper (cupronickel, brass, bronze) and stainless steels.

Decrease in prime cost of Units and production is possible provided replacement traditionally used materials by some considerably cheaper and available aluminium alloys which are almost 3 times lighter and 5-6 times cheaper than the copper ones of the same size.

Corrosive and electrochemical characteristics as well as protective effect mechanism for number of aluminum alloys during thermal desalination of Caspian water have been studied under heat balance and intermixing of medium [1-6], i.e. when the metal-electrode and the solution-electrode temperatures are the same. However, the heat transfer surface (metal) temperature differs from the cooling (or warmed) liquid medium temperature in the heat transfer systems, i.e. the metal-liquid interaction process is on, under the heat transfer. Mixing up of the liquid may not also correspond to the actual speeds of movement observed in the heat exchangers.

According to the procedure [7] the anodic potentio-static polarization curves have been read from the three-electrode cell made of pyrex-glass with electrode spaces for divided by taps, at the laboratory plant with rotating heat transfer disk electrode. Disk electrodes have been made of the Al-Mn alloy (1,0 – 1,4 % Mn; 0,2 – 0,5 % Mg, everything else is of – Al) – which is one of the most corrosion resistant alloys to sea water [1 – 6]. Natural Caspian sea water from the Absheron seacoast has been used as an electrolyte (total salt content is apprex. 13g/l ; Cl^- ≈ 5,35 g/l; SO_4^{2-} ≈ 3,1 g/l; $(Ca^{2+}+Mg^{2+})$≈80,0 mg-ekv/l; $(HCO_3^- + CO_3^{2-})$≈4,0 mg-ekv/l; $(Na^+ + K^+)$≈3,4 g/l.

Model aluminum or it's alloy anodic potentio-static polarization curve in the sea water is shown on the fig.1. As it is seen, there is no active dissolution area on this curve and metal is in passive state when corrosion potential is (φ_{cor}). As soon as definite pitting-formation potential (φ_{pf}) is achieved, drastic rise in anode current is registered, caused by local breach of passivity and formation of pittings.

According to general theory of this process offered by Ya.M. Kolotirkin [8], migratory accumulation of activated anions takes place by the most active parts of the metal surface. When $\varphi=\varphi_{pf}$ the anions force out the passivated oxygen and take part in the local dissolution process (as catalyst) at this places. Passive area width is defined by the $\Delta\varphi_p = \varphi_{pf} - \varphi_{cor}$ difference during the anodic polarization. Potential at which the direct and back stroke anodic curves are intersected is defined as the pittings repassivation potential (φ_{rp}). Density of anodic current in passive area i_p corresponds to the metal corrosion speed in current units.

According to the published works [9,10] formation of pitting could not happen in the $\varphi < \varphi_{rp}$ area, arose pittings may develop and formation of pittings could happen during sufficient time delay in the $\varphi_{rp} \le \varphi \le \varphi_{pf}$ area and pittings arise practically at once in the $\varphi > \varphi_{pf}$ area. Development of pittings which are already arose will be stopped only in case if the potential becomes lower than φ_{rp}.

Thus, location of φ_{cor} potential regarding φ_{pf} and φ_{rp} potentials defines, in essence, the stability to the pitting corrosion. Movements speed impact on parameters of the Al-Mn alloy anodic polarization curves is studied in the sea water warmed up to 90^o C under the disk electrodes rotation speeds of 1000, 2000, 3000, 4000 rpm that corresponds to the linear speeds of the liquid movement of 0,84; 1,19; 1,45 and 1,68 m/s inside the pipe.

Electrochemical measurements have been made in the thermostatic three-electrode cells made of pyrex glass with electrode spaces divided by taps. Investigated heat transmitting disk electrode has been placed in the middle part of the cell and connected to the reference electrode by Luggin capillary. Platinum has been used as an auxiliary electrode (AE) and silver chloride in the saturated solution of KCl – as a reference electrode.

The cells had plane bottom enabling mixing up of solution by MM – 3 type magnetic mixer when necessary. Working volume of the cell (investigated electrode's section) is 50 ÷ 100 sm^3, quantity of solution in it is 20 ÷ 50 sm^3.

Polyethylene hose connected the cell to the vessel for preparation of solution, equipped by casing for thermostating purpose like the cell itself. U-1, U-10, LP-201, TC-16

thermostats have been used for thermostatting. The thermostat's liquid is distilled water (up to 90°C) or glycerol (over 90°C).

Investigated disk electrodes have been made of aluminum alloy reds pressed into the teflon. To avoid gap effects, close fitting to the insulating material's metal had been carefully checked.

Before experiment the disk electrodes have been cleaned out by fine files of different numbers with consecutively decreasing size of the abrasive grains, degreased by ethyl alcohol, washed by distilled water and working solution.

Polarization curves have been taken based on steady-state corrosion potential (φ_{cor}) after 1-2 hours following immersion of the electrode. The potential have been changed by 10 – 30 mV steps with 2 – 3 min time delay per step. The delay have been extended up to 10 – 20 min nearly the pitting formation potential φ_{pf} (when potentials were approx. 100 mV lower than φ_{pf}). To take cathode curves the polarization have been stopped at potentials 0.5 – 0,6V lower φ_{cor}. Each polarization curve have been taken 3–6 times. Findings have been averaged.

Taking into consideration the recommendations [5, 6], stability to pitting have been estimated according to conventional width of passive area $\Delta\varphi_p=\varphi_{pf} - \varphi_{cor}$, i.e. according to potentials interval higher φ_{cor}, where metal is passive as well as according to difference between repassivation potential and corrosion potential ($\varphi_{rp} - \varphi_{cor}$) i.e. according width of the area where pittings could not happen; to measure the pittings repassivation potential (φ_{rp}) after the current density achieves approx. 10^{-3} A/sm^2 during the anodic activation process, polarization have been changed in the opposite direction and back stroke anodic polarization curve have been taken with the same speed until intersection with the part of the direct stroke curve corresponding to the passive area.

Time delay per each potential have been extended up to 5–7 minutes nearly φ_{rp}. Results of the φ_{rp} measurement by potentio-static method (potential shifting speed is 20mV/min) are the same.

Findings (fig.2) show that along with increase in the disk rotational speed the corrosion and repassivation potentials are changing a little like the corrosion current in the passive area, passive area $\varphi_{rp} - \varphi_{cor}$ width exceeds 200 mV all over the investigated liquid speeds' range (the potential values are shown reduced to the n.h.e. – normal hydrogen electrode). Along with increase in rotation speed up to 2000 rpm, the φ_{pf}, potential is shifting into the passive side (that is in conformity with data [11] for aluminum in the (NaCl) solution at 110 mV); further increase in the electrode rotation speed shifts the φ_{pf} into the more negative values' side, however this potential is more positive than in the static conditions ever when n = 4000 rpm.

Experiments with disk electrodes have been made under heat transfer conditions with n = 1000 rpm (0,84 m/s). Presented in the table are the parameters of received anodic polarization curves competitive to the relevant characteristics under the heat balance.

As it seen from the table, if there are no descalers in the water, the corrosion speed and pittings repassivation potential are unchangeable under heat transfer through the disk, φ_{cor} potential is shifted first 30 mV into the negative side under the temperature drop of 120° C/90° C and then 90 mV – into the positive side under the temperature drop of 140° C/90° C. φ_{pf} Potential is shifted into the negative side maximum 100mV under the temperature drop of 140° C/90° C, however $\Delta\varphi_p$ (0,28V) and $\varphi_{rp} - \varphi_{cor}$ (0,21V) values are quite sufficient to avoid pitting corrosion in this case.

Under the temperature drop of 140° C/90° C and the electrode rotation speed of 1000 rpm the anodic polarization curves have been also taken in the modes of scale prevention by acidification of water by sulfuric acid ($5,7 \le pH \le 6,3$) and injection of 100 mg/kg of anionic surfactant – sulphonic carbonate acid dysodium salt.

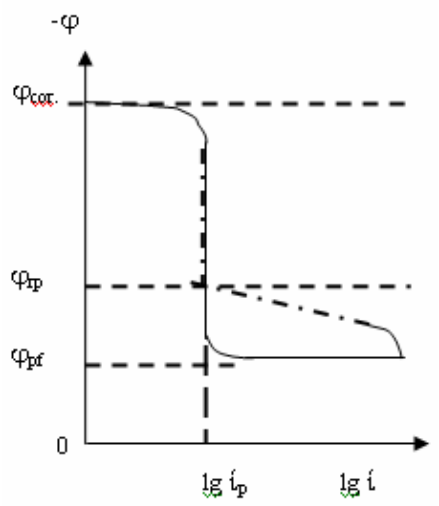

Fig.1. Schematic anodic potentio-static polarization curve of direct (——) and back (– · · –) stroke for aluminium and its alloys in the Caspian sea water.

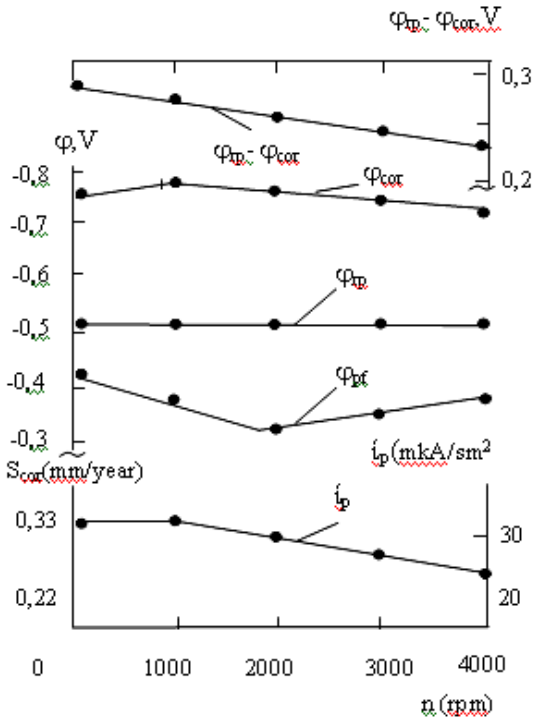

Fig.2. $\varphi_{rp} - \varphi_{cor}$, φ_{cor}, φ_{rp}, φ_{pf} and dependences of the Al-Mn alloy in sea water under 90°C on disk electrode rotation speed.

Acidification itself shifts φ_{cor} to 40 mV into the negative side and φ_{pf} to 30 mV into the positive side under some increase

of corrosion current in the passive area (from 28 up to 50 mkA/cm^2). Injection of surfactant shifts φ_{cor}, to 80 mV into the negative side and φ_{pf} to 100mV into the positive side increasing significantly the passive area width $\Delta\varphi_{pf}$. Thus, the alloy corrosion speed decreases 17,5 times (from 28 to 1,6 mkA/sm^2).

Pittings repassivation potential is unchangeable in the scale prevention modes mentioned, however φ_{pf} - φ_{cor} and φ_{pf} - φ_{rp} values are increased 70 and 30 mV accordingly in case of acidification and 180 and 100 mV accordingly – in case of descaler injection (anionic surfactant) due to change of φ_{cor} and φ_{pf}. So, from the stability to pitting corrosion standpoint, movements of the sea water is a favorable (factor) facilitating removal of the metal dissolution products out of metal surface. As a result, the, φ_{pf} potential is more positive in dynamic conditions than in static conditions. Heat transfer through the surface doesn't lead as well to the dangerous contraction of passive area especially when descaler (anionic surfactant exists).

Table

Corrosion potential and parameters of anodic polarization curves for the Al - Mg alloy in the sea water under the heat balance and the heat transfer conditions (n = 1000 rpm)

Measurement conditions	φ_{cor}, V	φ_{pf}, V	φ_{rp}, V	$i_p \cdot 10^5$, A/sm^2	$\Delta\varphi_p$, V	φ_{rp}-φ_{cor}, V	φ_{pf}-φ_{rp}, V
Heat balance, 90^o C	-0,79	-0,35	-0,52	3,0	0,44	0,27	0,17
Heat transfer, 120^o C/90^o C	-0,82	-0,43	-0,52	3,2	0,30	0,30	0,09
Heat transfer, 140^o C/90^{o}C	-0,73	-0,45	-0,52	2,8	0,28	0,21	0,07
The same in acidified sea water (5,7 ≤ pH ≤ 6,3)	-0,77	-0,42	-0,52	5,0	0,35	0,25	0,10
The same in the sea water with 100 mg/kg of anionic surfactant additive	-0,81	-0,35	-0,52	0,16	0,46	0,29	0,17

[1] A.F. Aliyev. Investigation of influence of temperature and Caspian Sea water compositions on corrosion and electrochemical behavior of some alloys. Transaction of the A – URI "Vodgeo". Moscow, 1974, 45 edition, p.103-115.

[2] *A.A. Abdulla-zade, A.F. Aliyev.* Some ways of Efficiency Increasing of Sea Water Desalination by Distillation, Reprinted from Proceedings of the Second World Congress. Intern. Water Resources Association, New Delhi, December, 1975, vol.3. p. 73-75.

[3] *A.F. Aliyev.* Corrosion and electrochemical behavior of aluminum alloys in Caspian sea water thermal desalination in accordance to the methods of scaling prevention. Transaction of the A – URI "Vodgeo". Moscow, 1975, 53 edition, p. 63-73.

[4] *A.F. Aliyev*, *L.I. Freynman.* Investigation of electrochemical behavior of aluminum alloys in Caspian Sea thermal desalination plants working condition. "Metal protection" Moscow, 1976, №4, p. 387-392.

[5] *A.F. Aliyev*, *L.I. Freynman.* Investigation of impact of water rewime parameters of Caspian Sea distillation plants on electrochemical behavior of aluminum alloys. The II All – Union scientific and technical conference Reports on "Utilization of sea and saltish waters on TES and problems of scientific investigation". Baku, 1976, p.230-233.

[6] *A.F. Aliyev*, *L.I. Freynman, A.A. Abdulla-zade.*, Investigation of anionic surfactants impact on corrosion and electro-chemical behavior of aluminum alloys in thermal desalination of Caspian Sea. The II All – Union conference reports on Utilization of Sea and saltish waters on TES and problems of scientific investigation. Baku, 1976, p. 233-235.

[7] *L.I. Freynman*, *V.A. Makarov, I.E. Briksin.* Potentiostatic methods in the corrosion investigations and electrochemical protection. House "Chimiya", Leningrad, 1972.

[8] *Ya.M. Kolotirkin.* The pitting corrosion of metals "Chemicheskaya promishlennost", Moscow, 1963, №9, p. 678.

[9] *R.A.Bonewits*. «Corrosion» (USA), 1973, 29, №6, 215.

[10] R.A. Bonewits. The Intern. Corrosion Forum Devoted Exclusively to the Protection and Performance of Materials. March 19-23, 1973, Anaheim, Calif, Paper №66.

[11] *F. Frans, P. Novak*. Sponsored by the National Association of Corrosion Engineers (Dec. 6-10, 1971), Williamsburg, Virginia, USA, 576.

[12] *L.I. Freiman, Lap Le Min*. Z.phys. Chem. (Leipzig), 1973, 252, № 12,65.

[13] *I.L. Rozenfeld*. Corrosion and metal protection. (Local corrosion processes) House "Metallurgiya", Moscow, 1970, p. 292.

A.F. Əliyev

DİNAMİK İSTİLİK ÖTÜRMƏ ŞƏRAİTİNDƏ XƏZƏR DƏNİZİ SUYUNDA ALÜMİNİUM ƏRİNTİSİNİN ELEKTROKİMYƏVİ CƏHƏTDƏN ÖZÜNÜ APARMASI

Xəzər dənizi suyunda müxtəlif hərəkət sürətlərinin və istilik ötürmə parametrlərinin alüminium ərintisinin elektro-kimyəvi təsiri, o çümlədən suyun turşusunu artırmaqla və anionlu səthi-aktiv maddələrin daxil edilməsi üsullardan istifadə olunması tədqiq edilib.

Müəyyən olunmuşdur ki, 2 m/s – dək sürətin artması, pitting-korroziyasının dayanıqlığı ücün əlverişli amildir, amma səthdən istilik ötürmə maye-metal sistemində temperaturun 90 ºC / 140 ºC – dək dəyişilməsi passiv sahənin təhlükəli daralmasına gətirmir, yəni nöktəli-yaralı korroziyanın əmələ gəlməsinə təhlükə yaratmır.

А.Ф. Алиев

ЭЛЕКТРОХИМИЧЕСКОЕ ПОВЕДЕНИЕ АЛЮМИНИЕВОГО СПЛАВА В КАСПИЙСКОЙ ВОДЕ ПРИ ДИНАМИЧЕСКИХ УСЛОВИЯХ ТЕПЛОПЕРЕДАЧИ

Исследовано влияние различных скоростей движения и параметров теплопередачи на электрохимическое поведение алюминиевого сплава в каспийской морской воде в том числе при использовании методов предотвращения накипи подкислением воды и введением анионных поверхностно-активных веществ. Установлено, что увеличение скорости до 2 м/с является благоприятным фактором устойчивости к питтинговой коррозии, а теплопередача через поверхность при перепаде температур в системе жидкость-металл до 90^{o} C / 140^{o} C не приводит к опасному сужению пассивной области, т.е. не представляет опасности с точки зрения возникновения точечно-язвенной коррозии.

Received: 14.09.04

THE OPTICAL PROPERTIES OF Fe:$LiNbO_3$

TALAT R. MEHDIYEV
Institute of Physics, National Academy of Sciences of Azerbaijan
Baku, Az-1143, pr. H. Javid, 33

The present paper is the continuous of publications of complex of optical properties investigations, which are perspective for the practical additions of nonlinear crystals of $LiNbO_3$+0,03%Fe with the aim of the usage in the systems of transmission, reception, treatment and storage of the optical information.

After the recording of the interference figure of the interaction of two plane waves in lithium niobate, he can be considered as a crystal, the index of refraction of which is periodic function.

$$n^2(z) = n_0^2\left(1 + 2\sum_{m=1}^{\infty} x_m \cos\left(\frac{2\pi}{\Lambda} mz\right)\right) \qquad (1)$$

If the crystal thickness us more than the sizes of the recorded interference figure, so the hologram will have the properties of three-dimensional diffraction grating. Thus, the plane wave propagation along the trajectory is in the conditions of the periodic modulation of the lateral component of wave vector k_x and consequently, the longitudinal component k_z, connected with it by ratio $k_x^2+k_z^2=k_0^2n^2$. The TE-wave amplitude, propagating in the medium, the index of refraction of which is defined by the expressions (1), satisfies to the Hill equation [5]:

$$\frac{d^2u}{d\varsigma^2} + \left(\theta_0 + 2\sum_{m=1}^{\infty} \theta_m \cos(2m\varsigma)\right)u = 0,$$

the solution of which, according to Flow theorem, can express in the form $u(\varsigma) = Ae^{-\frac{i\delta\varsigma}{n}} f(\varsigma) + Be^{\frac{i\delta\varsigma}{n}} f(-\varsigma)$, where δ is the some characteristic constant, $f(\zeta)$ is the periodic (with period π) function and $\varsigma = \left(\frac{\pi z}{\Lambda}\right), \theta_0 = \left(\frac{2\Lambda}{\lambda}\right)^2, \theta_m = X_m\theta_0$.

After substitution of the decomposition $f(\zeta)$ in Fourier series in (2), the characteristic constant δ is defined from the solutions of equations $\Delta(\delta)=0$ or

$$\sin\left(\frac{\delta}{2}\right) = \pm\sqrt{\Delta(0)}\sin\left[\left(\frac{\pi}{2}\right)\sqrt{\theta_0}\right], \text{ in which}$$

$$\Delta(\delta) = \frac{1}{\theta_0 - 4n^2}\left[\left(2n - \frac{\delta}{\pi}\right)^2 f_n - \sum_{m=\infty}^{\infty} \theta_m f_{n-m}\right] = 0,$$

$\Delta(\delta)$ is Hill determinant. It is easy to note, that in the general case at $\delta=0$, the necessity in the calculations of the determinant of infinite dimension matrix. However, for the case $\theta_0 \approx 1$ the approximated solution (6) shows that periodic medium under the condition $\left|\lambda - \lambda_0\right| < \frac{2\left(\left[\Delta_0(0)\right]^{1/2} - 1\right)\lambda_0}{\pi}$ behaves itself as Bragg reflector and diffraction, propagating in wave crystal, will be described by Bragg reflective angles, correspondingly. It is noted, that z axis situates parallel to vector difference vector ($\boldsymbol{k_1} - \boldsymbol{k_2}$), where $\boldsymbol{k_1}$ and $\boldsymbol{k_2}$ are the wave vectors of two plane waves.

From the other side, the effects, connected with the attenuation of the luminous radiation, which is caused by the scattering, caused by the density fluctuations on the microscopic and atom levels, and absorption, and geometrical distortions of form, thickness and etc. also. For example, in the case of lithium niobate crystals, the space-time changes of the coefficient of refraction, appearing under the action of incident light, depending on its wavelength and intensity, lead to the trajectory change of the luminous beam propagation, geometrical sizes and form of output light spot. The last circumstance is demonstrated in the fig.2 by the intensity propagating in the region of output light spot, the maximum of which in the limits of general accuracy, should be situated in the center. It is clear, that all characteristics of incident light on crystal, were stable during the time of experiment carrying out, the influence of external factors, which can influence on the investigation results, is equal to zero. Thus, it is followed from the figures 1,2,3 and, 4 the consideration of space-time changes of index of refraction, kinetics of scattering and transmission processes, is the obligatory condition in the optical experiments with given crystal. It is need to note, that change of angle of incidence of light from 0 till $\pi/3$, leads to the decrease of the scattered light intensity, at the same moment as scattering indicatrix doesn't change. This statement is stable till the crystal thickness is less than $3\text{-}4\mu$. In the other case, maximums of intensity of scattered light to 0 and π and scattering indicatrix becomes more diffusive.

As forms of curves of coefficient of refraction change are close to Gaussian profile, so it can be proposed that

$$n^2(\rho, z, t) = n_z^2 f(t) e^{-\frac{bp^2}{n_0}} \qquad (2)$$

where $\rho = x^2+y^2$, $f(t)$ is function on time, b is some constant, n is coefficient of refraction.

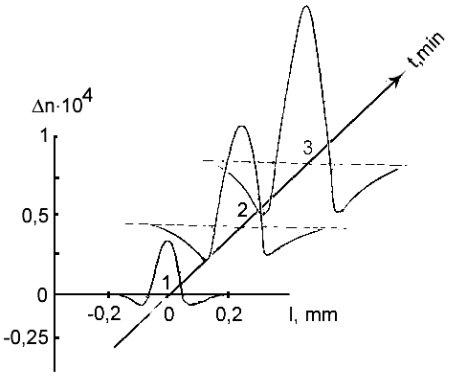

Fig.1. Space and time dependencies (t=1,2,3 min.) of the change of coefficient of refraction in lithium niobate crystals.

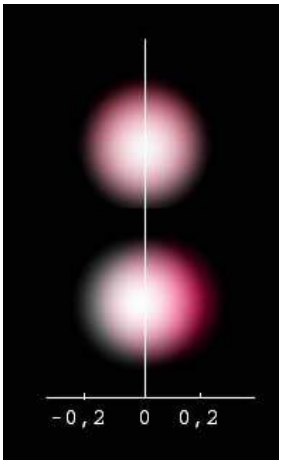

a

b

Fig.2. The time changes of the form and distribution of the intensity in the output light spot region in lithium niobate crystals (*a* – *t=0*; *b* – *t = 2* min).

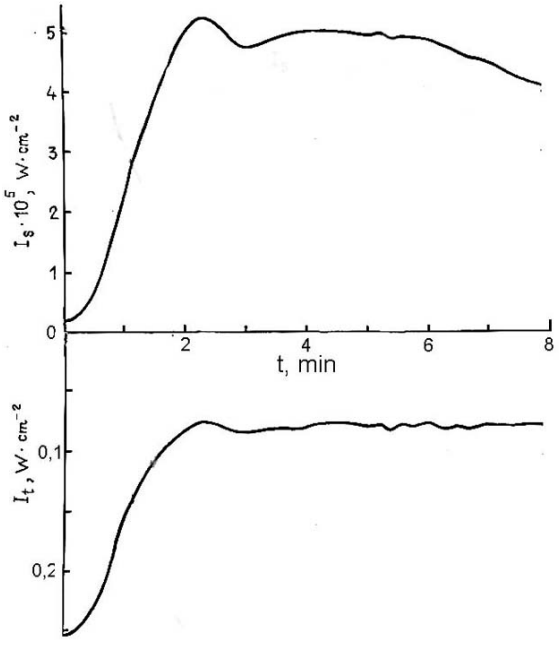

Fig.3. The time changes of transmission (I_t) and scattering (I_t) of the light in $LiNbO_3$ +0,03%Fe ($L=2\mu$, thickness of the sample is 2mm, $\lambda = 440$ nm).

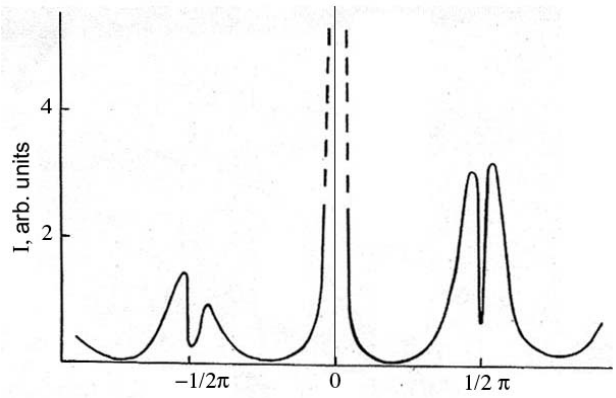

Fig.4. The scattering indicatrix (I_s) for $LiNbO_3$ +0,03%Fe ($L=2\mu$, the thickness of the sample is 2mm).

Taking into consideration, that the index of refraction of crystal doesn't depend on x and y, i.e. we consider unlimited layered medium, and at z =-∞ $u_i = e^{-i\vec{k}_0 n_0 (z\cos\theta + x\sin\theta)}$ also, the field has the form of plane wave u_i, propagating under the angle θ to z axis: $x = x_0 + \int_{z_0}^{z} \frac{adz'}{\sqrt{n^2(z) - a^2}}$. The trajectory of any beam in the Cartesian coordinates for the considered case can be recorded in the form, where z_o and x_o are coordinates of the trajectory point, $a = n_0 \sin\theta$ .The observable inclinations are well described by the given approach till the crystal thickness isn't so bigger, than the sizes of recorded interference figure. From the other side, such approach doesn't take into consideration this fact at all, that as of light propagation in the crystal, the intensity of the interacted pencils of light change because of the their interaction with the recorded holographic lattice by them. Such dynamic process leads to the essential coordinate dependence of amplitude and phase of the recorded lattice. According to the ref [2], the phase difference of two interacted pencils change thus, that surfaces of maximal and minimal change of the index of refraction generally stop to be the planes. However, if phase shift is equal to 0 and π, inspite of the unequal to 0 value of the diffraction efficiency, the intensity of the recorded pencils on the crystal output doesn't change. For the case of phase shift, which is equal to $\pi/4$, the recorded lattice has the alternating contrast on the crystal thickness. In many cases, after the recording of the interference figure in lithium niobate crystals (by the thickness, satisfying the condition $(2\pi\lambda z)/(nL^2)>10$ [1], where L is the constant of holographic lattice), the obtained holographic lattice can be related to the phase volume one. The limiting recording density for the volume holograms is estimated by the dependence of the diffraction efficiency on the inclination from Bragg angle. At the small intensities, this dependence well coincides with the estimate, given in the ref [1], $\Delta\theta \approx L/z$. The further increase of the diffraction efficiency is accompanied by the broadening, connected with the presence of the efficiency nonhomogeneous on the crystal thickness. The more big the z value, the more big the nonhomogeneous and the broadening also. In the case of the $LiNbO_3$ +0,03%Fe crystal ($L=2\mu$, sample thickness-2mm) the reason of the nonhomogeneous can be energy exchange [3,10] between recorded beams, at which the contrast of interference figure changes (because of the change of phase F

and oscillating character η).From the other side, as it is followed from the analysis of time changes of transition and scattering. The big value has the exposition time of recorded hologram on this crystal. The value of crystal absorption at the above mentioned parameters, in the region 440nm near 1,5 sm^{-1} and the peculiarities of angular selectivity of diffraction efficiency also weak dependence from this process. The obtained experimental dependencies of the diffraction efficiency on the value of phase shift and angle of reading information for $LiNbO_3$+0,03%Fe are presented on the fig.5,6.

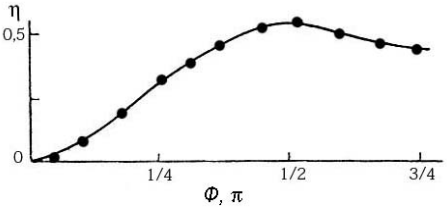

Fig.5 Dependence of diffraction efficiency η on phase displacement angle.

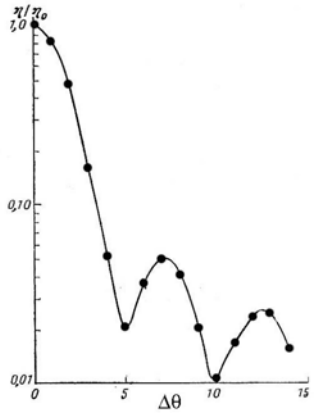

Fig.6 Dependence of diffraction efficiency η/η_0 on angle of reeding information of holographic lattice in the crystal $LiNbO_3$ +0,03%Fe ($L=2\mu$, sample thickness is 2mm, η_0=20%).

They are well accord to the results of the ref [3].

The theoretic model, taking into consideration the nonlinear dynamic processes at the recording of the stationary holographic lattices with the taking into consideration of diffusion and drift of photocarriers, change of crystal dipole moment in the result of the elimination, was introduced in the ref [4]. The change of crystal ΔP, dipole moment, appearing in the generation and recombination processes of current carriers, was taken into consideration phenomenologically in the prediction, that it is proportional to the concentration change of the charged centers, i.e. in the form: $\Delta\vec{P} = \vec{d}(N_D^+ - N_A)$. The connection of dipole moment change only with the change of the charge impurity state, probably doesn't correct at all. It is possible to show, that absence of the consideration of ion arrangement relatively each other changes neglible few the value of sum crystal dipole moment. The questions, connected with the change nature of crystal dipole moment, were discussed in refs [5,6] and as analysis of the given experimental results show, the nature of these changes for the pure crystals and crystal with impurity is different. In our case we consider $LiNbO_3$ with impurity 0,03%Fe, and the expression application (fP_s), where $\alpha^*(fP_S)$ -is impurity polarizability; f- is Lorentz factor; (fP_s) is the macroscopic field; &(*)(fP_s) is the impurity dipole moment. For the case of shallow impurities: $f=0$. Thus, deposit in the polarizability change will be put by the deep levels. As at the homogeneous elumination of short-circuit crystal the macroscopic field has tendency to the zero, so dipole moment changes connect with the change of the polarizability and deformation of the space region near impurity atom. Experimentally, the dipole moment value can be defined, measuring the polarization currents [8]. The obtained results are well correspond with the ones, given in the ref [6] and P_s value is equal to 0,71 cm^{-2}. All above mentioned allows to take into consideration the time changes of dielectric constant. They can be easily obtained from the experiments, given not only in the present publication, but in the refs [3,5,6,7] also.

[1] *H. Kogelnik.* The Bell System Technical Journal, 1969, 48,9, 2009.
[2] *V.L.Vinetskii, H.V.Kukhtarev.* I drPreprint IFAN USSR, 1976, №14.
[3] *V.B.Markov, S.G.Odulov, M.S. Soskin.* Izv. AN SSSR, 1977, v.41, №4, 821.
[4] *V.L.Vinetskii,N.V.Kukhtarev,V.B.Markov,C.G.Odulu v,M.S.Soskin.* Izv.AN SSSR, 1977, t.41, №4, 811.
[5] *T.R. Mehdiyev* Fizika, 2002, VIII, 4, 50-56.
[6] *T.R. Mehdiyev* Fizika, 2003, IX, 1, 31-34.
[7] *D.L. Staebler, J.J. Amodei,* J.Appl. Phys., 1972,43,1042.
[8] *V.V. Voronov, P.V. Ionov.* FTT, 1976, 18, 28.

Tələt R. Mehdiyev

Fe:$LiNbO_3$-ÜN OPTİK XÜSUSİYYƏTLƏRİ

Təklif olunan iş praktik tətbiqlərdə böyük perspektivi olan qeyri-xətti $LiNbO_3$+0,03%Fe kristallarının optik xassələrinin kompleks tədqiqinə həsr olunmuş işlərin davamıdır.Tətqiqatlar optik məlumatı xaricə yayan, qəbul edən, yenidən işləyən və özündə saxlayan sistemlərdə istifadə oluna bilmək məqsədini daşıyır.

Талат Р. Мехтиев

ОПТИЧЕСКИЕ СВОЙСТВА Fe:$LiNbO_3$.

Настоящая работа является продолжением публикаций комплекса исследований оптических свойств перспективных для практических приложений нелинейных кристаллов $LiNbO_3$+0,03%Fe с целью использования в системах передачи, приема, обработки и хранения оптической информации.

Received: 20.04.04

THE MICROWAVE POLYMER ABSORBENTS

S.T. AZIZOV, M.A. SADIKHOV
Institute of Physics, Azerbaijan National Academy of Sciences,
AZ-1143, Baku, G.Javid ave., 33

The technique of the layer thickness selection and composition of the binary absorbent microwave coverings are presented in the paper.

INTRODUCTION

The essentiality of the papers, connected with the theoretical analysis of the appearing condition of the non-reflecting absorption of the electromagnetic radiation in the layer of the polar dielectric, taking into consideration its characteristics, treatment of the methodological and algorithmic software with the treatment of the methods of the measurements of the strongly-absorbent materials in the high-frequency range, based on the non-reflecting wave absorption effect, makes them very perspective.

The existence the non-reflecting wave absorption effect in the polar liquids and their solutions in the non-polar absorbents makes the perspective of their using in the capacity of the non-reflecting absorbents of high-frequency radiation. Such coverings may be used in the location techniques in the action band of the radio transmitting devices, at the creation of the dead rooms, and in the other areas of techniques and ecology, where appears the necessity in the absorption of the electromagnetic radiation of the given frequency, also. The existing absorbents of the electromagnetic radiation are carried out, as a rule, on the base of the compositional materials and have in their composition the thin metallic wires or high-disperse metallic particles. Moreover, the dissipation of the electromagnetic radiation takes place in the surface layer because of skin-effect [1,2,3].However, in such absorbents the effective dissipation of the electromagnetic radiation decreases with the increase of its frequency, and that makes difficultness of the creating the high-frequency absorbents of electromagnetic radiation on the base of existing conducting materials.

In such cases, when absorbents of the electromagnetic radiation have the metallic base, covered by dielectric film on it, in the capacity of which the polar substance with the maximal dispersion near given range of wavelength was used, it is hardly to select the material of the absorbing film, the dielectric properties of which satisfy to the conditions of the non-reflecting absorption of the incident electromagnetic radiation of the given frequency.

In this direction prefer in the capacity of the material of the absorbing covering to use the homogeneous mixture, consisting on the polar dielectric with dispersion near the given range of wavelength and non-absorbing radiation of the non-polar substance, but not the concentration of the polar component of the mixture, and thickness of the covering layer it is need to choose from the theoretical positions, concluded for the case of the absence of the reflection of the electromagnetic radiation of the given frequency from dielectric-metal system.

THE MAIN CONTENT

It is known, that at the presence of the absorption of the electromagnetic radiation in the dielectric layer, covered on the metallic base, the dependence of the amplitude of the reflected wave on the thickness l of the covering layer has oscillating and damped character. The state and value of the module of the wave *R* reflection coefficient in the external points of this dependence is defined by the dielectric parameters of the covering substance and radiation frequency f .Moreover, the non-reflecting wave absorption in the considered two-layered system dielectric-metal realizes in the minimum points of the dependence *R* on l at the carrying of the following conditions

$$\left(1+y^2\right)\cdot\lambda/\lambda_g = th\left(2\pi l_0 y/\lambda_g\right) - y\cdot tg\left(2\pi l_0/\lambda_g\right)$$
$$y\cdot sh\left(4\pi l_0 y/\lambda_g\right) + \sin\left(4\pi l_0/\lambda_g\right) = 0 \qquad (1)$$

where

$$y = tg\,\delta/2\,,\ \delta = arctg\,{}^{\varepsilon''}\!/_{\varepsilon'}\,,\ \varepsilon',\varepsilon''$$

is the dielectric constant and dielectric loss of covering substance, correspondingly; λ , λ_g are wavelength in the vacuum and dielectric, correspondingly, l_0 is the thickness of covering layer, at which *R* becomes equal to 0).

So

$$\varepsilon' = \left(1-y^2\right)\cdot\left(\frac{\lambda}{\lambda_g}\right)^2;\quad \varepsilon'' = 2y\cdot\left(\frac{\lambda}{\lambda_g}\right)^2; \qquad (2)$$

the joint decision of the equations (1), (2) is defined the functional connection between λ , l_0 , ε' and ε"of material of the absorbing film, corresponding to the case of the complete extinction of radiation in the covering layer by the way of the deletion from the equations of λ and y .

The results of calculations by the equations (1), (2) are presented graphically in the axis of ordinates *[ε', ε"]* (fig.1). They are equal to the first three minimums of curve *R* on l , under the condition, that in the chosen its points of extremum points the wave reflection is absent. Every point of these dependencies is equal to definite value of the given thickness l_0/λ of covering layer, at which the conditions of non-reflecting wave absorption are carrying out.

If absorbent's covering is formed in the type of binary mixture of absorbent and nonabsorbent material, so values of the concentration dependencies ε″ and ε′of mixture at the chosen radiation frequency are necessary for the finding of

the resonance composition of mixture φ and thickness l of the layer.

In this case it is necessary to cover the found dependence of ε′′and ε′ in the fig.1.

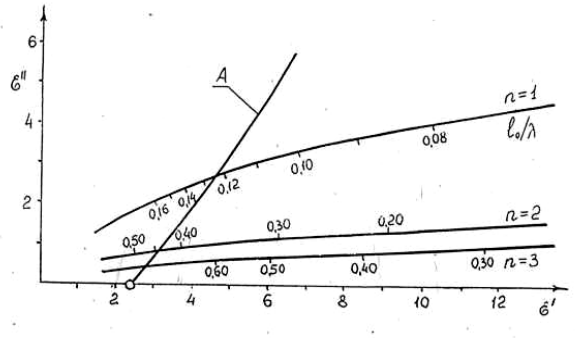

Fig.1. The illustration of the graphical method of the finding of the resonance concentrations of polar component in the absorbent.

Then the points of intersection of this dependence with the curves, described by equations (1) and (2), allow to define the looking for the set of values φ_0 and l_0 for every N value. As the concentration dependence ε′′and ε′ of the concrete mixture it is difficult to express analytically, so we use the graphic method of the finding of resonance values φ_0 and l_0 for their calculation, which was described in the ref [4].

In the table as a example are given the results of the calculation of the parameters of the non-reflecting coverings of the solutions of dimetilformamide-dioxan.

N	φ %	l/λ
1	4	0,1
2	8	0,3
3	19	0,7

CONCLUSION

Thus, the search of the resonance values l and λ, at which the conditions of non-reflecting wave absorption becomes unique. If the frequency dependencies ε"and ε'of the concrete covering material are known. In the dispersion region of the polar substance, its dielectric properties are well described by Debye equations. From the joint solution of Debye equations and equations (1) and (2), it is followed, that any covering substance has the frequency discrete spectrum and the spectrum of the thicknesses of covering layer, corresponding to it, at which the resonance non-reflecting wave absorption effect appears.

[1] *E.R.Kasimov, S.T.Azizov,R.M. Kasimov , Ch.O.Kadjar*. Izvestiya AN Azerbaydjan, ser. fiz.-tex. I mat. nauk, 1995,t. 16, N5-6,s. 22-29.

[2] *V.D.Saxachkiy*. Izv. vuzov. Radioelektronika, t 41, N1-2,1998, c 78-80.

[3] *R.M. Kasimov, M.A. Kalafi, Ch.O.Kadjar, E.R.Kasimov.* Injenerno-fizicheskiy jurnal, t. 71, N2, 1998.

[4] *S.R.Kasimova, S.T.Azizov, R.M.Kasimov, Ch.O.Kadjar, M.A.Sadixov*. Izvestiya AN Azerbaydjan,Fizika I astronomiya, t. XXIV, №5, 2004, (v pechati).

S.T.Əzizov, M.A.Sadıxov

MİKRODALĞALI POLİMER UDUCULAR.

Məqalədə mikrodalğalı binar uducuların tərkibi və qalınlıq layları seçilmə metodikası göstərilib.

С.Т.Азизов, М.А. Садыхов

МИКРОВОЛНОВЫЕ ПОЛИМЕРНЫЕ ПОГЛОТИТЕЛИ.

В статье приведена методика выбора толщины слоя и состава бинарных поглощающих микроволновых покрытий.

Received: 16.09.04

THE INVESTIGATION OF MORFOLOGY AND CONFORMATION CHANGES OF THE THIN POLYMERIC FILM, FILLED BY THE THIN-DISPERSION FERROELECTRIC PARTICLES

E.M. HAMIDOV, M.K. KERIMOV, A.M. MAGERRAMOV, N.N. GADZJIEVA
Institute of Radiation Problems of NAS of Azerbaycan, AZ 1143, av. H. Javid, 31A, Baku

The separation method of thin-dispersion ferroelectric particles and their input in the crystallizing polymeric matrix have been described. The morphology of the obtained thin polymer composite films have been investigated. It is shown, that the increase of the part of the crystallic β-phase of the polymer matrix is observed at the volume content of the filler up to 15%, but at the high filler content the tendency to the clusteroformation takes place. It is established, that clusteroformation and conformation changes in PVDF, observed on the lines 840 and 813 sm^{-1} are interconnected.

Introduction

The obtaining and investigation of the properties of thin ferroelectric and electro active polymeric films is the actual problem with the aim of their application in the different converters [1-2]. It is known, that the sizes and volume part of filler particles play the determinative role in the process of the formation of composite material structure [3]. With the increase of the particle sizes, the specific surface increases, therefore the peculiarities of the interphase interaction and the size effects are strongly revealed [4-6]. The character of phase transitions changes at critic sizes of the filler or the thickness of the film, or in a particular, the decrease of the particle size leads to the decrease of tangent of dielectric loss angle [5]. It is need to note, that the substrate surface, on which these films have been obtained or treated, influences on the physical state of the thin films essentially. We informed about the influence of the substrate type on the submolecular structure (SMS) and showed, that by the choice of the corresponding substrate one can make dielectric properties of ftorpolymers better [6].

The study of the structure peculiarities and properties of the thin polymer composite materials (PCM) with the thin-dispersion ferroelectric fillers (particle diameter d<5mkm) opens the possibility of the revealing of the main regularities of the modification influence of surface and distribution of fillers on the electret and dielectric properties [4-8].

The modification influence of filler on the structure and electroactive properties of PCM have been made by different ways: plasmolysis, nanotechnology, using of the Lengmure-Blodjet technology, selection of solvent and e.t.c. The application borders and realization possibilities of these methods are significantly differed. Moreover, as the analysis of the obtained data shows, the PCM can be created with the definite connectivity, morphology and improved electro active properties at the optimal their combinations in the dependence on the filler dispersion degree and polymer type.

In the present work the method of separation of thin-dispersion particles, the obtaining of the polymeric thin films on the base of the polyvinylideftoride (PVDF), filled by the thin- and monodispersion particles of ceramic powders by the PZT-19 type and investigation of their morphology and conformation changes in the dependence on the filler volume content, are described.

The experimental part

It is known, that the base of the sedimentation particle generation, having different sizes, according to which, particles, precipitating in the viscous medium, have constant velocity, depending on their sizes is the Stocks law [9]. For the spherical particle this velocity is expressed by the following form: $u = \frac{4}{3}\pi r^3(\rho_m - \rho_l)g / 6\pi r\eta$, where r is particle radius, η is dynamic medium viscosity, ρ_m and ρ_l are densities of material particle and liquid correspondingly. At the uniform motion $u=const=H/\tau$, where H is precipitation height of particle, τ is precipitation time. Taking into consideration that $d=2r$, so for the determination of the particle diameter the following formulae is obtained: $d = \sqrt{18H\eta / g(\rho_m - \rho_l)\tau}$ In the practical aims it is necessary to calculate the precipitation time on the fixed height of the particles, having the different diameters, by the formulae: $\tau = 18H\eta / g(\rho_m - \rho_l)d^2$.

It is note that the given formulas are correct for the spherical particles and are applied for the diluted suspensions. For the particles of the irregular form, the representation about equivalent radius is used, corresponding to the radius of the spherical particle velocity.

In our case the separation of the particles by the type PZT-19 was carried out in the dimetylformamide medium (DMF) in the measuring glass of 1l volume. The sampling time in the dependence on the choice of ceramic particle sizes is given on the table 1.

Table 1
The sampling time in the dependence on the particle size for the suspension DMF/PZT-19

Diameter of particle is less, than mkm	The sampling depth, sm	The sampling time DMF/PZT-19, sec.
50	10	6
10	10	146
5	10	584
1	10	14600
0,5	10	58400

The polymeric composite films with the thickness $h<10$ mkm are obtained by the way of thermal evaporation of 1% solution of polymer PVDF in DMF and colloid ceramic suspension with chosen particles at the temperature 370 K on Al substrate. For the obtaining of the homogeneous degree of dispersion the particles are separated in the opposite order, i.e. the beginning of the small sizes. The ceramic particle

concentration in the colloid suspension with chosen sizes of the particles is found by the weighing of the average trial volume. The mass ratio of the filler and polymeric matrix is obtained by adding of the known volume of the colloid ceramic suspension to the known volume of the polymeric solution. The thickness of the samples is found with the help of the thickness meter IZV-2. The samples are treated by the heat treatment at the temperature 393 K during one hour. The micro photos are taken on the scanning electronic microscope (Nanoscope IIIa, Multimode SPM). IR-spectrums of the samples are investigated in the range 950-750 sm^{-1} on the spectrophotometer Specord 71JR at the room temperature by the reflection absorption spectroscopy method (RAS). The measurements are carried out at the angles of incidents, which are closed to the normal ones ($\varphi=10°$) in the unpolarised light with the help of special reflection device (Shimadzu, Japan). Polymer films were polarized in the field of Corona discharge at polarization voltage of 7kV at room temperature. The distance between the films and electrode was 10mm, polarization duration 180 sec. Surface potential if the electrets were measured by the vibration electrode method. The surface charge density б and then charge Q were calculated by the formulae:

$$\sigma = U_c\, \varepsilon\varepsilon_0/h,$$

where U_c is the compensation voltage; ε, the relative permittivity of the composite; ε_0, the permittivity of the free space, equal to 8.854×10^{-12} Fm^{-1}; h, is the electret thickness.

The results and their discussion

Earlier we informed, that the more narrow dispersed distribution of the ceramic particles, and the particles of the size 1mkm [10] also, can be obtained at the exact calculation of the parameters, including in the Stocks equation and at the sampling selection in the opposite order. At the small content of such quazimonosize filler (till 15%), on the data of SEM images, the horizontal and vertical clusters are absent. But at the increasing of the filler concentration till 20%, the aggregation process of the ceramic particles takes place that leads to the cluster formation. SEM images of the composite film with the 20% of the filler volume content is represented by fig.1.

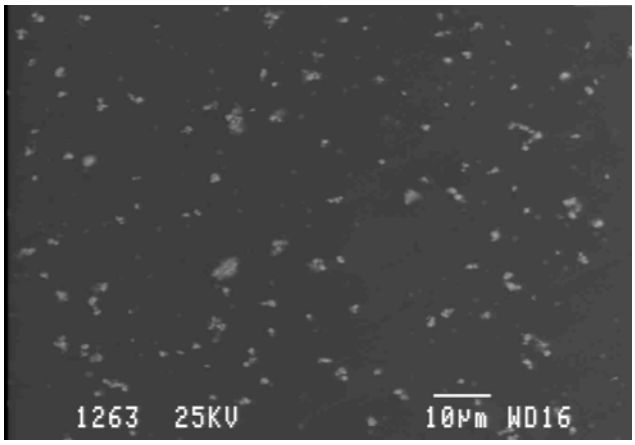

Fig.1. SEM microphotography of the polymeric composite film on the PVDF base and PZT-19 with the particle sizes of the filler d~1mkm at the volume filler content 20%.

From fig.1 it is seen that particles with the sizes about 1 mkm combine and form the clusters of the form either line chains or lumps. The cluster sizes change from 2 to 10 mkm. SEM images of such a clusters is given in the fig.2.

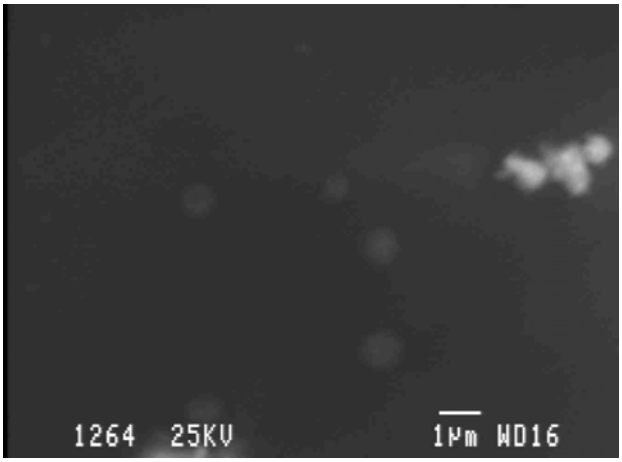

Fig.2. SEM images of the separate cluster of the composite film on the PVDF base and PZT-19 with the particle sizes of the filler d~1 mkm at the volume filler content 20%.

It is seen that the size of this line cluster is about 3 mkm. The appearance of the clusters destroys the morphology of the polymeric film. That's why at increase of filler concentration because of the increase of sum specific surface of the ceramic particles and appearance of the vertical clusters, the composite material with the ratio *h/d~2* isn't obtained.

AFM micro photos of free surface and the surface turned to substrate of the composite material with the scanning area 5x5 mkm^2 on the base PVDF/PZT-19 at 20% of the filler volume content are shown in fig.3 and fig.4.

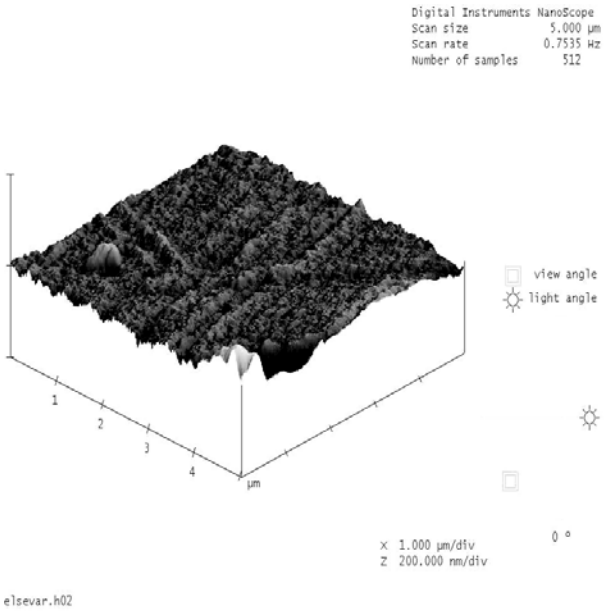

Fig.3. AFM microphotography of the free surface of the composite film PVDF/PZT-19at the volume filler content 20%.

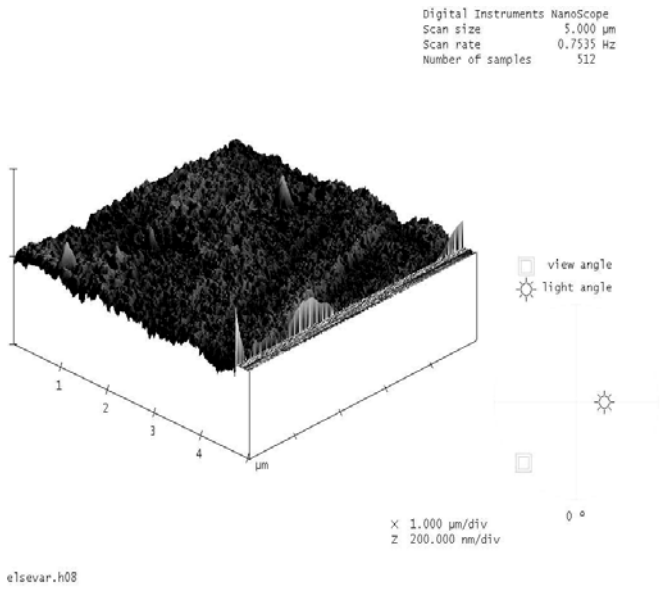

Fig.4. AFM microphotography of the surface, turned to the substrate of the composite film PVDF/PZT-19 at the volume filler content 20%.

From that figures it is seen the formation of the vertical clusters of the ceramic particle in the ledge form that destroys the polymer structures – the ferroelectric particle – polymer. Indeed, these morphological offences will influence on the dielectric properties of the composite as a whole. From the comparison of these images we can see that the surface composite-substrate is rougher that the surface composite-air, i.e. the surface of the substrate also deposit in the formation of the near-surface layer. From the references it is known that the surface tension of the film from side of the solid substrate differs strongly from the surface bounded by air [10]. In this work it is established by authors that the solubility parameter of the near-surface layer differs also from the solubility parameter in the polymer volume that leads to the change of the polymer density in the near-surface region.

Thus, the surface state of the film depends on the volume content of the filler, energetic parameters of the substrate, solubility parameter of the polymer, parameter caused by adhesive properties and etc.. The morphology of the near-surface region formed by such complex method plays an essential role in the formation of a submolecular structure as the polymer film, so the composite material on the base of these polymers and therefore influences on the dielectric properties [6].

The doping of the thin-dispersion filler to the polymeric matrix allows also revealing the structure transformations caused by interphase interactions with the help of IR-spectroscopy. Taking into consideration that the sum of specific filler surfaces causing the interphase interaction between the polymer and the doped particle can purposefully change by the change of the volume content of the filler of the determined size. So it is possible to observe the change of the conformational transformations. The IR-spectrums of the initial film (1) and composite films, filled by the thin-dispersed particles (*d~1* mkm) with the volume content 10 (2) and 15% (3) are given in fig.5.

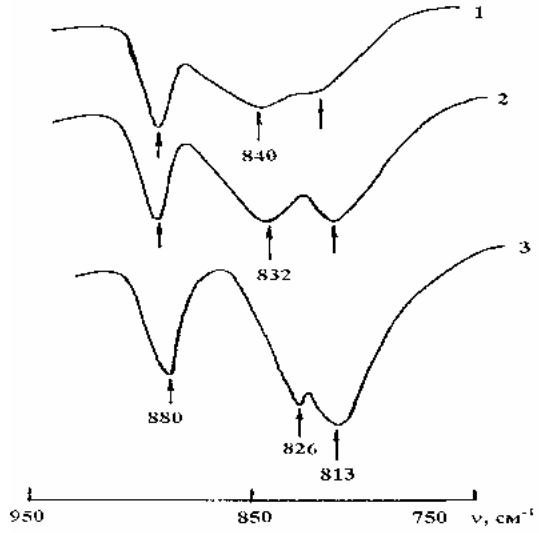

Fig.5. IR-spectrums of the initial film (1) and composite films, filled by the thin-dispersed particles (*d~1* mkm) with the volume content Φ=10(2) and 15%(3).

From fig.5 it is seen that the optical absorption of the conformational sensitive band is 840 cm^{-1}, which characterizes the crystal *β*-phases, increases with the increase of the volume content Φ. This increase accompanies with the shifting of the maximum of this frequency and decrease of the half-width. The band 880sm^{-1} is conformational insensitive, but the band 813sm^{-1} characterizes the amorphic phase [10]. The data, reflecting the band changes 840 sm^{-1} are given in the table2.

Table 2

The change of the parameters of the crystallic *β*-phase (band 840 sm^{-1}) from the volume content

Sample	Volume content Φ, %	D_{840}	$\nu_{1/2}$ of the band 840 sm^{-1}	ν_{max} of the band 840 cm^{-1}
1	0	0,025	50	840
2	5	0,05	40	832
3	10	0,065	32	830
4	15	0,075	15	826
5	20	0,068	22	823

The dependence of the optical absorption *D* and the half-width of the frequency 840 sm^{-1} ($\nu_{1/2}$) on the volume content Φ is shown on the fig.6. From the plot it is seen, that both dependencies have the extreme characters. The content of the crystal *β*-phase increases and the increase of the crystallinity takes place at the volume content of the filler till 15%. Evidently, the fillers in the form of the thin particles in the polymeric matrix behave themselves as the crystallinity

centers. However, the value of the optical absorption of the frequency 813 sm^{-1} also increases, that shows the simultaneous appearance of the crystallinity and amorphization processes (growth β and γ phases).

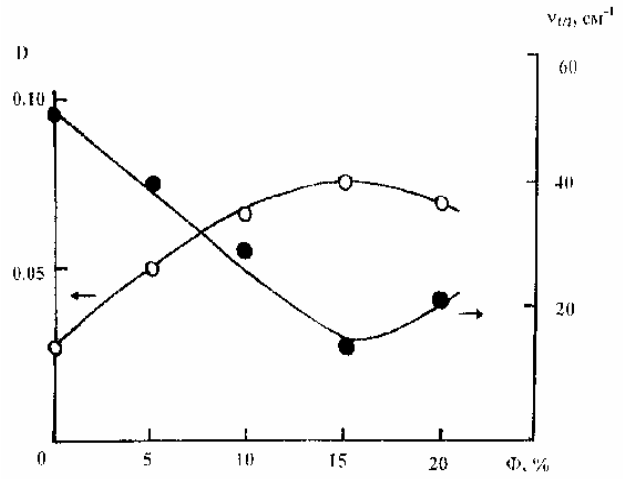

Fig.6. The dependence of the optical absorption *D* and frequency half-width 840 sm^{-1} ($\nu_{1/2}$) on the volume content Φ.

The cristallinity change directly influence on the electret properties, in a particular, on the effective electret charge of Corona polarized composite films. The dependence of the relative initial electret surface charge Q/Q_0 on the volume content of the filler Φ is given in the fig.7.

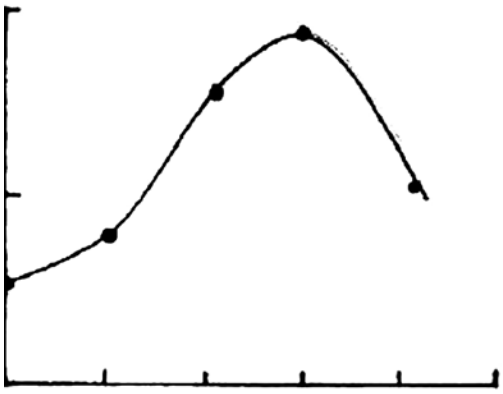

Fig.7. The dependence of the relative initial electret surface charge Q/Q_0 on the volume filler content Φ.

From fig.7 it is seen, that the initial electret surface charge achieves its maximum value at te volume content Φ=15%. The comparison of the figures 6 and 7 shows, that the direct correlation, which is proved by our experiments takes place between the cristallinity of the polymer matrix, volume content of the filler and electret properties of the composite material.

The external form of the dependence of crystallinity on the volume content corresponds to other reference data. In particular, in the work [7] at the studying of the electret properties of polystirol with the thickness 1,2mm, filled by silicooxides, the extremum dependence of the effective surface charge 6 on the volume content of the filler Φ is obtained by authors and is shown that 6 has the maximum value at Φ=12%. This probably can be connected with the change of the conductivity of the surface layer and decrease of the quantity of the polarized polymeric material.

On our opinion, in the case of the thin films, the observable extreme dependence can be explained by the change of the submolecular structure. The near-surface layer forms around the doping particle and it can be proposed that the crystallization process of the polymer takes place in the near-surface layer of this particle. The sum specific surface of the particles increases with the increase of the filler concentration increase that leads to the increase of the polymer crystallization region. However, at the volume content of the filler 20%, as it is seen from the fig.1-4, the clusters form. This is caused the decrease of the sum specific surface of the particles. And in the result, the crystallization region of the polymer decreases. That we can observe on the IR-spectrums.

From the other side, the each particle in the polymer matrix behaves itself as the center of the mechanical stress, acting in the near-surface region, the size of which changes in the dependence on the particle size and filler volume content [11]. These changes cause the change of the mechanical stress in the disperse volume of polymer, that leads to the change of the conformation state. In the work [12], the change of the conformation states, oriented by PVDF films with the width 28 mkm by IR spectroscopy methods the different degrees of deformation, is investigated. These data prove our prediction about the interphase interaction takes place with the help of the mechanical stresses forming in the near-surface layer of the doping particle in the thin filled polymers.

Thus, the separation technique of the thin-dispersed ferroelectric particles with their following doping in the polymer matrix is treated. It is shown, that the surface morphology of the obtained composite materials changes under the influence of the substrate and the change of the filler volume content. By the studying of the conformation changes, obtained by this method of the PVDF films, filled by the thin-dispersed ferroelectric particles it is established, that by the variation of the filler volume content, the content of the crystallic β-phase can be modificated and improved of the electret properties of the polymer composite materials.

The authors thankful to the scientists of Norvegian University of Science and Technology Kjell Evjen and Tanem S.Bern for realization of SEM and AFM images.

[1] *E.B. Araujo, J.A. Eiras.* Material research, 1999, v.2, №1, p.17-72.

[2] *E. Bormashenko, S. Sutovsky, R. Rogreb, A. Sheshnev, A. Sulzinger, M. Levin, Z. Barkay, A. Katzir.* SPIE Proceedings, 4695, 2002, 465-472.

[3] *I.D. Simonov-Emelyanov, V.N. Kuleznev, L.Z.Trofimicheva* Plasticheskiye massi. 1989, № 8. p.61-64.

[4] *A.M. Magerramov.* Structural and radiation modification of electret, piezoelectret properties of polymer composites. Baku, «Elm», 2001, 327 p.

[5] *V. Platonova, S.N. Gorshkov, S.A. Taraskin, A.E. Bilan, A.M. Shetinin.* Naukoemkiye tekchnologii" 1, 2004. v. 5, p. 9-13.

[6] *Mark P. McNeal, Sei-Joo Jang,, Robert E. Newnham.* Journal of Applied Physics. v. 83 (6), pp.3288-3297. March 15, 1998.
[7] *E.M. Hamidov, Tanem S. Bern, A.M. Mageramov, M. A. Nuriyev.* Tretya vserossiyskaya Karginskaya konferenchiya "Polimeri –2004". 2004, M. MSU. v.2. p. 103 M.F.
[8] *M.F. Galikhanov, D.A. Eremeev, R.Ya. Deberdeev*. Russian Journal of Applied Chemistry. Vol. №10, 2003, pp. 1651-1654.
[9] *E.S.Lukin, N.T.Andrianov.* Technicheskiy analiz i kontrol proizvodstvo keramiki M.: Stroyizdat, 1986, 272p.
[10] *E.M. Hamidov, Tanem S. Bern, A.M. Magerramov, M.A. Nuriyev*. «Aktualniye problemi fiziki». Materiai III Respublikanskoy nauchnoy konfernchii, Baku, fevral, 2004, p. 127-128.
[11] *V.B. Busigin, A.E.E. Chalix* Chimiya i kompyuternoe modelirovaniye. Butlerovskiye soobsheniya 1999. v. 2.
[12] *S. Lanceros-Mündez, M.V. Moreira, J.F. Mano, V.H. Schmidt, and G. Bohannan.* Ferroelectrics 273, 2002, 2393-2398.

E. M. Həmidov, M. K. Kərimov, A.M. Məhərrəmov, N. N. Hacıyeva

XIRDADİSPERSLİ SEQNETOHİSSƏCİKLƏRLƏ DOLDURULMUŞ NAZİK POLİMER TƏBƏQƏLƏRİNDƏ MORFOLOJİ VƏ KONFORMASİYA DƏYİŞİKLİKLƏRİNİN TƏDQİQİ

Xırdadispersli seqnetoelektrik hissəciklərinin ölçüyə görə ayrılması və onların polimer matrisasına daxil edilməsi üsulu təsvir edilmişdir. Alınan kompozit materialların morfoloji tədqiqatı aparılmışdır. Göstərilmişdir ki, doldurucuların həcm payı 15 % olduqda polimer matrisanın kristallik β-fazasının miqdarının artması və yüksək həcmi faizlərdə isə klasterlərin yaranması müşahidə olunur. Müəyyən edilmişdir ki, PVDF təbəqələrində 840 və 813 sm^{-1} zolaqlarına görə öyrənilən dəyişikliklər və klasterlərin yaranması qarşılıqlı surətdə əlaqədardır. Göstərilmişdir ki, doldurucuların həcm payını seçməklə elektret xassələrini yaxşılaşdırmaq olar.

Э.М. Гамидов, М.К. Керимов, А.М. Магеррамов, Н.Н. Гаджиева

ИССЛЕДОВАНИЕ МОРФОЛОГИИ И КОНФОРМАЦИОННЫХ ИЗМЕНЕНИЙ ТОНКИХ ПОЛИМЕРНЫХ ПЛЕНОК, НАПОЛНЕННЫХ ТОНКОДИСПЕРСНЫМИ СЕГНЕТОЭЛЕКТРИЧЕСКИМИ ЧАСТИЦАМИ

Описан метод сепарации тонкодисперсных сегнетокерамических частиц и их введение в кристаллизующуюся полимерную матрицу. Исследована морфология полученных тонких полимерных композитных пленок. Показано, что при содержании наполнителя до 15% об. наблюдается увеличение доли кристаллической β-фазы полимерной матрицы, а при высоком содержании наполнителя – тенденция к кластерообразованию. Установлено, что образование кластеров и конформационные изменения в ПВДФ, прослеживаемые по полосам 840 и 813 $см^{-1}$ взаимосвязаны. Показано, что электретные свойства могут быть улучшены выбором оптимального значения объемного содержания наполнителей.

Received: 07.09.04